A Laboratory Experiment of Axisymmetrical Infiltration Into a Layered Soil

by

Stephen E. Heermann

Submitted in Partial Fulfillment of
the Requirements for the Degree of
Master of Science in Hydrology

New Mexico Institute of Mining and Technology

Socorro, New Mexico

February, 1986

Abstract

An axisymmetrical sand tank model was used to study the anisotropic behavior of a variably saturated, layered soil. The soil was composed of cyclic layers or a fine-grained and a medium-grained sand. Water was introduced from a point source located at the soil surface. The movement of the wetting front was observed and the steady-state total hydraulic gradients and streamlines were mapped. Observations of wetting front behavior for three experiments, conducted at three different flow rates, revealed that the wetting front movement in the radial direction was as high as 27 times greater than wetting front movement in the vertical direction at the lowest flow rate. The ratio of the radial and vertical distances to the wetting front decreased as the flow rate increased. Analysis of steady-state gradient and streamline behavior revealed that anisotropy increased with increasing distance from the source and with decreasing moisture content and pressure head, supporting the conceptual models of Mualem (1984) and Yeh (1985). As the anisotropy increased, the streamlines diverged from the average total hydraulic gradients. The anisotropies observed from the sand tank model were much greater than those predicted using the hydraulic conductivity - pressure head relationships of the individual soils. The observations of this study are highly relevant to the study of pollution migration in the vadose zone and to the study of flow from trickle irrigation systems

TABLE OF CONTENTS

LIST OF FIGURES

LIST OF TABLES

Acknowledgements

I would like to acknowledge Jim McCord for constructing the sand tank and I would like to thank Ed Weeks of the U.S. Geological Survey and Dr. John Wilson for their advice on the design of the experiment.

I would especially like to thank Amy Childers, Steve Conrad, Tom Duval, John Hanson, Diana Holford, Tracy McFarland, Richie Spangler, Todd Stein, and Valda Terauds, for their invaluable help in setting up and conducting the experiments.

I would like to thank Valda Terauds for her encouragement and moral support and well as for her help with typing the report.

Finally, I would like to thank Dr. Dan Stephens, my advisor, for providing the initial idea to conduct the study, for providing the funding, and for his guidance and time spent advising and reviewing.

Chapter 1

INTRODUCTION

The study of infiltration through soils is greatl complicated by layering in the soil profile. In a unsaturated, homogeneous and isotropic soil, infiltrati behavior is relatively easy to predict using eithe analytical or numerical solutions. In an unsaturat layered soil, however, the variability of hydraul parameters governing the flow of water greatly reduces t ability to predict infiltration behavior. The implicatio of this inability to predict flow can be found in studies the transport of contaminants in the vadose, the study recharge, either from precipitation or from streams, and the study of flow from irrigation systems

Crosby and others (1968) studied the migration pollutants from a 150 square meter sewage drain field in layered glacial outwash deposit. They found that aft several years of infiltration, at flow rates of 40,0 liters per day, the polluted water did not penetrate mo than approximately 8 meters. Instead, it moved lateral through the fine-grained layers. Due to the increase lateral spread and decrease in vertical penetration, it w predicted that the pollutant would not reach the wat table, 40 meters below, in any harmful concentratio

Routson and others (1979) studied the movement of radionucleides through a relatively dry, layered, coarse-grained soil after 435,000 liters of high-level nuclear waste leaked from a buried storage tank. It was found that the plume moved further laterally than it did vertically. Due to this lateral movement, it was predicted that the plume would take over 23,000 years to reach the water table 50 meters below the storage tank. After this period of time, the radionucleides would reach the water table in harmless concentrations, owing partly to radioactive decay.

Zaslavsky and Sinai (1981) developed a conceptual model of infiltration from precipitation into a sloping, layered soil. They found that the layering in the soil increased the lateral component of flow.

These three studies have all shown that layering in unsaturated soils increases the lateral movement of water relative to the vertical movement and may even cause the lateral component of flow to become greater than the vertical flow component. Little is known on how to actually predict the flow of water in unsaturated, layered soils. The variability and discontinuity of the hydraulic parameters controlling flow makes the use of analytical solutions to flow equations very difficult if not impossible to use and greatly increases the work involved in using numerical solutions to flow equations.

Some of the problems faced in the study of flow through layered media can be simplified by integrating the hydrauic properties of the layers. In doing so, the heterogeneous flow system is transformed into an equivalent homogeneous but anisotropic system, (Bear, 1972, pg. 156) which is one in which the hydraulic conductivity of the porous medium varies in direction but not in space. In layered soils, the hydraulic conductivity is greatest in the direction parallel to layering and obtains its lowest value normal to that direction.

For two-dimensional or axisymmetrical flow, where the coordinate axes are parallel to the principal directions, anisotropy can be mathematically defined by the equation

$$A = K_p/K_n \qquad (1.1)$$

where K_p is the component of the hydraulic conductivity tensor occurring parallel to bedding and K_n is the component in the direction normal to bedding. Within the zone of saturation, the value of anisotropy is constant with respect to pressure head because the hydraulic conductivities of the individual layers remain constant with respect to this parameter. Within the vadose zone, however, the hydraulic conductivity varies with pressure head and with the degree of saturation. As the pressure head decreases from 0, the moisture content decreases from the ~~effective~~ porosity and the hydraulic conductivities of the individual layers

decrease. According the findings of Mualem (1984) and Yeh (1985), the hydraulic conductivities of different soils diverge with decreasing pressure head, which result in an increase in anisotropy with decreasing pressure head. Since anisotropy is a function of pressure head, ψ, equation 1.1 becomes

$$A(\psi) = K_p(\psi)/K_n(\psi) \qquad (1.2)$$

The principal effect of an anisotropic porous medium on flow is that the hydraulic gradient and flow vectors do not coincide, except if flow is in one of the pricipal directions. Instead, the flow vector occurs at some angle from the hydraulic gradient in the direction of greatest hydraulic conductivity, In the case of layered media, this direction is parallel to the layers. An increase in anisotropy results in an increase in the angle between these vectors.

In the case of flow from a point source located above the water table, such as a leak from a sewage treatment pond or an underground storage tank, the soil becomes dryer with distance from the source. As a result, anisotropy may increase with distance from the source in which case the pathlines of the pollutant will diverge from the hydraulic gradients.

This divergence between the hydraulic gradient and flu directions was the focus of the study. An axisymmetrica laboratory model was set up in which water was allowed t infiltrate at a constant flow rate from a point source int a layered soil. The soil consisted of a fine-grained san and a coarse-grained sand placed horizontally in thi alternating layers.

Steady-state flow was of most interest because i provided the best conditions in which to study th divergence of the flowpath from the hydraulic gradient Flow was observed through many layers so that the porou media could be homogenized into an equivalent homogenou anisotropic porous medium. Steady-state hydraulic gradient were mapped with tensiometers and streamlines were mapped b observing the movement of dyes.

Transient-state infiltration was studied in terms o wetting front behavior. In the transient-flow study, th hydraulic properties of the individual soils, for the mos part, were not integrated into a homogeneous but anisotropi soil. Instead, the wetting front movement was studied as function of the contrasting hydraulic properties of th individual layers.

There were two main objectives for this study. Th first objective was to observe the steady-state anisotropi behavior of the flow system in terms of the total hydrauli gradients, the streamlines, and the pressure hea

distribution within the soil profile, and to determine if this anisotropic behavior could be predicted from the unsaturated hydraulic conductivities of the individual soil layers. The second objective was to observe the movement of the wetting front in terms of the wetting front geometry and the relative velocity of the wetting front through the individual layers.

This paper will first present a more detailed and theoretical analysis of the problem, the previous work done on the topic and the approach that this study has taken to the problem. Next, the design of the model and the execution of the experiments will be examined. This will be followed by a presentation of the results of the experiment and a discussion of these results.

Chapter 2

THEORY

2.1 Steady-State Anisotropy in Layered Soils

For axisymmetric flow through an anisotropic porous medium, in which the radial and vertical axes are directed parallel and normal to bedding, Darcy's law can be written in the form

$$q_r = K_{rr} \cdot J_r$$
$$q_z = K_{zz} \cdot J_z \qquad (2.1)$$

where q_r and q_z are the specific flux vectors in the radial and vertical directions, respectively. K_{rr} and K_{zz} are the components of the hydraulic conductivity tensor and J_r and J_z are the gradient vectors.

According to Bear (1972, pg. 157), a layered soil can be made equivalent in its average behavior to an anisotropic soil if the layers are thin with respect to the over-all dimensions of the flow domain. The principal directions of hydraulic conductivity in this anisotropic soil occur parallel and normal to the layering. Since K_{rr} and K_{zz} are the principal directions, they can be expressed simply as K_r and K_z, respectively.

Given a layered medium composed of many alternating layers of two soils, each of equal thickness and having saturated hydraulic conductivities of K_1 and K_2. The directional hydraulic conductivities in the directions parallel to the radial and vertical axes are theoretically equal to the arithmetic and harmonic means, respectively, of K_1 and K_2. Mathematically this can be expressed as

$$K_r = K_a = \frac{K_1 + K_2}{2}$$
$$K_z = K_h = \frac{2}{\frac{1}{K_1} + \frac{1}{K_2}} \qquad (2.2)$$

where K_a and K_h represent the arithmetic and harmonic means, respectively.

In an unsaturated soil, K_1 and K_2 are no longer constant but become dependent on the pressure head, ψ . In this case, K_r, K_z, K_a and K_h also become dependent on pressure head.

$$K_r(\psi) = K_a(\psi) = \frac{K_1(\psi) + K_2(\psi)}{2}$$
$$K_z(\psi) = K_h(\psi) = \frac{2}{\frac{1}{K_1(\psi)} + \frac{1}{K_2(\psi)}} \qquad (2.3)$$

If equation 2.3 is substituted into equation 1.2 with K_p =

anisotropy in terms of the hydraulic conductivities of the individual layers.

$$A(\psi) = \frac{K_r(\psi)}{K_z(\psi)} = \frac{K_a(\psi)}{K_h(\psi)} = \frac{(K_1(\psi) + K_2(\psi))\left(\frac{1}{K_1(\psi)} + \frac{1}{K_2(\psi)}\right)}{4} \qquad (2.4)$$

Anisotropy reaches a minimum value of 1 when K_1 and K_2 are equal.

The relationship between the gradient vector and the specific flux vector, as a function of the anisotropy, can be derived from Darcy's law. Equation 1.1 can be rewritten in the following form

$$K_r = \frac{q_r}{J_r} \qquad (2.5)$$

$$K_z = \frac{q_z}{J_z}$$

Using the relationships between the specific flux vectors $q_{r,z}$, the gradient vectors, $J_{r,z}$ and angles a and

b shown in Figure 2.1, equation 2.5 can be rewritten as

$$K_r = \frac{q \cdot \cos a}{J \cdot \cos b}$$

$$K_z = \frac{q \cdot \sin a}{J \cdot \sin b} \qquad (2.6)$$

Substituting this into equation 1.1 with K_p and K_n equal to K_r and K_z, respectively, the following relationship results.

$$A = \frac{K_r}{K_z} = \frac{\tan b}{\tan a} \qquad (2.7)$$

From equation 2.7 it can be seen that as the anisotropy increases from a value of 1, angles a and b must diverge. Angle a, the angle between the specific flux vector and the radial axis can be related to angle b and the value of anisotropy with the following equation:

$$a = \tan^{-1}\left[\frac{\tan b}{A}\right] \qquad (2.8)$$

If the angle of the gradient vector, b, is fixed, then the angle of the specific flux vector, a, must diverge as anisotropy increases from a value of 1. From equation 2.7 if the specific flux vector becomes horizontal, angle a becomes 0 and anisotropy becomes infinite

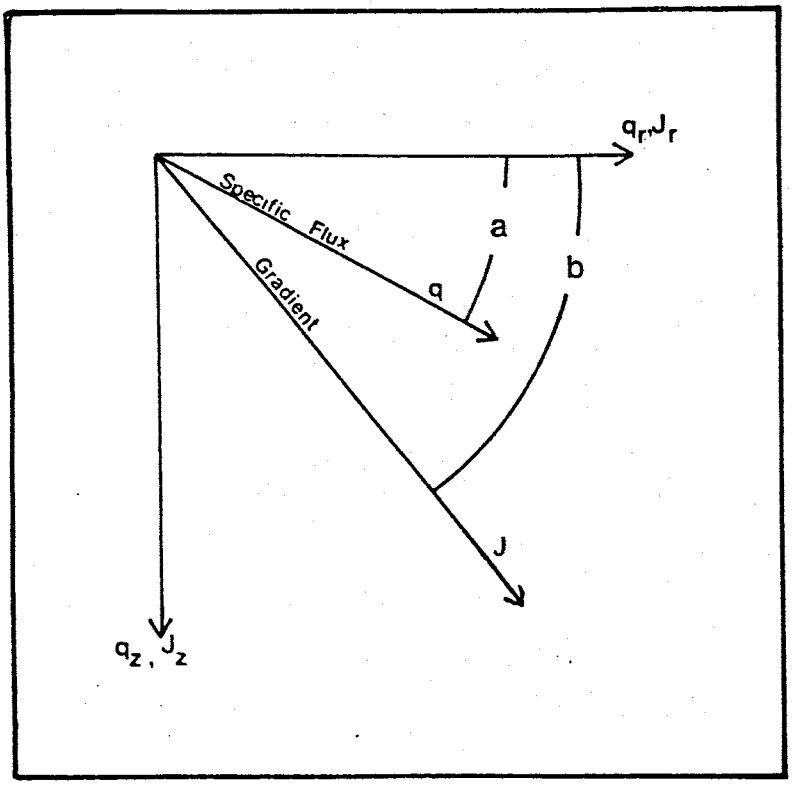

Figure 2.1 Diagram showing the relationship between the specific flux vector, the gradient vector, and the principal axes.

Under steady-state conditions, streamlines are everywhere tangent to the specific flux vector. In addition, at steady-state, streamlines coincide with pathlines (Bear, 1972,pg. 224). A pathline is defined as being the locus of positions in space and time of a fluid particle (Bear, 1972). If a dye is placed into a soil in which flow is at steady-state, its movement maps the pathline of the fluid particles. This pathline coincides with the streamline and is therefore tangent to the specific flux vector.

If the direction of the specific flux vector is determined from the movement of the dye and the direction of the gradient vector is known from tensiometer measurments, then using equation 2.7, the anisotropy can be determined at different locations within the soil. Thus two independent methods are available for determining the anisotropy of an unsaturated soil: the conceptual model of equation 2.4 and a direct measurement of the flow system through the use of dyes, tensiometers, and equation 2.7.

Three previous studies have presented conceptual models of anisotropy in unsaturated soils. Zaslavsky and Sinai (1981) produced a mathematical model of anisotropy in unsaturated, layered soils based on the pressure head distribution found within a medium consisting of cyclic layers of two homogeneous, isotropic soils. This study discussed briefly in chapter 1, is very relevant to the

present study because the soil profile that they used in their mathematical model is very similar to the cyclic profile used in the laboratory model. Their model differed in that flow was introduced from precipitation rather than from a point source. They computed average anisotropy as a function of the precipitation rate and found that as the rainfall rate decreased and the soil became unsaturated, anisotropy initially decreased. As rainfall rate decreased further, anisotropy eventually increased.

Mualem (1984) provided a mathematical model of the anisotropy of unsaturated, layered soils in which he assumed that the soil profiles were composed of an infinite number of individual soil layers, each having a different hydraulic conductivity. The saturated hydraulic conductivities of these layers were uniformly distributed between an upper and lower limit. He further assumed that the hydraulic conductivities parallel and normal to the layering were represented by the arithmetic and harmonic means of the individual soil layers. Finally he assumed power function relationships between hydraulic conductivity and pressure head and determined values for the parameters that decribe these relationships on data collected from various naturally occuring soils. From these assumptions and empirical relationships, Mualem computed anisotropy - pressure head relationships for different ranges of saturated hydraulic conductivity. He found that as pressure head decreased from zero, anisotropy first decreased and then rapidly increased

to values much greater than the anisotropy at saturation Mualem also determined that soils with low saturate hydraulic conductivities displayed a much smaller increas in anisotropy with increasing soil dryness than did soil with higher saturated hydraulic conductivities

Yeh and others (1985) provided a model of anisotropy i unsaturated soils based on stochastic theory. Thei approach looked at the spatial variability of pressure head saturated hydraulic conductivity, and the pore siz distribution index. Their model required severa assumptions. They assumed that hydraulic conductivity an pressure head were exponentially related. They assumed gravity driven flow field with an average gradient directe downwards. Finally, they assumed that hydrauli conductivity varied only in the vertical direction. Thei findings were very similar to Mualem's in that they foun that anisotropy increased with increasing soil dryness an that contrasts in anisotropy were greatest in soils wit high saturated hydraulic conductivities. Their finding differed in that they found no initial decrease i anisotropy upon desaturation.

These three models show that below a certain negativ pressure head, anisotropy increases with decreasing pressur head. Assuming this relationship and the relationship between gradient vectors, specific flux vectors an anisotropy given by equation 2.7, the pathline of a dye

placed near a point source, should become increasingl horizontal as the distance from the source increases, and a the soil becomes dryer.

2.2 Wetting front movement in a layered soi

Most of the work done on wetting front movement i layered soils has involved one-dimensional vertica infiltration. Miller and Gardner (1962) conducte laboratory studies that showed that vertical wetting fron movement from a fine-grained layer to a coarse-grained laye was temporarily inhibited at the layer boundary. Thi occurred until the pressure of the wetting front increase enough to allow the pores of the coarse-grained layer t fill with water. They also found that the water move through the coarse-grained layer in distinct fingers

The movement of water through these fingers, also knov as unstable wetting front movement, was further investigate by Hill and Parlange (1972), Raats (1973), Phillips (1975) and Diment and Watson (1985).

Palmquist and Johnson (1962) studied the effects (layering in soils on two-dimensional infiltration from point source. They conducted two infiltration experiment into a large sand tank. One involved a homogeneous profil consisting of 0.47 mm glass beads and the other involved layered profile consisting of three layers of 0.037 mm glas

the first experiment, water infiltrated downwards through the homogeneous medium, displaying very little lateral movement. In the second experiment, water moved downwards through the fine layer until it reached the layer of larger beads. Vertical infiltration stopped until the wetting front had spread laterally to the boundaries of the tank. When the wetting front penetrated the layers of 0.47 mm beads, it did so in discrete fingers leaving portions of that layer unwetted.

2.3 Steady-State Analytical Solutions For Flow From A Point Source

Richard's equation for axisymmetrical, steady flow through a homogeneous, anisotropic, unsaturated soil can be written in the form

$$\frac{1}{r}\frac{\partial}{\partial r}\, r\, (\underline{\underline{K_r}}(\Psi)\frac{\partial \Psi}{\partial r}) + \frac{\partial}{\partial z}\,(\underline{\underline{K_z}}(\Psi)\frac{\partial \Psi}{\partial z}) + \frac{\partial K}{\partial z} = 0 \qquad (2.9)$$

This equation is non-linear because hydraulic conductivity is a function of the dependent variable, Ψ . This equation is further complicated by the fact that hydraulic conductivity - pressure head relationships vary with direction. No known analytical solutions exist for Richard's equation in this form.

The only analytical methods presently available for solving flow problems in homogeneous, anisotropic conditions are to first solve the flow equation for homogeneous, isotropic conditions and then scale the coordinate system to account for anisotropy. Richard's equation for axisymmetrical steady flow through a homogeneous, isotropic unsaturated soil is written in the following form

$$\frac{1}{r}\frac{\partial}{\partial r} r\,(K(\psi)\frac{\partial \psi}{\partial r}) + \frac{\partial}{\partial z}(K(\psi)\frac{\partial \psi}{\partial z}) + \frac{\partial K}{\partial z} = 0 \qquad (2.10)$$

Raats (1971) used a linearized form of this equation,

$$\frac{\partial^2 \Phi}{\partial r^2} + \frac{1}{r}\frac{\partial \phi}{\partial r} + \frac{\partial^2 \phi}{\partial z^2} - \frac{\partial K}{\partial z} = 0 \qquad (2.11)$$

where

$$\phi = \int_{\psi_0}^{\psi} K(\psi)\,d\psi \qquad (2.12)$$

to produce an analytical solution for axisymmetrical flow from a point source located at the soil surface.

$$\Phi_{R,Z} = \frac{2}{\rho}\exp(Z-\rho) - 2\exp(2Z)\,E_1(Z+\rho) \qquad (2.13)$$

In this equation, $\Phi = 8\pi\phi/\alpha q$, $R = \alpha r/2$, $Z = \alpha z/2$, $\rho = \sqrt{R^2 + Z^2}$ q is the flow rate at the source (in ml/sec), E_1 is the

index (in cm^{-1}) determined by the relationship

$$K(\psi) = K_s \exp(\alpha\psi) \qquad (2.14)$$

where K_s is the saturated hydraulic conductivity of the soil.

McKee and others (1984) presented a method of scaling the coordinate system of the linearized flow equation (in three dimensions) in order to account for anisotropy.

$$x^T = x\sqrt{\frac{K_y}{K_x}}$$

$$y^T = y\sqrt{\frac{K_x}{K_y}}$$

$$z^T = z\frac{\sqrt{K_x \cdot K_y}}{K_z} \qquad (2.15)$$

$$\alpha^T = \alpha\frac{K_z}{\sqrt{K_x \cdot K_y}}$$

The values x^T, y^T and z^T are distances along the transformed coordinate axes and α^T is the scaled value of the pore size distribution index.

Assuming that $K_x = K_y = K_r$, then equation 2.1 simplifies to

$$r^T = r \frac{K_r}{K_z}$$
$$z^T = z \qquad (2.16)$$
$$\alpha^T = \alpha$$

which may be aplied to Raats (1971) analytical solution This transformation assumes a constant anisotropy

Use of the analytical solution in combination with th coordinate transformation, which assumes a fixed anisotropy contradicts the purpose of of the present study which is t establish a relationship between anisotropy and pressur head. However, it provides the researcher with a limite ability to predict the total head and pressure head profile within a small range of pressure head values where change in anisotropy may be limited. It also provides a means c comparing the observed pressure head and total head profile with profiles predicted under the assumption of a constar anisotropy. This then would allow one to observe th effects of a changing anisotropy on the pressure head ar total head profiles.

Chapter 3

DESIGN AND EXECUTION THE EXPERIMENT

The design of the experiment may be summarized as follows: a soil consisting of alternating layers of two homogeneous isotropic soils, each of equal thickness, but each having unique hydraulic properties was infiltrated from a point source located at the surface. The soils were enclosed in a tank constructed of steel and transparent plastic sheet designed to accommodate axisymmetrical flow. The wetting front behavior was observed and recorded with photographs. Tensiometers were used to map gradients and dyes were used to map streamlines. A total of three experiments were conducted, each at different flow rates and each involving infiltration into an air-dry soil.

This chapter provides a detailed description of the design of the experiment and the procedures followed in the execution of the experiment. This discussion is subdivided into eleven topics: 1) the design of the tank, 2) the hydraulic characteristics of the soils and how they were determined, 3) the number of layers and their thickness, 4) the design of the tensiometers, 5) the use of the dye, 6) the locations of tensiometer and dye ports, 7) the method of filling the tank, 8) the design of the point source, 9) the methods used in photographing the experiments, 10) the actual procedures followed in the execution of the

experiments, and 11) the use of a steady-state analytical solution to predict the total head distribution for each of the experiments.

3.1 Design of the Sand Tank.

A large tank was constructed in the shape of a triangular prism (Figure 3.1). It was constructed of 0.63 cm (1/4 in.) steel plating and 1.27 cm (1/2 in.) polycarbonate sheet and was held together by a frame constructed of 2.5 cm (1 in.) angle iron. Polycarbonate was used in the construction because it does not easily crack, as does acrylic sheet, and could therefore be drilled into without concern of cracking. Polycarbonate was used on two sides so that one could check for radial symmetry.

The angle between the vertical faces of the tank is 30 degrees. This angle allows the shape of the tank to represent 1/12th of a cylinder and could therefore accomodate a cylindrical or axisymmetrical coordinate system with an origin located in the upper corner bounded by the 30 degree angle. The large size of the tank, $0 \text{ cm} \leq z \leq 150 \text{ cm}$ and $0 \text{ cm} \leq r \leq 175 \text{ cm}$, where r and z are distances in the radial and vertical directions, respectively, allowed steay-state conditions to be reached behind the wetting front.

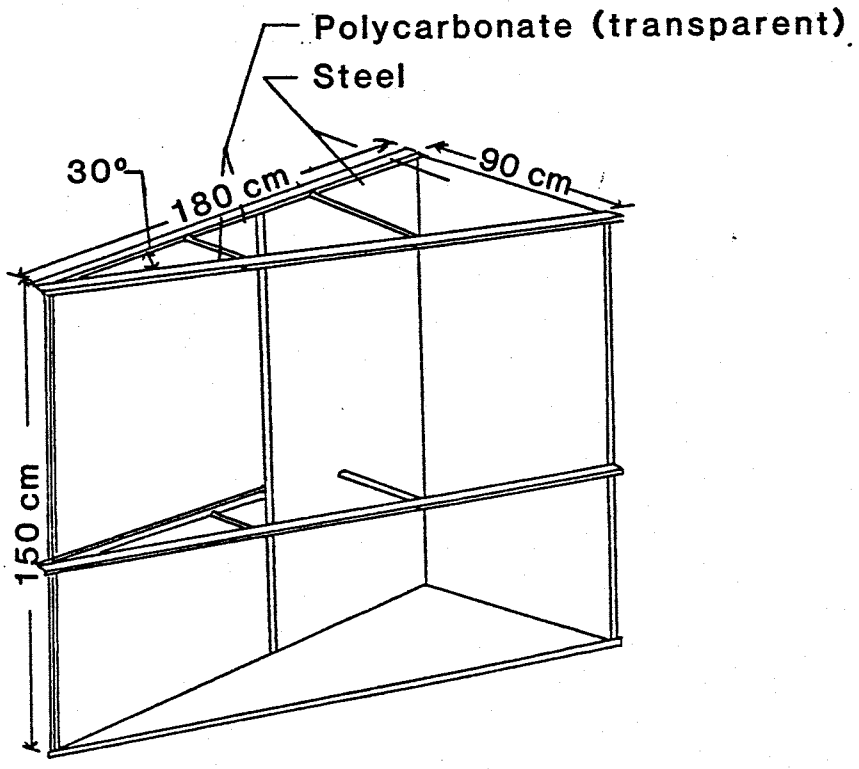

Figure 3.1 Isometric drawing of the sand tank.

3.2 Selection and Testing of the Soils

Four criteria were used in the selection of the two soils: 1) Sand should be used in preference to finer grained materials. It is much easier to work with and, according to Yeh (1985), displays a greater contrast in anisotropy at different moisture levels than do silts or clays. 2) The textures of the soils should not be so different that one material falls into another. A clay placed on top of a sand would readily mix with the sand and unique layers would not be maintained. 3) There should be a large contrast in the hydraulic properties of the materials. Saturated hydraulic conductivities should be at least one order of magnitude apart. Unsaturated hydraulic conductivities should diverge with increasing soil dryness. 4) Finally, the soil should be cost-effective and obtaining it should be time-effective. Over two tons of soil were needed and it would not have been time-effective to hand seive desired fractions from a poorly sorted soil.

The soils selected for the experiment included a dune sand from the Sevilleta Wildlife Refuge located 20 miles north of Socorro, N.M. and a commercially produced sand sold for the purpose of sand blasting. These are informally designated as the Sevilleta dune sand and the medium blasting sand.

The Sevilleta dune sand is a well-sorted fine to medium grained quartz sand. It was obtained without cost and required no further seiving. The medium blasting sand is a pre-seived coarse to very coarse, well sorted quartz sand purchased at a reasonable cost. It was sold as a sand passing through a No. 16 sieve but retained by a No. 30 sieve. Due to the nature of commercial scale processing, this sand contained many particles smaller than what should have passed through the No. 30 seive. These fine-grained particles were removed by hand sieving.

3.2.1 Sieve Analyses

Cummulative-frequency curves for the Sevilleta dune sand and the medium blasting sand are shown in Figure 3.2. By U.S.D.A. soil classification standards, they categorize as a fine to medium grained sand and a coarse to very coarse sand for the Sevilleta dune sand and the medium blasting sand, respectively. Their d_{10} and d_{60} grain sizes and uniformity coefficients are shown in Table 3.1.

Table 3.1. d_{10}, d_{60} grain sizes and uniformity coefficients (C_u) for the Sevilleta dune sand and the medium blasting sand.

	d_{10}(mm)	d_{60}(mm)	C_u
Sevilleta dune sand	0.175	0.305	2.4
Medium blasting sand	0.480	0.830	1.7

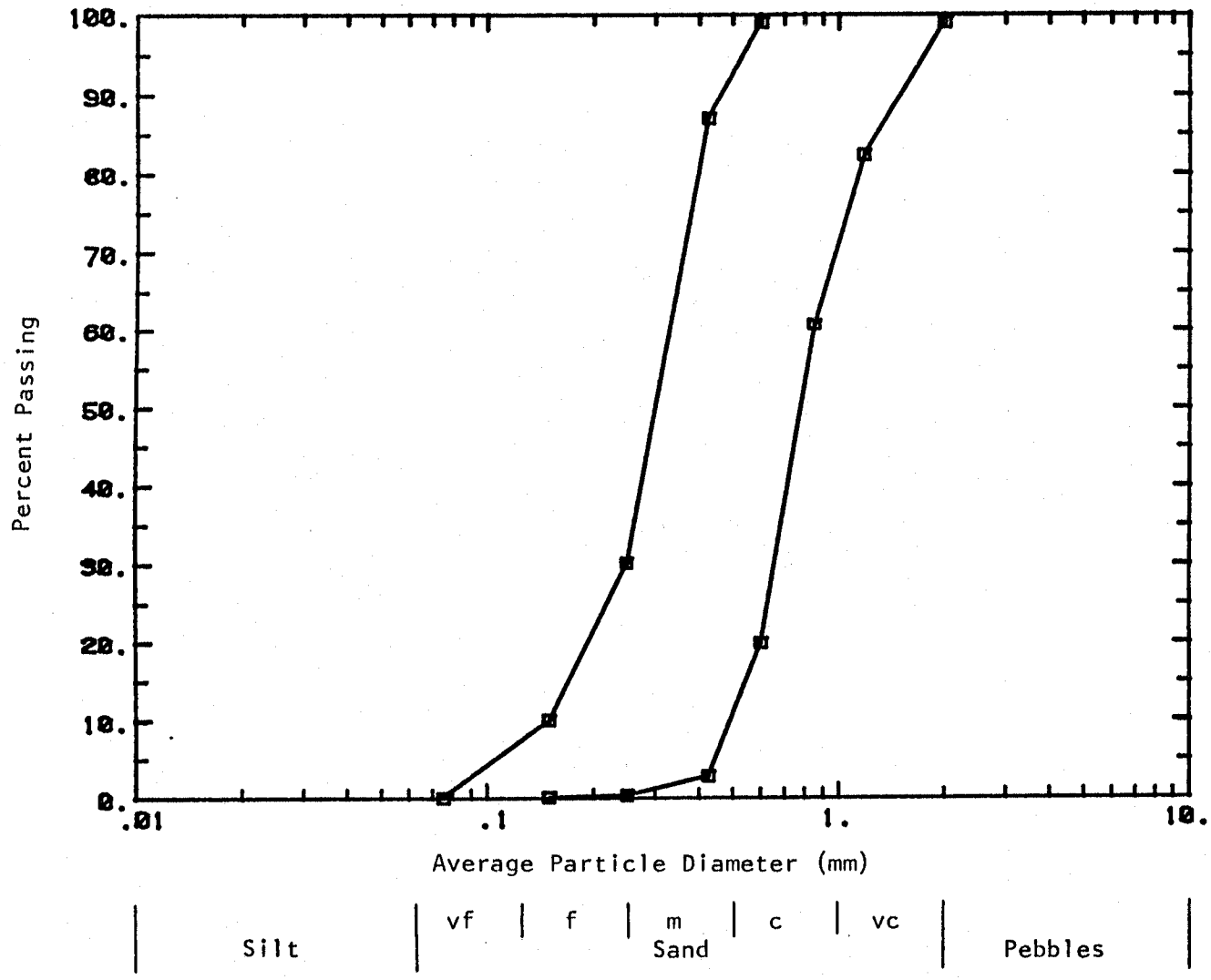

Figure 3.2 Cumulative-frequency curves for the Sevilleta dune sand and the medium blasting sand in relation to the U.S.D.A. soil classification system.

3.2.2 Porosity

The porosity, n, was determined from the relationship

$$n = 1 - \rho_b / \rho_m \qquad (3.1)$$

where ρ_b is the dry bulk density (g/cm^3) and ρ_m is the particle density (g/cm^3). The sand was essentially pure quartz so that $\rho_m = 2.65\ g/cm^3$. Ten values of bulk density and porosity were obtained for each sample. In determining these values, the sands were packed by passing them through 3 screens, as was done when the tank was filled. (This packing procedure is explained further ahead in this chapter in the section on filling the sand tank.) The values of dry bulk density and porosity are given in Table 3.2. The mean values of porosity are 0.363 for the Sevilleta dune sand and 0.358 for the medium blasting sand.

3.2.3 Soil Moisture Characteristic Curve

Moisture content - pressure head relationships were obtained by the hanging column method introduced by Bouma (1974). The relationships obtained are shown in Figure 3.3. The air entry values are -10 cm-H_2O and -7 cm-H_2O for the wetting curves of the Sevilleta dune sand and medium blasting sand, respectively. The residual moisture content for the range of 0 to -200 cm-H_2O is 0.07 cm^3/cm^3 for the Sevilleta dune sand and 0.04 cm^3/cm^3 for the medium blasting sand.

Table 3.2 Values of dry bulk density (ρ_b) and porosity (n) for the Sevilleta dune sand and the medium blasting sand. Values were determined from 100 cm^3 repacked samples used in various soil characteristics tests.

	Sevilleta dune sand		medium blasting sand	
	ρ_b (—)	n (—)	ρ_b (—)	n (—)
	1.71	0.355	1.71	0.355
	1.71	0.355	1.76	0.336
	1.75	0.340	1.80	0.321
	1.71	0.355	1.58	0.404
	1.65	0.377	1.67	0.370
	1.74	0.343	1.68	0.360
	1.58	0.404	1.51	0.430
	1.77	0.332	1.57	0.408
	1.71	0.355	1.80	0.321
	1.76	0.336	1.61	0.392
	1.67	0.370	1.75	0.340
	1.63	0.385	1.74	0.343
Mean	1.70	0.358	1.68	0.365
Std.Dev.	0.06	0.022	0.10	0.036

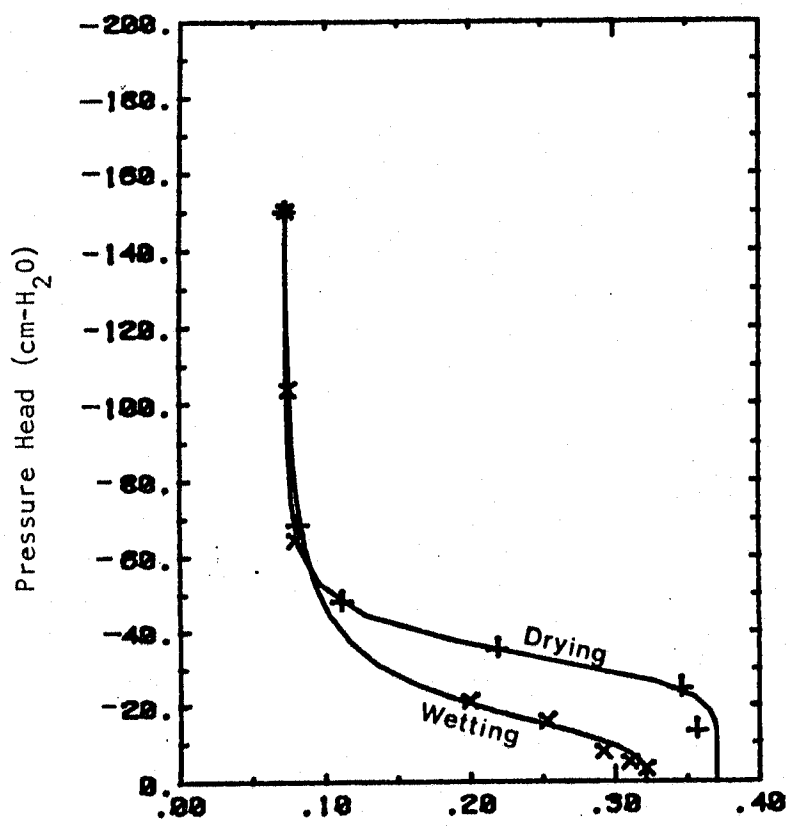
-200.
-160.
-160.
-140.
-120.
-100.
-80.
-60.
-40.
-20.
0.
.00
.10
.20
.30
.40
Drying
Wetting
Pressure Head (cm-H2O)
Volumetric Moisture Content
(cm3/cm3)

(a)

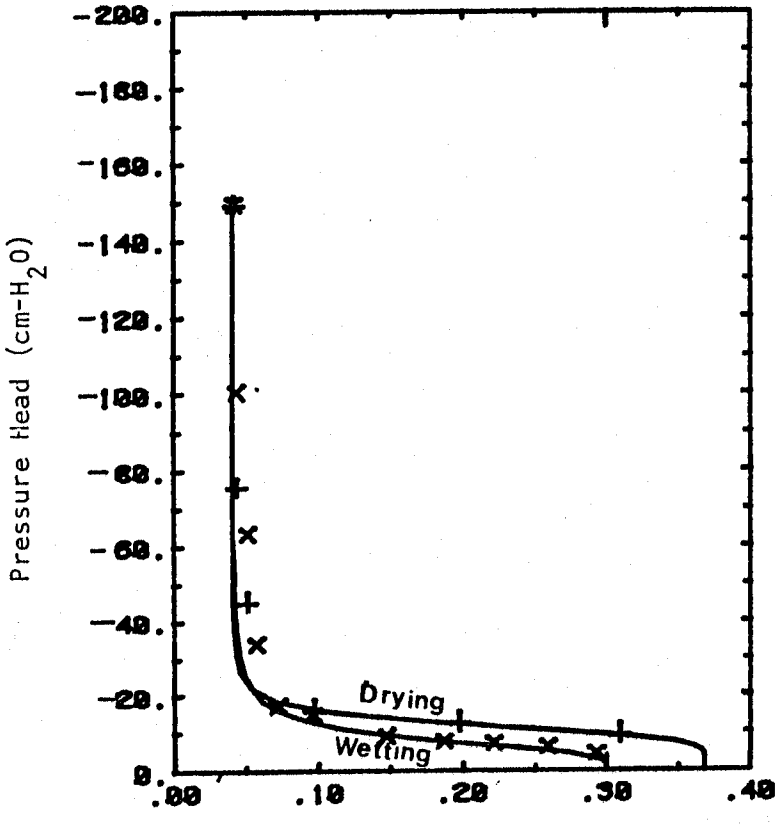
-200.
-160.
-160.
-140.
-120.
-100.
-80.
-60.
-40.
-20.
0.
.00
.10
.20
.30
.40
Drying
Wetting
Pressure Head (cm-H2O)
Volumetric Moisture Content
(cm3/cm3)

(b)

relationship

$$c(\psi) = d\theta / d\psi \qquad (3.2)$$

was computed as a function of pressure head from the wetting cycles of the soil moisture characteristic curves (Figure 3.4). The maximum value of the specific moisture capacity is nearly one order of magnitude greater for the medium blasting sand than for the Sevilleta dune sand. This peak in the medium blasting sand also occurs at a higher pressure indicating that the moisture content of the medium blasting sand changes over a higher and much narrower pressure range than the moisture content of the Sevilleta dune sand.

3.2.4 Hydraulic Conductivity

Saturated hydraulic conductivities were determined using a constant-head permeameter. For each soil, three 100 cm^3 samples were analyzed. The results are shown in Table 3.3.

Table 3.3. Saturated hydraulic conductivities for the Sevilleta dune sand and the medium blasting sand as determined by constant-head permeameter tests.

Soil type	K_{20^oC} (cm/s)	Avg. K_{20^oC} (cm/s)
Sevilleta dune sand	0.035 0.047 0.013	0.032
Medium blasting sand	0.233 0.143 0.236	0.201

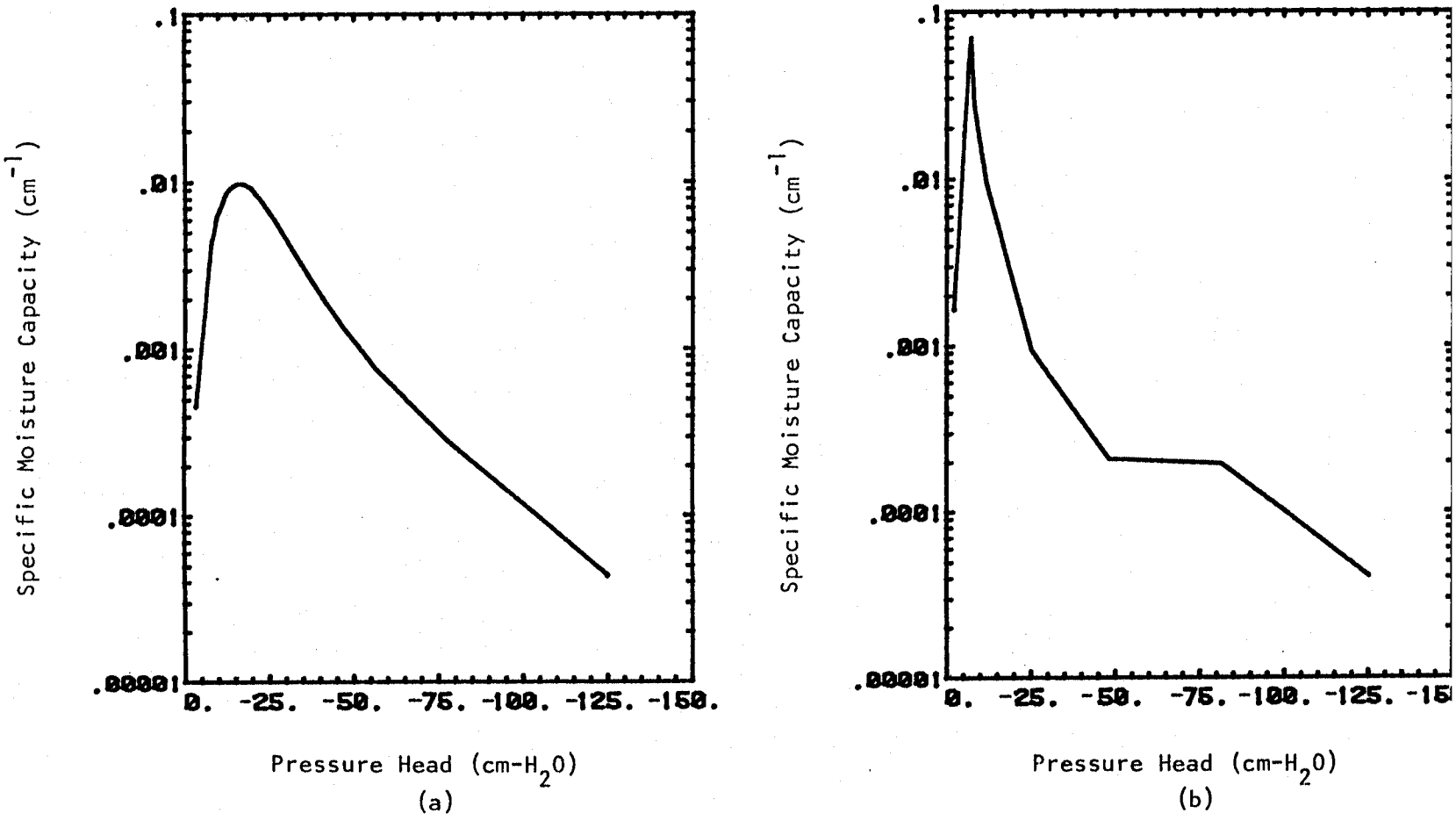

Figure 3.4 Specific moisture capacity versus pressure head for the wetting curves of (a) the Sevilleta dune sand and (b) the medium blasting sand.

Unsaturated hydraulic conductivities were determined using the method of Bruce and Klute (1956). In this method, soil diffusivity was determined through analyses of horizontal infiltration tests performed on repacked samples in the laboratory. The apparatus used in these experiments is shown in Figure 3.5. A detailed procedure is given in Appendix 1. Water was introduced into the column at a constant head of 0 cm-H_2O. After a specified time, usually 60 to 180 seconds, the column was quickly removed from the source. The soil in the column was then separated into 1 cm sections and volumetric moisture contents were determined for each section.

From these tests, profiles of volumetric moisture content versus the Boltzman variable, λ , were constructed (Figure 3.6). The Boltzman variable is defined by the equation

$$\lambda = xt^{-1/2} \qquad (3.3)$$

where x is the distance along the column and t is the time specified for imbibition. Use of the Boltzman variable allows several tests of different imbibition times to be overlain for each soil. Two horizontal infiltration experiments for two different lengths of time were conducted for each soil.

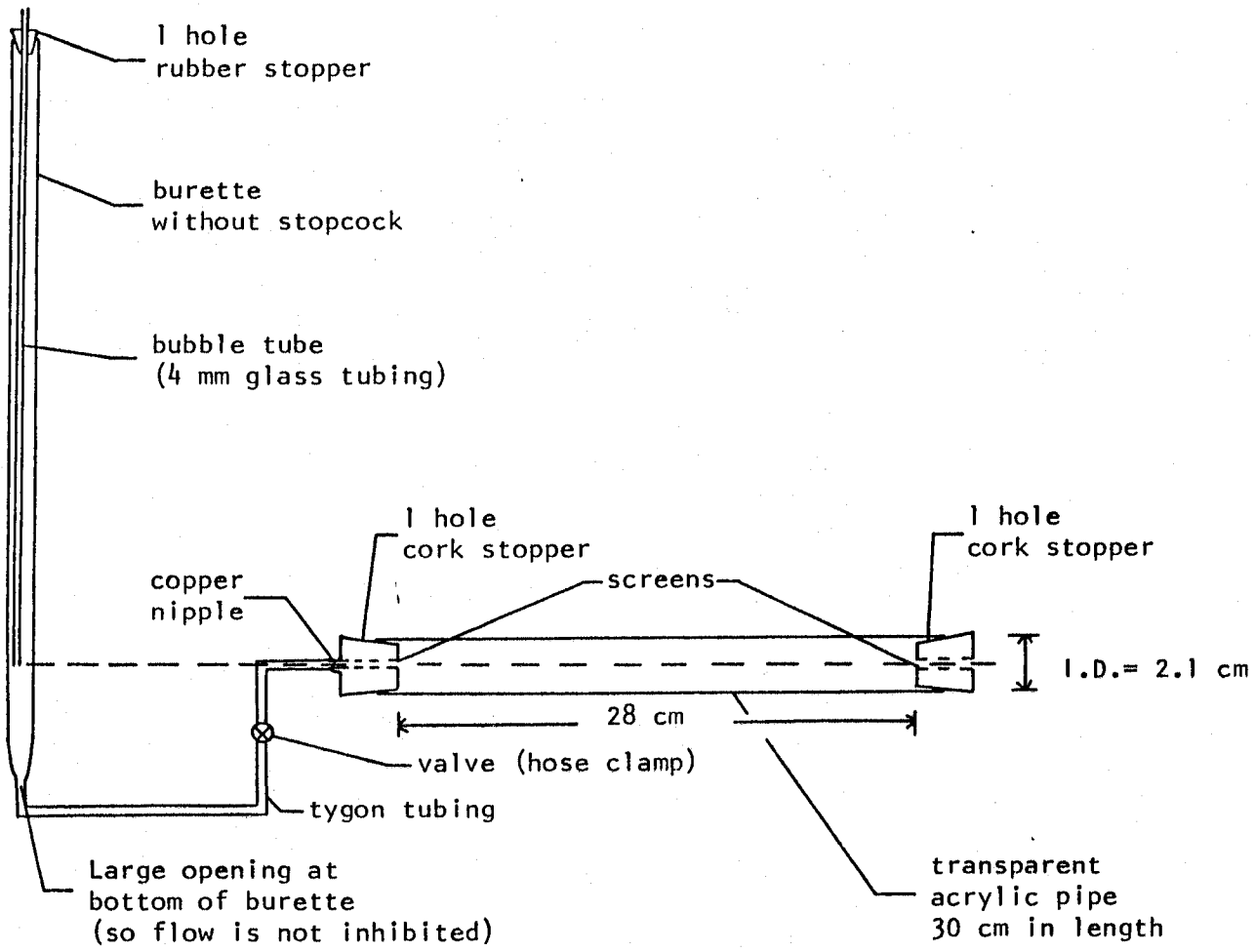

Figure 3.5 Apparatus used to determine soil diffusivity.

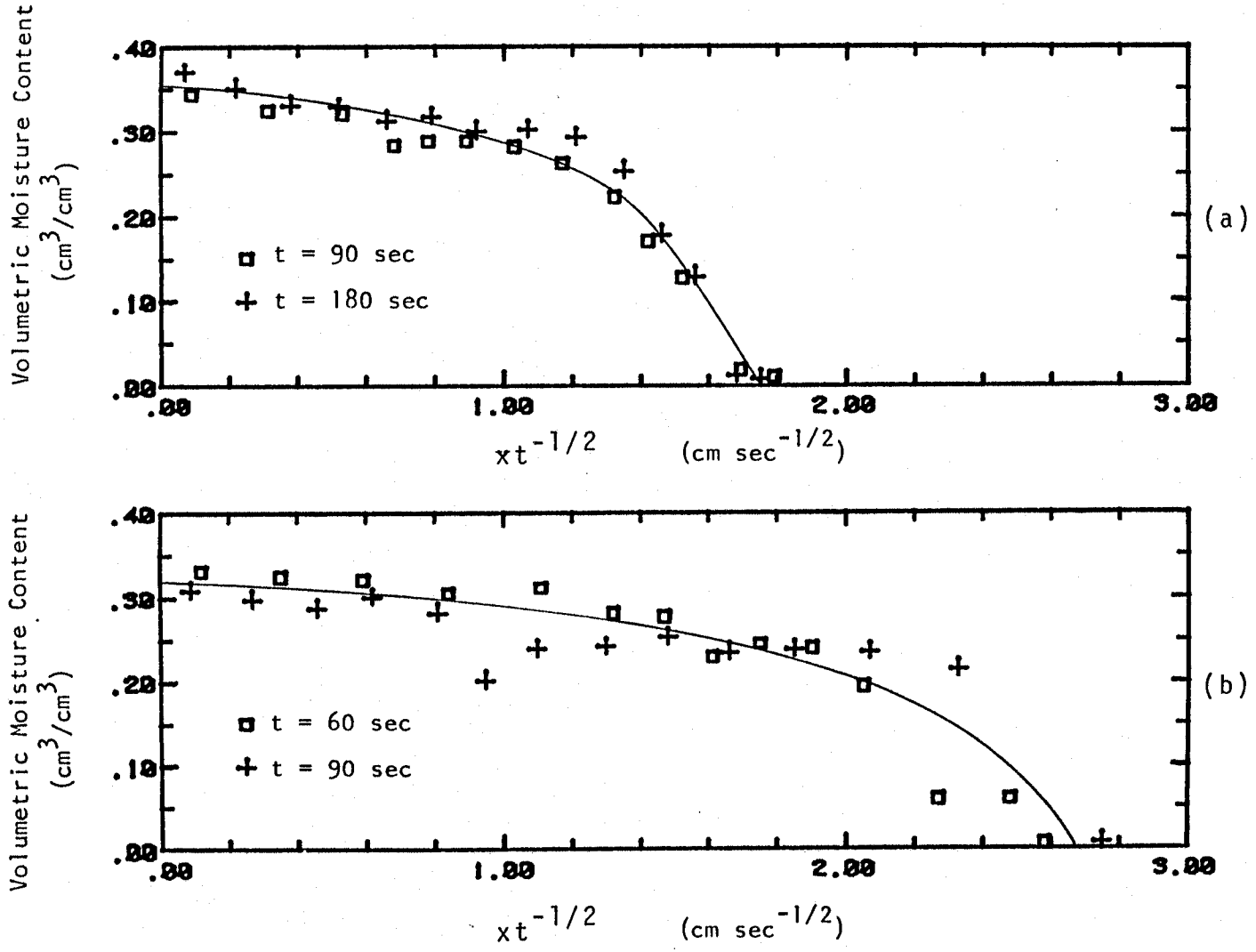
Volumetric Moisture Content
(cm3/cm3)
.40
.30
.20
.10
.00
t = 90 sec
t = 180 sec
1.00
2.00
3.00
xt-1/2 (cm sec-1/2)
(a)
Volumetric Moisture Content
(cm3/cm3)
.40
.30
.20
.10
.00
t = 60 sec
t = 90 sec
1.00
2.00
3.00
xt-1/2 (cm sec-1/2)
(b)

A hand-drawn curve was fit through the data as shown in Figure 3.6 Values of for each value of moisture content were obtained from this curve and used to compute soil diffusivity using the equation given by Bruce and Klute (1956):

$$D(\theta) = -\frac{1}{2}\frac{d\lambda}{d\theta}\int_{\theta_i}^{\theta} \lambda \, d\theta \qquad (3.4)$$

where $D(\theta)$ is the soil diffusivity at volumetric moisture-content θ . This equation was solved numerically using the fortran program DFSVTY listed in Appendix 1. Diffusivity versus moisture content for the Sevilleta dune sand and the medium blasting sand is plotted in Figure 3.7. The Sevilleta dune sand has a greater soil diffusivity between moisture contents of 0 and 0.20 cm^3/cm^3. At moisture contents greater than 0.20 cm^3/cm^3 the medium blasting sand exhibits a greater soil diffusivity.

Unsaturated hydraulic conductivity can be determined by the equation

$$K(\theta, \psi) = D(\theta)\ C(\theta, \psi) \qquad (3.5)$$

where $K(\theta,\psi)$ is the hydraulic conductivity as a function of moisture content (θ), or pressure head (ψ) and $C(\theta, \psi)$ is the specific moisture capacity from Figure 3.4.

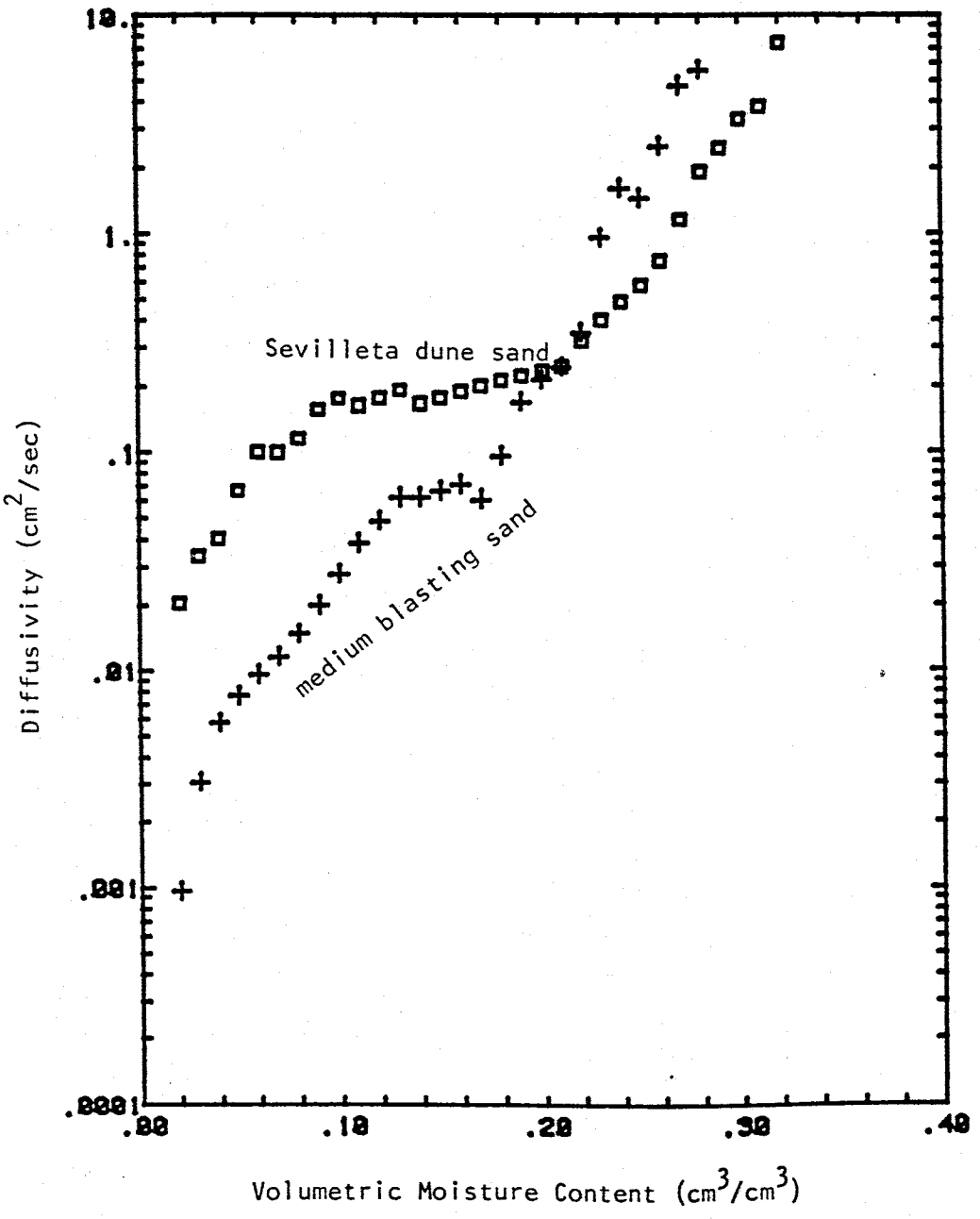

Figure 3.7 Soil diffusivity versus moisture content for the Sevilleta dune sand and the medium blasting sand as determined by the method of Bruce and Klute (1956).

Hydraulic conductivity is plotted as a function of pressure head in Figure 3.8 for the wetting cycle of the Sevilleta dune sand and the medium blasting sand. Saturated hydraulic conductivities determined by this method are similar to those determined using the constant-head permeameter method. A value of 0.019 cm/s for the Sevilleta dune sand was found using this method, whereas a mean value of 0.032 cm/s was determined using the constant-head permeameter. For the medium blasting sand, a value of 0.23 cm/s was determined using the method of Bruce and Klute. This is slightly greater than the mean of 0.20 cm/s determined using the constant-head permeameter. As the pressure head decreases less than -7 cm-H_2O, the hydraulic conductivities converge becoming equal at -9.5 cm-H_2O. At pressure heads below -9.5 cm-H_2O, the hydraulic conductivities diverge. Below -25 cm-H_2O pressure head, however, the hydraulic conductivities of the two soils begin to converge.

If the arithmetic and harmonic means of the hydraulic conductivities (K_a and K_h, respectively) are determined for different values of pressure head, two additional hydraulic conductivity - pressure head curves are obtained. These curves K_a-ψ and K_h-ψ represent the directional hydraulic conductivity - pressure head relationships found parallel and normal to the layers, respectively. These two curves, along with the K-ψ curves for the Sevilleta dune sand (K_{sd}) and the medium blasting sand (K_{bs}) are plotted in Figure

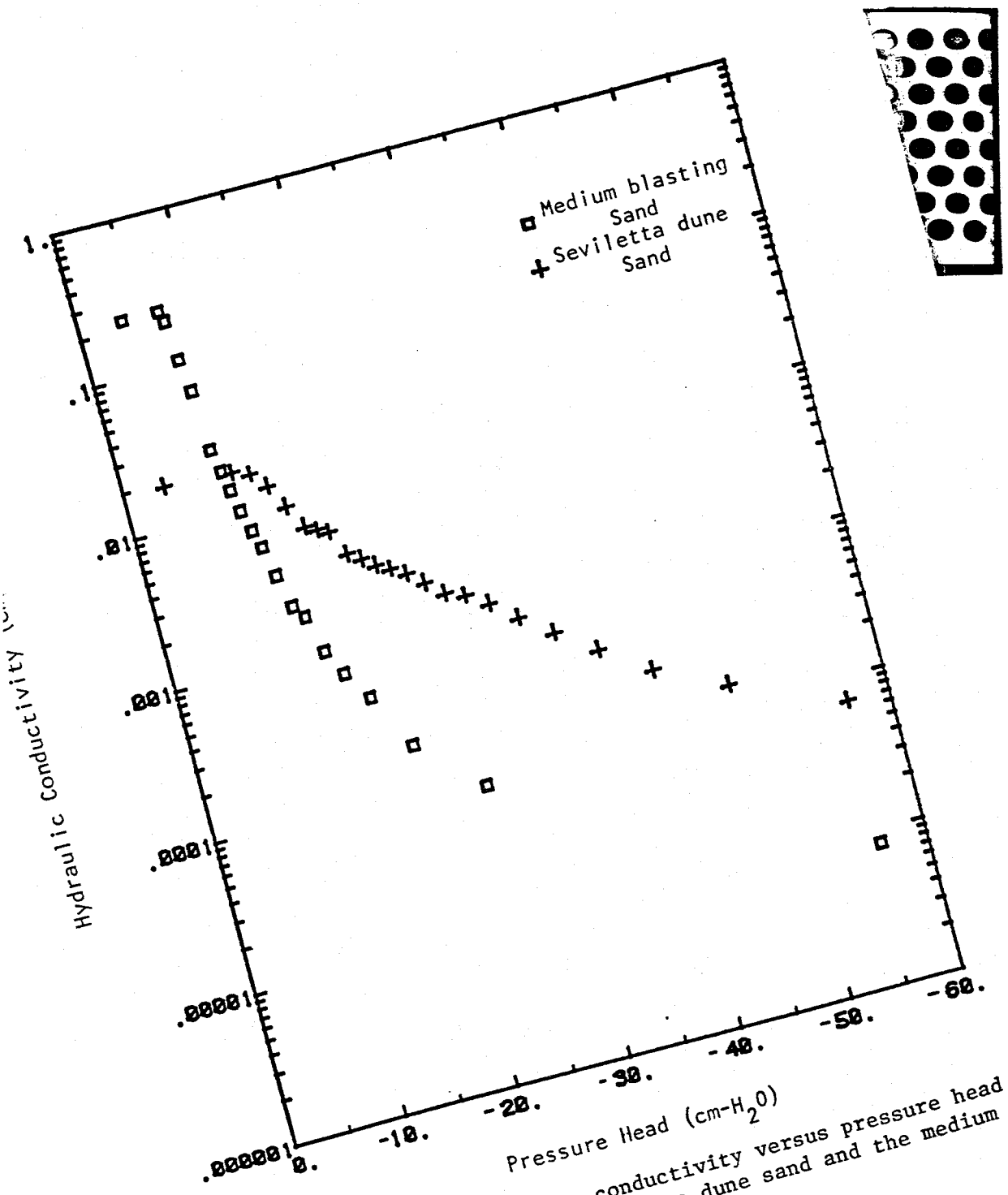

Figure 3.8 Hydraulic conductivity versus pressure head for the Sevilleta dune sand and the medium ...ing sand.

3.9.

Anisotropy was computed as a function of pressure head by dividing the arithmetic mean of the hydraulic conductivities of the two soils by the harmonic mean of these hydraulic conductivities for different values of pressure head (Figure 3.10). As pressure head decreases from 0 to -9.5 cm-H_2O, anisotropy decreases from a value of 3.5 to 1.0, where it becomes nonexistant. Anisotropy increases to a value of 6 as pressure head decreases from -9.5 cm-H_2O to -25 cm-H_2O. It then decreases at lower pressures, reflecting the convergence of the hydraulic conductivities of the soils.

Also plotted in Figure 3.10 is the ratio of hydraulic conductivities of the two soils as a function of pressure head. For pressure heads greater than -9.5 cm-H_2O, this ratio is plotted as the hydraulic conductivity of the medium blasting sand (K_{mb}) divided by the hydraulic conductivity of the Sevilleta dune sand (K_{sd}) in as much as the blasting sand has a greater hydraulic conductivity than the Sevilleta dune sand. For pressure heads less than -9.5 cm-H_2O the ratio is plotted as K_{sd}/K_{mb}.

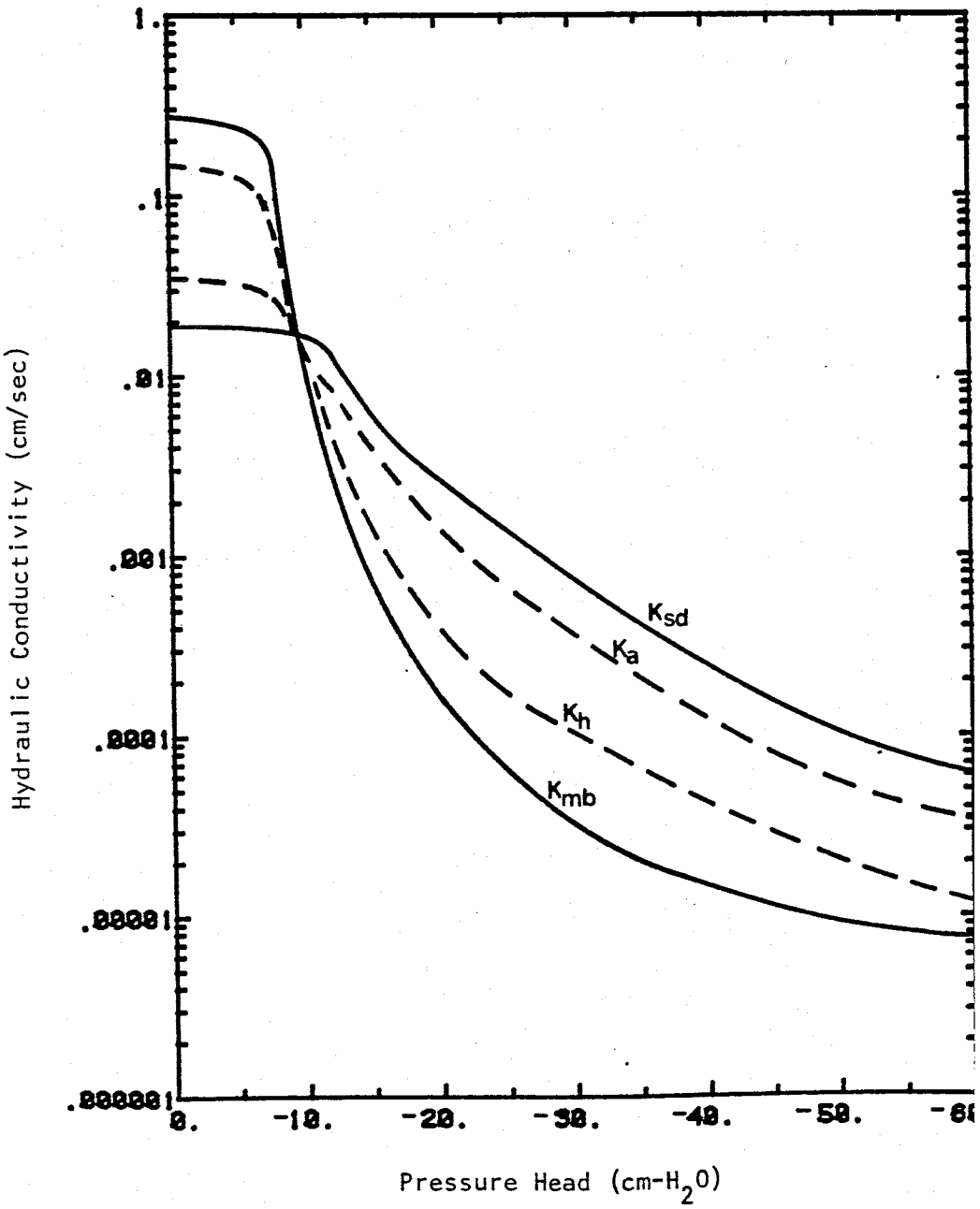

Figure 3.9 Hydraulic conductivity versus pressure hea for the Sevilleta dune sand (K_{sd}), the med blasting sand (K_{mb}), and for the arithmeti (K_a) and harmonic (K_h) means of the hydrau conductivities of the two soils.

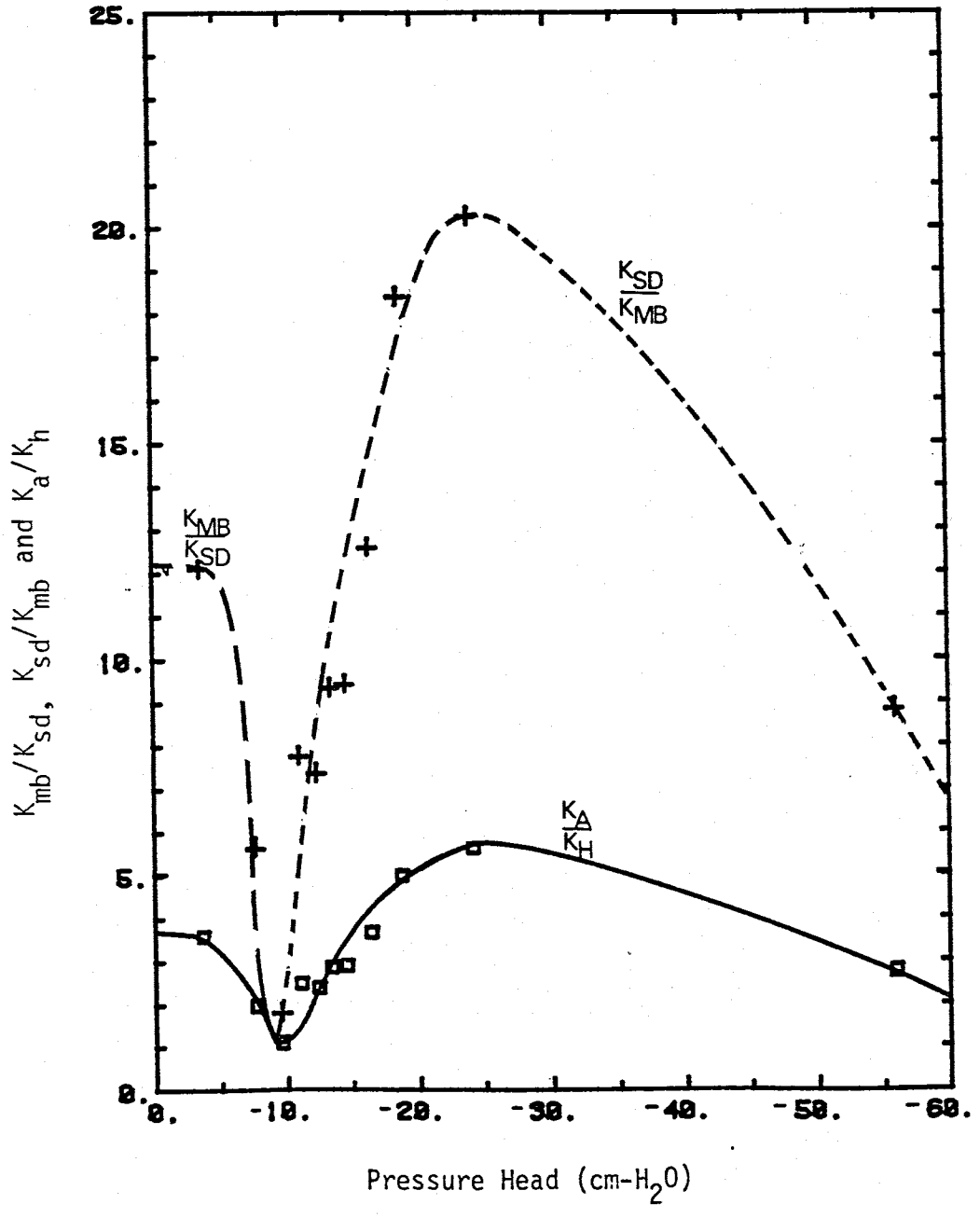

Figure 3.10 K_a/K_h and the ratios K_{mb}/K_{sd} and K_{sd}/K_{mb} determined from hydraulic conductivity-pressure head relationships.

3.3 Thickness and Number of Layers

The thickness of each layer was set at 2 cm. The choice of this thickness was based on two criteria. First, the layers should be as thin as possible. In order for a layered soil to be equivalent in behavior to an anisotropic system the thickness of the individual layers must be thin with respect to the flow domain (Bear 1972, pg. 157). Second, the layers should not be so thin that their individual hydraulic properties are not maintained. There is always some zone between the layers where the soils mix. If the layers are thick with respect to these transition zones, the layers are better represented by the previously determined hydraulic properties. Conversely, if the layers are thin with respect to the transition zones, then the transition zones would become an accountable third layer.

The number of layers was set at 50, making the total stratified thickness 100 cm. The design of the tank would have accomodated 75 layers, but it was felt that this was not necessary, since the wetting front would advance parallel to the stratification much faster than it would advance perpendicular to the stratification. A base layer 50 cm thick consisting of Sevilleta dune sand elevated the experiment so that it could be conducted in the top 2/3 of the tank.

3.4 Tensiometer Design

The design of the tensiometer used in the experiment is shown in Figure 3.11. Pressures were recordeed in two different ways. An aqueous manometer measured pressure heads near the source where pressure heads were greater than -25 cm-H_2O and a pressure transducer measured pressure heads far from the source where the pressure heads were less than about -25 cm-H_2O. The tensiometer was designed so that it could be read either with a manometer or a pressure transducer.

The advantage of the aqueous manometer is that it is extremely accurate. Values of pressure head can be read with a precision of $\pm$ 0.1 cm-H_2O. It also allows one to constantly monitor the pressures in the soil. The disadvantage of this type of tensiometer is that it is very slow to respond to pressure changes, especially in a dry soil. Because it is an aqueous manometer, large volumes of water must be transfered to or from the manometer through the tensiometer cup. This water must also be transferred to or away from the tensiometer cup through the soil. If the sand is at a moisture content well below saturation, it will have a very low hydraulic conductivity. As a result, water in this sand will travel very slowly away from or towards the tensiometer cup. In this experiment, pressure head profiles were of concern only for steady-state conditions [illegible] As

long as the pressure head in the soil was greater than 25 cm-H_2O, aqueous manometers were found to be an adequate method of measuring soil pressures.

The tensiometer used in conjunction with an aqueous manometer was filled as follows. The end of the manometer tubing that was not attached to the tensiometer was placed in a beaker of distilled, de-aired water. (The water was de-aired by bubbling helium through it for 15 minutes.) A syringe needle, attached by tygon tubing to a suction pump, was inserted into the tensiometer through the syringe stopper and between the manometer tubing and the glass wall of the tensiometer. Water was pulled in as air was removed through the syringe needle. In doing this, it was important that the manometer tubing inside the tensiometer extend all the way to the porous cup so that all of the air in the tensiometer would be flushed out. Before filling the tensiometer, a copper sulfate solution provided by the Soil Moisture Corporation was added to the distilled water at a concentration of 20 drops per liter of water as recommended by the manufacturers rers. This solution served to prevent algal growth in the tensiometer and to dye the water so that the air-water interface would be clearly visible in the manometer tubes.

The manometer tubes consisted of nylon tubing. Nylon was used because it does not admit air under high suctions as does vinyl. As shown in Figure 3.11, two sizes of tubing

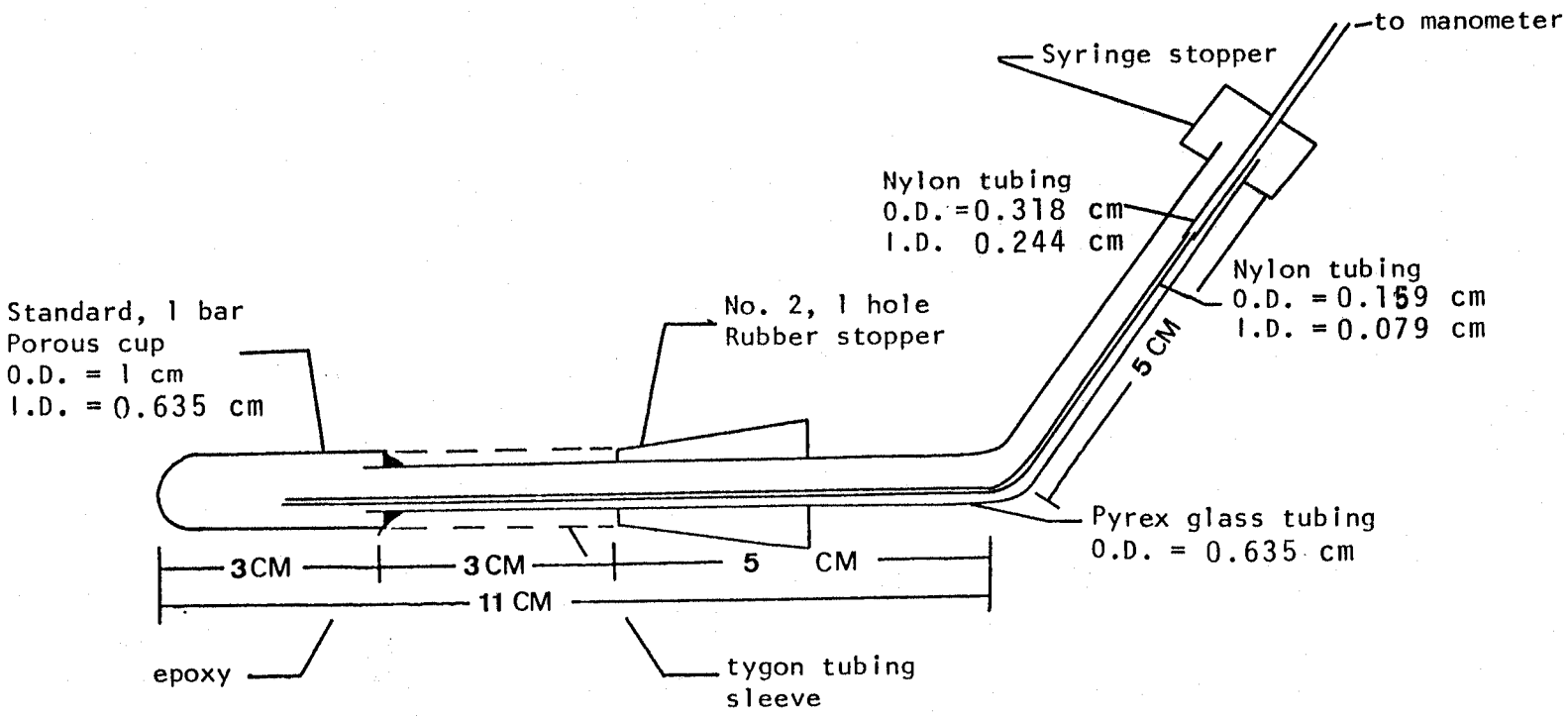

Figure 3.11 Design of the tensiometers.

were used. The large size was used outside the tensiometer because: 1) large quantities were needed and it was available at reasonable cost, and 2) its use did not result in capillary effects. Inside the tensiometer, the small diameter tubing was used because its size allowed enough space between the tubing and the glass so that air would not be entrapped between the nylon tubing and the glass. The two sizes of tubing fit tightly together without cement and were joined inside the tensiometers so that the leakage of air into the tubing would not be a problem. A manometer board was constructed so that pressure head in cm-H_2O could be read from the air-water interface as shown in Figure 3.12.

A pressure transducer was used to measure pressure in the tensiometers placed where the soil was at a pressure head less than approximately -25 cm-H_2O and at distances far enough from the source that the precision provided by the water manometer was not needed. The pressure transducer was part of a unit called the Tensimeter, distributed by Soil Measurement Systems of Las Cruces, New Mexico. The pressure transducer was connected to a syringe needle and to a digital display unit that displayed pressures in millibars.

The tensiometers were filled until there was approximately a 1 cm long air space at the end containing the syringe stopper. The transducer needle was inserted through the syringe stopper in order to measure the pressure

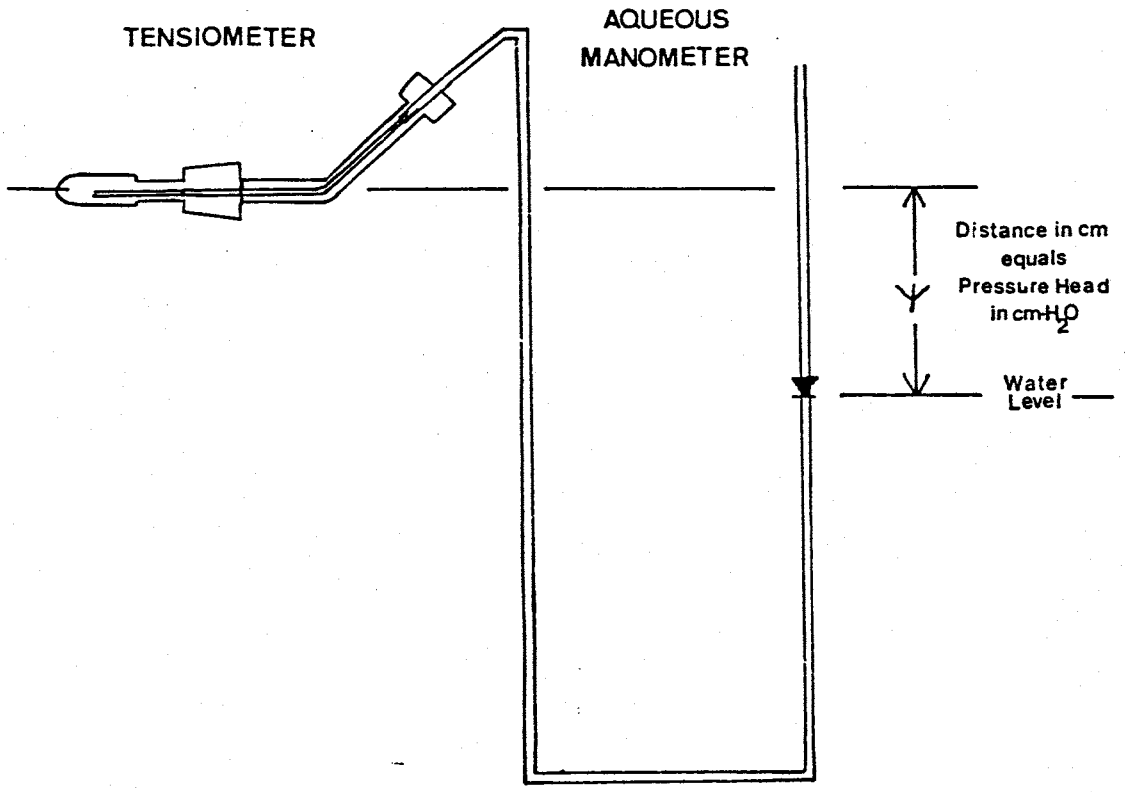

Figure 3.12 Method of determining the pressure head of the tensiometer using an aqueous manometer.

of the air space. The pressure head at the tensiometer cup was then the value measured (in cm-H_2O) minus the height of water between the air-water interface in the tensiometer and the porous cup (in cm). After reading the pressure in the tensiometer, the needle was removed and a thin layer of rubber adhesive was placed on top of the syringe stopper.

The tensiometers used in conjunction with a pressure transducer were filled in the following manner: the porous cups were immersed in a beaker filled with distilled de-aired water. A syringe needle, attached with tygon tubing to a vacuum pump, was inserted through the syringe stopper. Water was pulled into the tensiometer through the porous cup, displacing the air that was being removed through the syringe needle. The tensiometers were filled to within 1 cm of the top. The syringe stopper was coated with a thin film of rubber adhesive. Copper sulfate was not used in the water. It was not needed to dye the water and it was feared that it might clog the tensiometer cup during the filling process.

The soil was air-dry before each experiment. An air-dry soil has a pressure much less than the 1 bar air entry value of the tensiometer cup. Therefore, the tensiometer would not work in an air-dry soil and tensiometers had to be inserted after the wetting front had passed the position where the tensiometer was to be placed. A 1/4 in drill, rotated by hand, was used to core a 7 cm

hole into which the tensiometer was inserted.

3.5 Selection of the Dyes

Upon recommendation by John Helier, of the Petroleum Recovery Research Center located on campus, potassium permanganate was used as a dye in the experiment. It was purchased as a powder and was dissolved in water to a concentration of 50 mg/L. It was injected with a syringe needle into the soil through syringe stoppers located on the side of the tank. The dye was not conservative, but it was not necessary for it to be so, because it was used only to map pathlines and was not used to study solute transport.

3.6 Locations of Tensiometer and Dye Ports

The positions in which the tensiometers and dye ports were placed are shown in Figure 3.13. The tensiometer array was based on tensiometer pairs set 40 cm apart in the direction parallel to layering and 20 cm apart in the direction normal to layering. Near the source, the tensiometer pairs were placed in a more dense array. The tensiometer pairs consisted of one tensiometer in each soil and were aligned diagonally with respect to layering in order to minimize the influence of one on another. Prior to packing, holes for the tensiometers were drilled into the polycarbonate sheet with a 1.27 cm (1/2 in.) drill bit. The

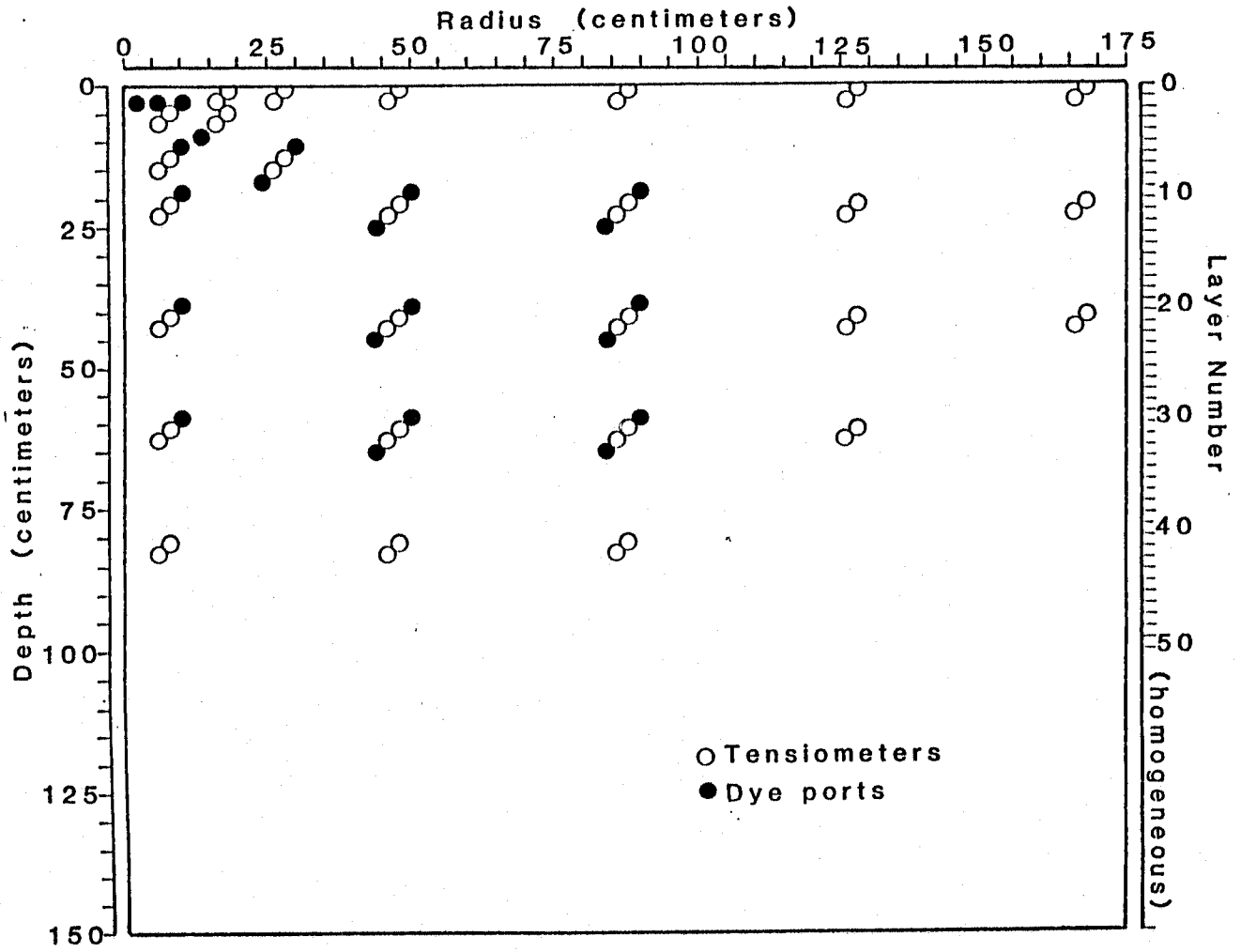

Figure 3.13 Locations of the tensiometers and dye ports.

positions of these holes were carefully surveyed, each hole being surveyed from two directions. The holes were expanded with a cone-shaped grinding wheel that melted the polycarbonate sheet and increased the diameter of the holes to 1.9 cm on the outside of the sheet. Number 2 rubber stoppers were cemented into these holes with rubber adhesive. Dye ports consisted of syringe stoppers placed into 1.27 cm (1/2 in.) holes drilled into the polycarbonate sheet. These were placed in diagonal lines with the tensiometer holes on both sides of the tensiometer pairs.

3.7 Filling the Sand Tank

The sand tank was packed following a method introduced by Wygal (1961). In this method, sand is passed through three screens situated 2 inches apart. The screens are coarse enough that the sand grains are not retained but fine enough that they are bounced around. As the grains bounce between the screens, grains of different sizes are mixed and fall at the same rate. This results in a much denser packing and minimizes stratification. If the tank is packed at a near maximum bulk density, then there is little chance of settling and the redistribution of grains during the experiment. The packer shown in Figure 3.14 is very similar to ones built by Wygal. It consists of three screens overlain by pegboard and enclosed by a wooden frame. It was computed, based on the cross-sectional area of the tank, and

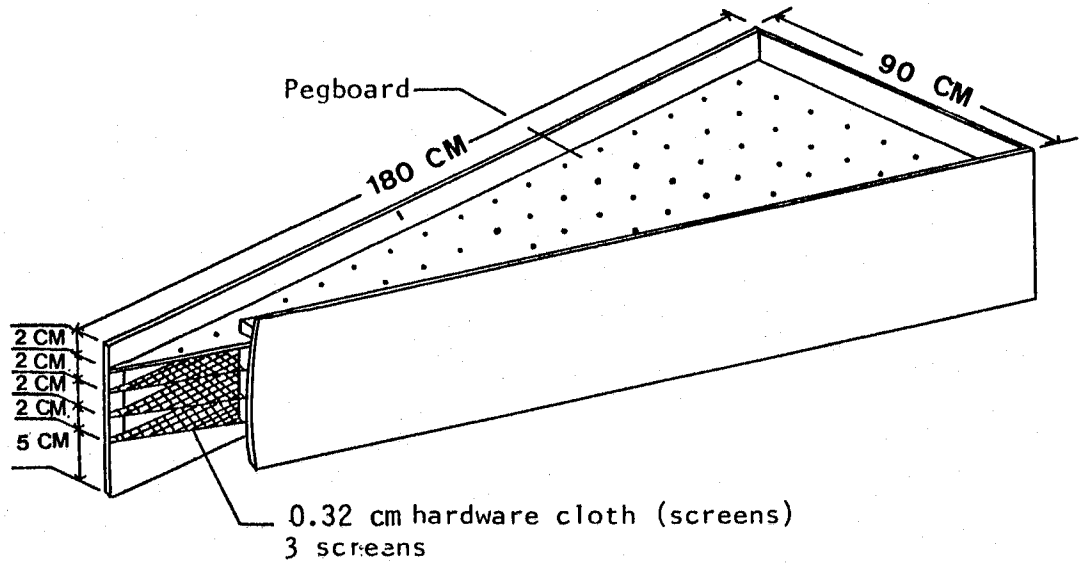

Figure 3.14 Isometric drawing of the packing device used to introduce sand to the tank.

the dry bulk density of the sand, that each 2 cm layer should weigh 30 kg. Both sands had the same bulk density and therefore, the mass of each layer should be equal. The 50 cm base provided ample opportunity to refine packing techniques. The refined method was composed of the following steps:

1. Place the packer on top of the tank.
2. With a grease pencil, draw a line around the box marking the position of the top of layer to be introduced.
3. Weigh 30 kg of the type of sand to be used for the layer.
4. Using a scoop, scatter approximately 2 kg of sand across the pegboard.
5. With smooth even hand motions, work the sand through the holes of the pegboard.
6. Repeat steps 4 and 5 until 25 kg of the sand are used up.
7. Remove the packing device from the box.
8. Using three coarse sieves (No. 10 and coarser) scatter the remaining 5 kg of sand in the low spots of the layer. Have an assistant on eye level with the top of the layer guide the placement of the sand.
9. Once the layer is nearly level, tamp lightly with a flat, metal tamper. Add additional sand as needed until the 30 kg of sand are used up or the layer is an even 2 cm thick. Do this under the guidance of an assistant.
10. Repeat steps 1 - 9 until all 50 layers are completed.

the tamper, however, caused some heterogeneities to occur as the fine grains separated from the coarse grainswithin each layer. Tamping, though, was found to be the only effective means of obtaining level layers of even thickness. By tamping lightly and by minimizing the tamping with the addition of sand to low areasof the surface, heterogeneities were minimized and generally limited to the top 1-2 mm of each layer. Preliminary trials indicated that raking the soil or smoothing it by hand resulted in very noticeable heterogeneities.

Due to outward pressures from the sand, the sides of the plastic sheet bulged in the middle. This increased the cross-sectional area of the tank slightly so that as much as 31.5 kg of sand were needed for several layers in the middle of the tank.

The 50 cm base consisted of Sevilleta dune sand. The lowermost and fiftieth layer was comprised of medium blasting sand. All even-numbered layers were made up of medium blasting sand and all odd-numbered layers were composed of the Sevilleta dune sand. The uppermost layer consisted of the Sevilleta dune sand.

Volumetric moisture contents were determined from 100 cm^3 repacked samples were found to be less than 0.01 but greater than 0.005 for both soils.

The source was constructed from a 25 cm length of PVC pipe (Figure 3.15). Twelve holes, 0.159 cm in diameter were drilled into the bottom 2 cm of the pipe. This perforated interval was filled with very coarse sand in order to provide a small amount of impedence so that water flowed out of all 12 holes instead of just the bottom holes.

The source was placed in the top 2 cm of the sand, thus fully penetrating the top fine-grained layer. The PVC pipe, which was placed into the 30 degree corner of the tank, portruded 2 cm radially into the sand. Thus the source had both an effective radius and a depth of 2 cm.

For the first experiment, the flow rate was 1 ml/min. A syringe pump delivered the water to the source at this rate. For the second experiment, the flow rate was 20 ml/min. This flow rate exceeded the capacity of the syringe pump, so instead, flow rates were controlled by maintaining a constant head reservoir and directing flow through capillary tubing. A needle valve, located in a flowmeter, added additional resistance to flow and allowed the flowrate to be fine-tuned to 20 ml/min. The flowrate for the third experiment was 100 ml/min. The capillary tubing was eliminated and flow was directed from the constant-head source through the needle valve and flowmeter into the source.

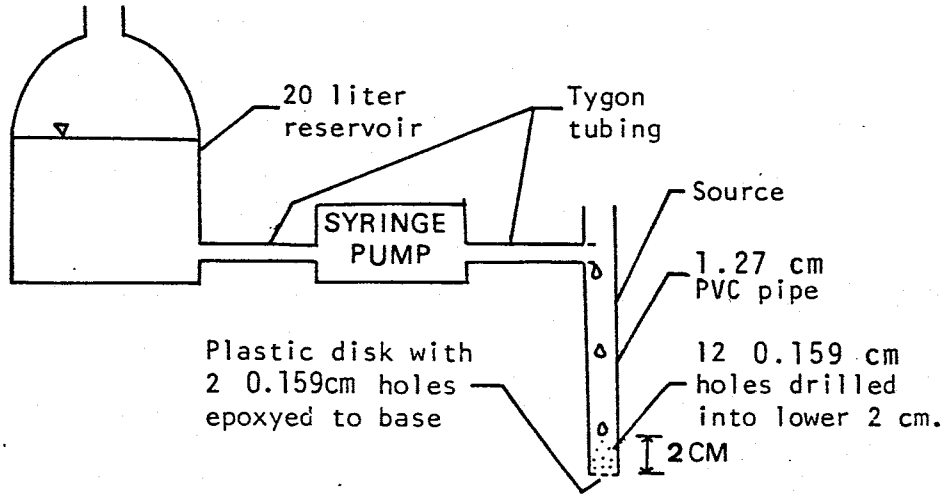

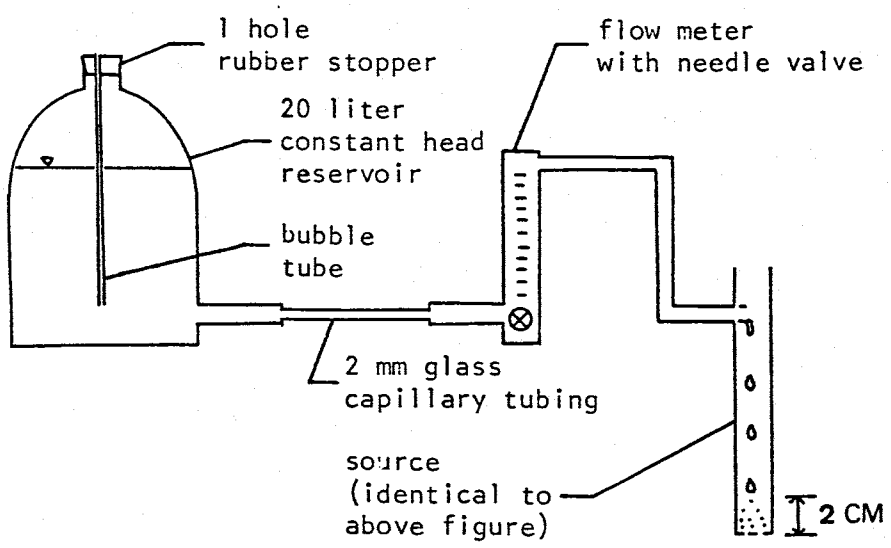

Figure 3.15 Methods of introducing water of (a) experiment 1 and (b) for experiments 2 and 3.

Three cameras and a videocassette recorder were used to record the experiment. Two cameras, one containing black and white print film and the other containing color slide film were set at fixed positions in front of the box. These two cameras along with the videocassette recorder were used to document the movement of the wetting front. A third camera, containing color slide film, documented the procedures.

Lighting was difficult. The room had many windows and the walls were covered with reflective aluminum foil. The walls, windows and many other objects were reflected by the glass and into the view of the cameras. To solve this, the windows were covered with black plastic and the cameras were placed behind a black curtain extending 12 ft lengthwise and 6 ft in height. Holes were cut into the black curtain for the camera lenses.

Lighting was provided by four 3200^{o}K tungsten floodlamps. Two were located on each side of the tank and made angles of approximately 30 degrees from the face of the tank. Because tungsten lights were used, 50 ASA tungsten film had to be used for the color slides. No special film was needed for the black and white prints, so Kodak 125 ASA film was used.

3.10 Execution of the Experiments

3.10.1 Experiment I

The first experiment was conducted at a flow rate of 1 ml/min. Water was delivered to the point source by means of a syringe pump. Before the experiment, 24 manometer-type tensiometers and 12 transducer-type tensiometers were filled with water. These were immersed in water so that the tensiometers and the entire lengths of the manometer tubes remained filled.

Two assistants were utilized during the first two hours of the experiment. One operated the cameras and the other operated the videocassette recorder. The source was inserted into the top layer. The tubing leading from syringe pump to the source was disconnected at the source. The syringe pump was turned on and the flowrate was adjusted using a stopwatch and graduated cylinder. The temperature of the water was recorded and the water level in the reservoir was marked.

The experiment was started by connecting the tube from the syringe pump to the source. Wetting front profiles were drawn, with grease pencil, on the back of the sand tank at various times. Tensiometers were inserted into the holes in the side of the tank as the wetting front passed. The manometer tubes were fed through a series of conduits and put in place on the manometer stand. The tubes were cut so

that the initial pressure in the tensiometer was approximately 0 cm-H_2O. Tensiometer pressure heads were recorded upon insertion and at 120, 180, 240, 360, 420, 600, 720, 1080, 1440, 1800, 2160, 3600, 4320, and 4680 minutes. Photographs were taken at 5, 10, 20, 30, 60, 90 minutes and whenever pressure heads were recorded. The reservoir was refilled to its initial level every 12 hours and the volume of water used in 12 hours was recorded. The temperature of the reservoir was recorded when pressure heads were recorded.

At 360 minutes into the experiment, a sheet of black plastic was laid over the soil surface. This was done to prevent evaporation.

At 4600 minutes, dyes were injected into the soil through dye ports and along the top layer. The paths of the dyes were recorded.

At 4680 minutes, the syringe pump was turned off. Cylindrical cores, 40 cm^3 in volume, were taken in each individual layer for those layers that were wet at radii of 8, 28, 48, 88, 128, and 148 cm. The coring tubes were pushed in from the top and removed after one layer had been sampled. Moisture contents were determined for each core sample. The wet layers were removed and replaced for the next experiment.

3.10.2 Experiment II

The second experiment was conducted at a flow rate of 20 ml/min. As before, 24 manometer-type tensiometers and 12 pressure-transducer tensiometers were filled prior to the experiment. As an improvement over the first experiment, the manometer tubes were put in their respective places on the manometer stand prior to the start of the experiment. The manometer tubes were pre-cut so that their lengths were correct. The tensiometers were placed in a bucket of water that was elevated so that the initial pressures of the tensiometers when placed in the soil would be in the -10 cm-H_2O to -20 cm-H_2O range. Equilibration times were greatly reduced using this method. When installing tensiometers, it was necessary to remove the manometer tubing from the board and feed the manometer lines backwards through the conduits and back onto the manometer board. This was necessary because the tensiometers would not fit through the conduits.

Four assistants were used during the first three hours of the experiment and one assistant helped for six hours. Two of these worked the cameras and videocassette recorder, a third injected dyes and traced dye front movement, and a fourth installed and monitored tensiometers.

The flowrate was adjusted prior to the experiment. The experiment was started, as before, by plugging the tubing, in which water was already flowing into the source,

Wetting front profiles were recorded on the back of the tank and with photographs. Pressure heads in tensiometers were recorded upon insertion and at 90, 120, 180, 240, 300, 360, 480, 600, and 720 minutes. Photographs were taken at 1, 2, 5, 10, 20, 30, 40, and 60 minutes and whenever pressure heads were recorded.

Dyes were injected and streampaths recorded at selected times. The water temperature was recorded when pressure heads were recorded.

The experiment was ended at 900 minutes. No cores were taken. Ten layers of sand and half of the eleventh were removed. Only the eleventh layer was replaced for the third experiment.

3.10.3 Experiment III

The third experiment was conducted at a flow rate of 100 ml/min. This experiment was conducted in nearly the same manner as experiment 2. The main exception, besides the flowrate, were that there were only forty layers, since the top 10 layers were not replaced and that the tensiometers were not as closely spaced around the source as they were in previous experiments. The experiment was ended at 780 minutes.

3.11 Steady-State Point Source Solutions

A steady-state solution for flow from a point source (Raats, 1971),(equation 2.13) was used in conjunction with the coordinate transformation presented by McKee and others (1984) in order to construct a total head profile based on the measured soil parameters and a constant anisotropy. The pore size distribution index, α , was determined from the slope of the K_h - ψ curve of Figure 3.8 for pressure head values ranging from -9 cm-H_2O to -25 cm-H_2O. Use of the hydraulic conductivity - pressure head curve representing the harmonic mean of the hydraulic conductivities of the two soil types produced a value of α that should best predict the pressure head distribution in the vertical direction. Equation 2.13 was scaled in the radial direction using an anisotropy of 3.5, the value at saturation, and was solved using a programmable calculator. The exponential integral was calculated using a series solution available in Abaromowitz and Stegum (1964). Profiles of total head were constructed from solutions to equation 2.13 for flow rates of 12 ml/min, 240 ml/min, and 1200 ml/min. Since the analytical solution is for full cylindrical flow and the sand tank is only 1/12 of a cylinder, the flowrates used in the analytical solution were twelve times greater than those used in the experiments. The total head profiles computed from the analytical solution are shown in Figure 3.15

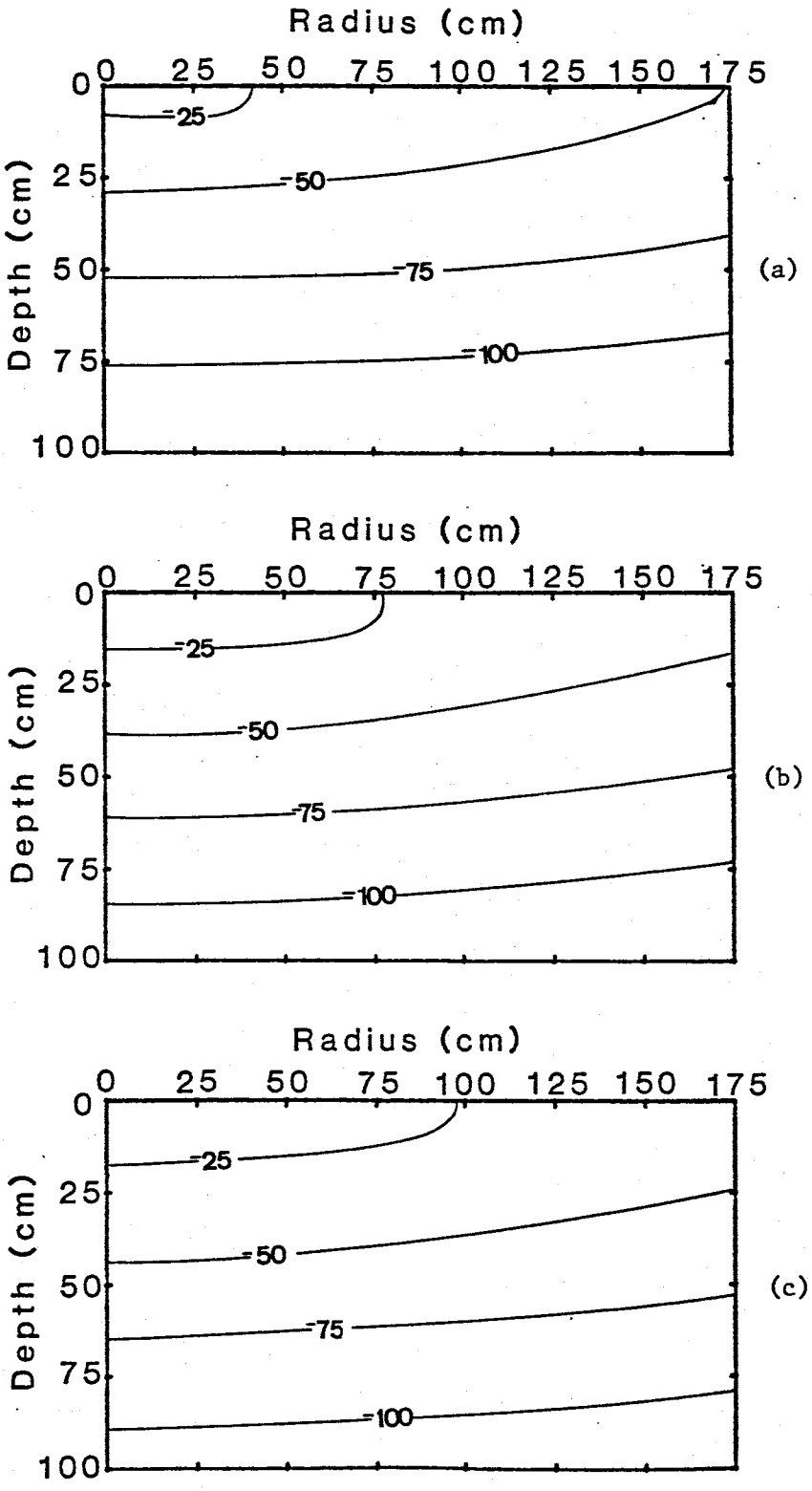

Figure 3.16 Total head profiles predicted using the analytical solution for flow from a point source (Raats, 1971) and by scaling the coordinate system to

Chapter 4

RESULTS AND DISCUSSION

4.1 Transient-State Behavior

Wetting front profiles were constructed from photographic slides taken during each of the experiments. These profiles can be found in Appendix 2.

4.1.1 Experiment I

A composite wetting front profile was constructed for the first experiment from profiles recorded at six times (Figure 4.1). During the 4680 minutes in which water infiltrated the sand layers, the wetting front travelled 165 cm radially and 9 cm vertically, infiltrating a maximum of 4.5 layers.

Radial movement of the wetting front occurred primarily through the fine-grained layers (the Sevilleta dune sand). The wetting front entered the coarse-grained layers (the medium blasting sand) vertically from the overlying and underlying fine-grained layers.

Early in the first experiment, from 0 to 720 minutes, the radial distance to the wetting front from the source was much greater in the fine-grained sand than in the coarse-grained sand making the wetting front profile highly irregular. Later in the experiment, the shape of the

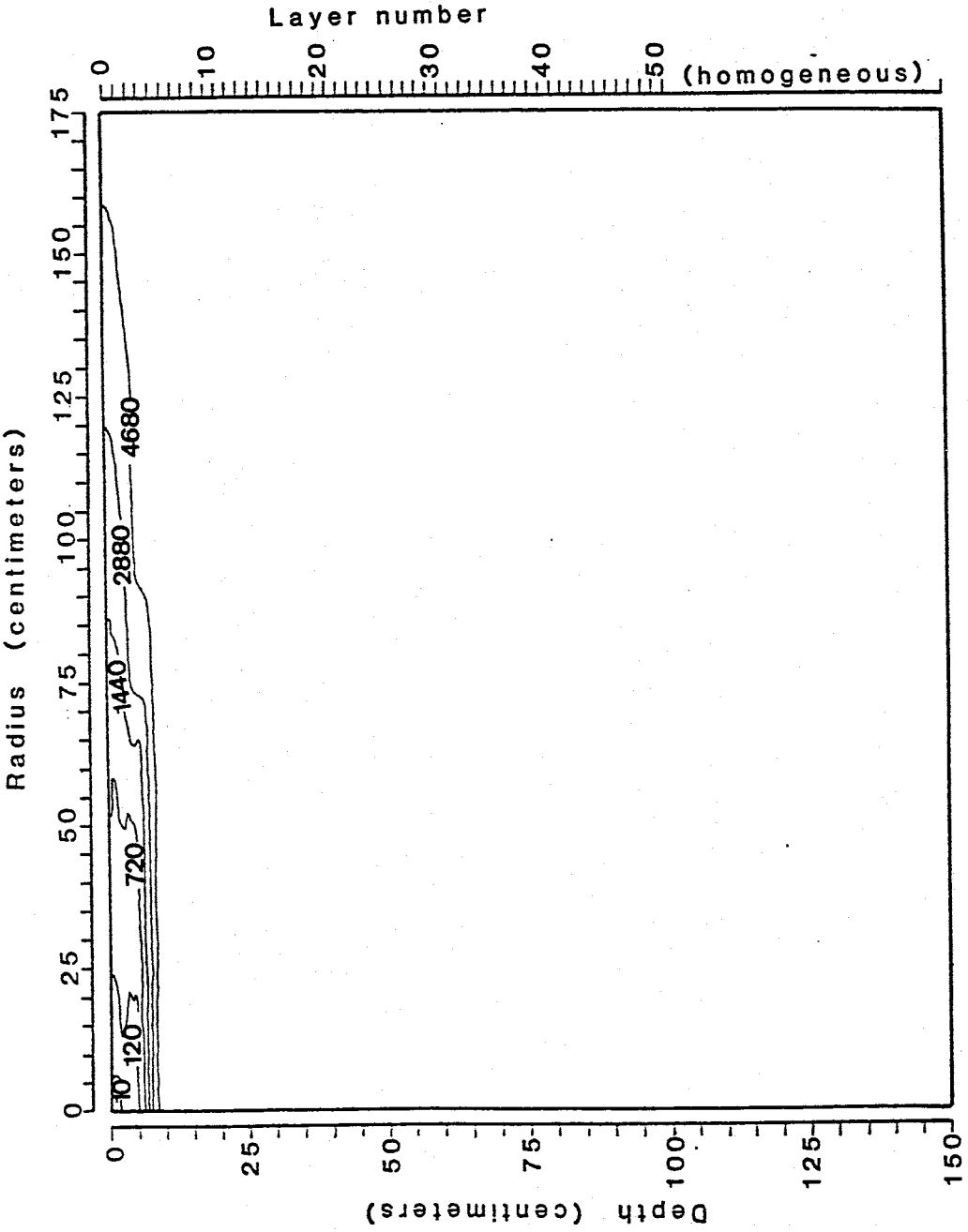

Figure 4.1 Wetting front profiles at indicated times (in minutes) for experiment 1.

wetting front became much more smooth, displaying little variation between layers. This occurred as the radial advance of the wetting front slowed to the point where it equilibrated with the vertical advance of the moisture from the fine-grained layers into the interlying coarse-grained layers.

4.1.2 Experiment II

A composite wetting front profile was constructed from profiles observed at five different times during the second experiment (Figure 4.2). In 720 minutes, the wetting front travelled 165 cm radially and 20 cm vertically, infiltrating a total of ten layers.

As in the first experiment, the wetting front moved faster, radially through the fine-grained layers ,except beneath the source and water entered the coarse-grained layers vertically from both the underlying and overlying fine-grained layers. The existence of a small amount of water between the source and the corner of the polycarbonate sheet suggested that the soil was saturated at the source and that the pressure head at the source was 0 cm-H_2O.

The wetting front profile was highly irregular at early time, but like the first experiment, it became smoother as time progressed. The profile remained somewhat irregular throughout the experiment. Given more time, however, and a greater distance to the radial boundary, the profile

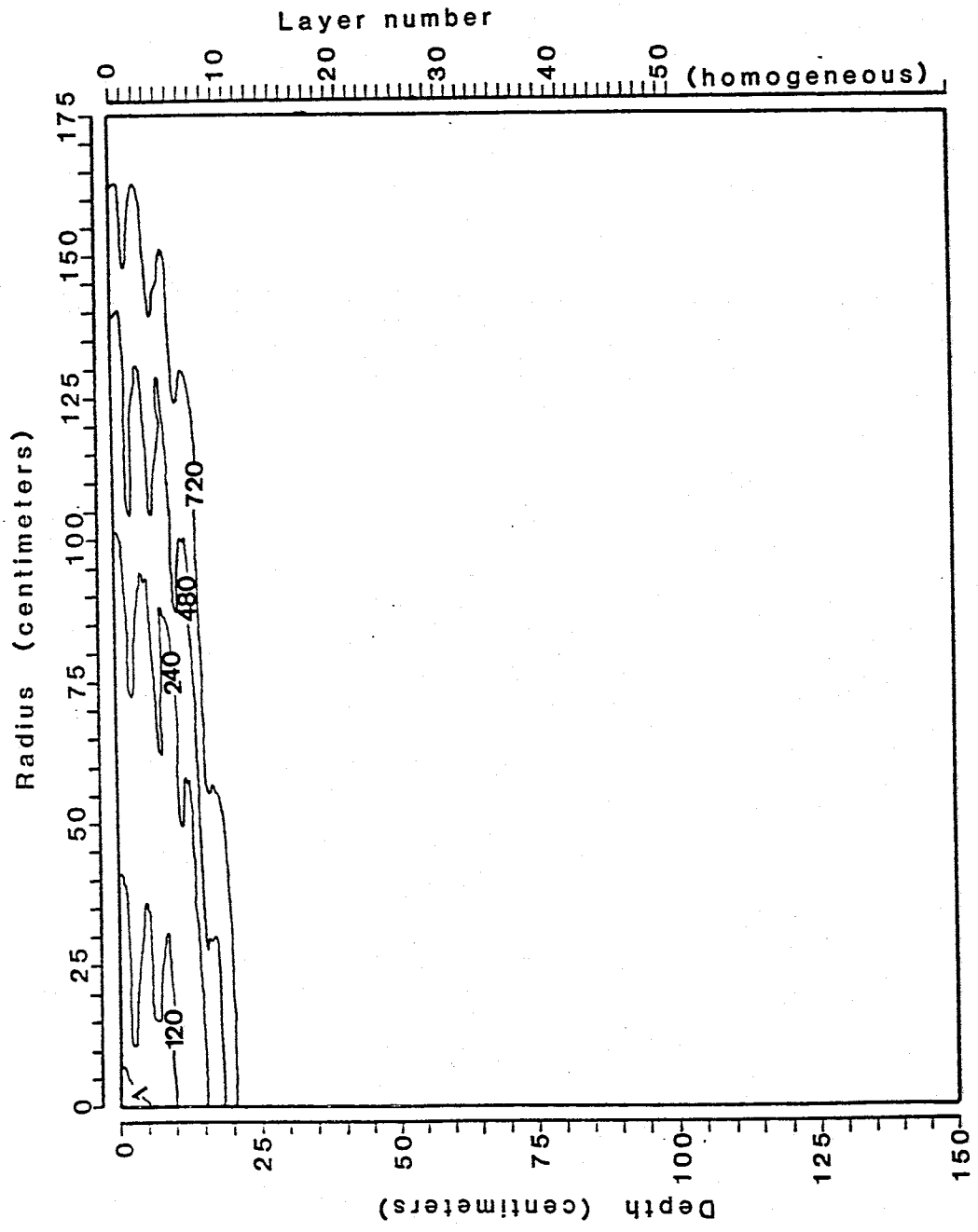

Figure 4.2 Wetting front profiles at indicated times (in minutes) for experiment 2.

probably would have had the smooth parabolic shape observed in the first experiment.

Outlines of the movement of the dye injected behind the wetting front at early time show the movement of water between and within the soil layers (Figures 4.3 and 4.4). Dyes injected into the coarse-grained layers moved vertically, both upwards and downwards into the fine-grained layers. This is in sharp contrast to to the movement of the wetting front where moisture moved vertically from the fine-grained layers to the coarse-grained layers. Once in the fine-grained layers, the dye moved parallel to the layer in the direction of the wetting front. One exception occurred immediately below the source where the dye moved vertically through several layers before travelling laterally through the fine-grained layers. A dye injected into the topmost layer (fine-grained) travelled radially away from the source.

4.1.3 Experiment III

A composite wetting front profile was constructed for the third experiment (Figure 4.5). At 720 minutes, the wetting front extended 172 cm radially and 116 cm vertically. The wetting front extended past the lower boundary of the layered soil, entering the underlying homogeneous Sevilleta dune sand at approximately 420 minutes.

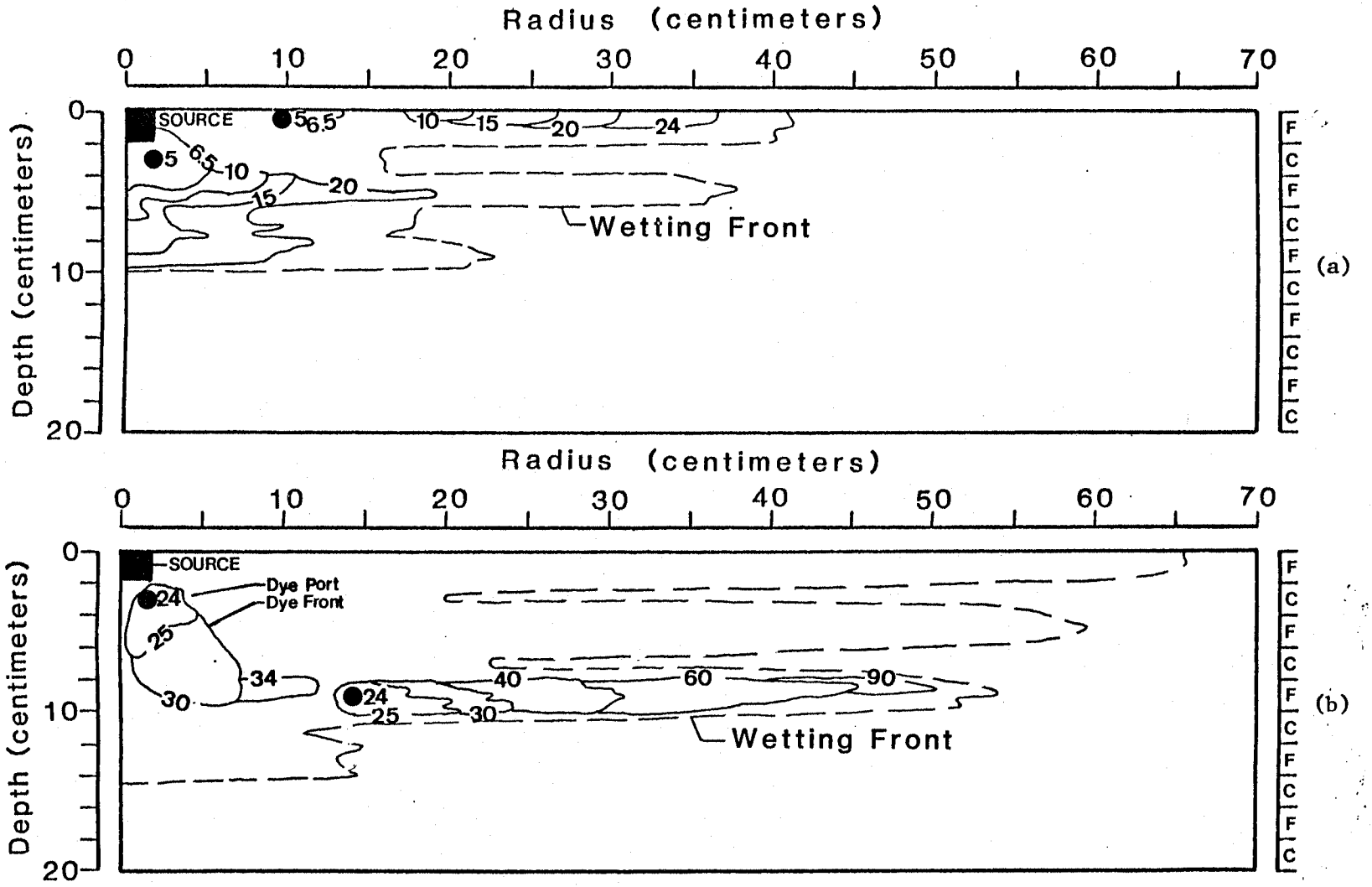

Figure 4.3 Outline of dye front movement for dye injected at (a) 5 min. and (b) 24 min. for experiment 2. F refers to the fine-grained layers and c refers to the coarse-grained layers. Solid circles are locations where dye was injected.

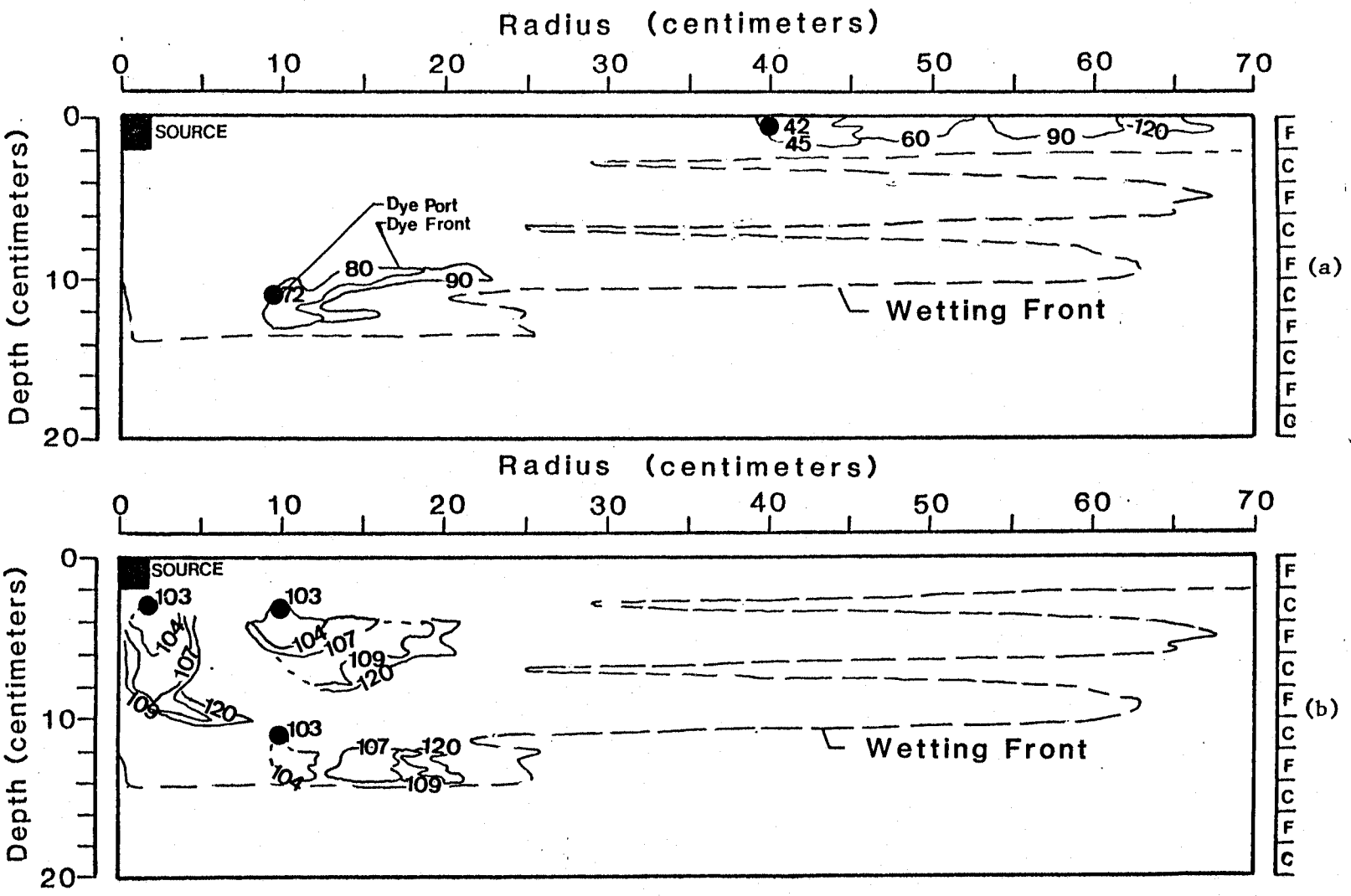

Figure 4.4 Outline of dye front movement for dye injected at (a) 42 min. and 72 min., and (b) 103 min. F refers to the fine-grained layers and c refers to the

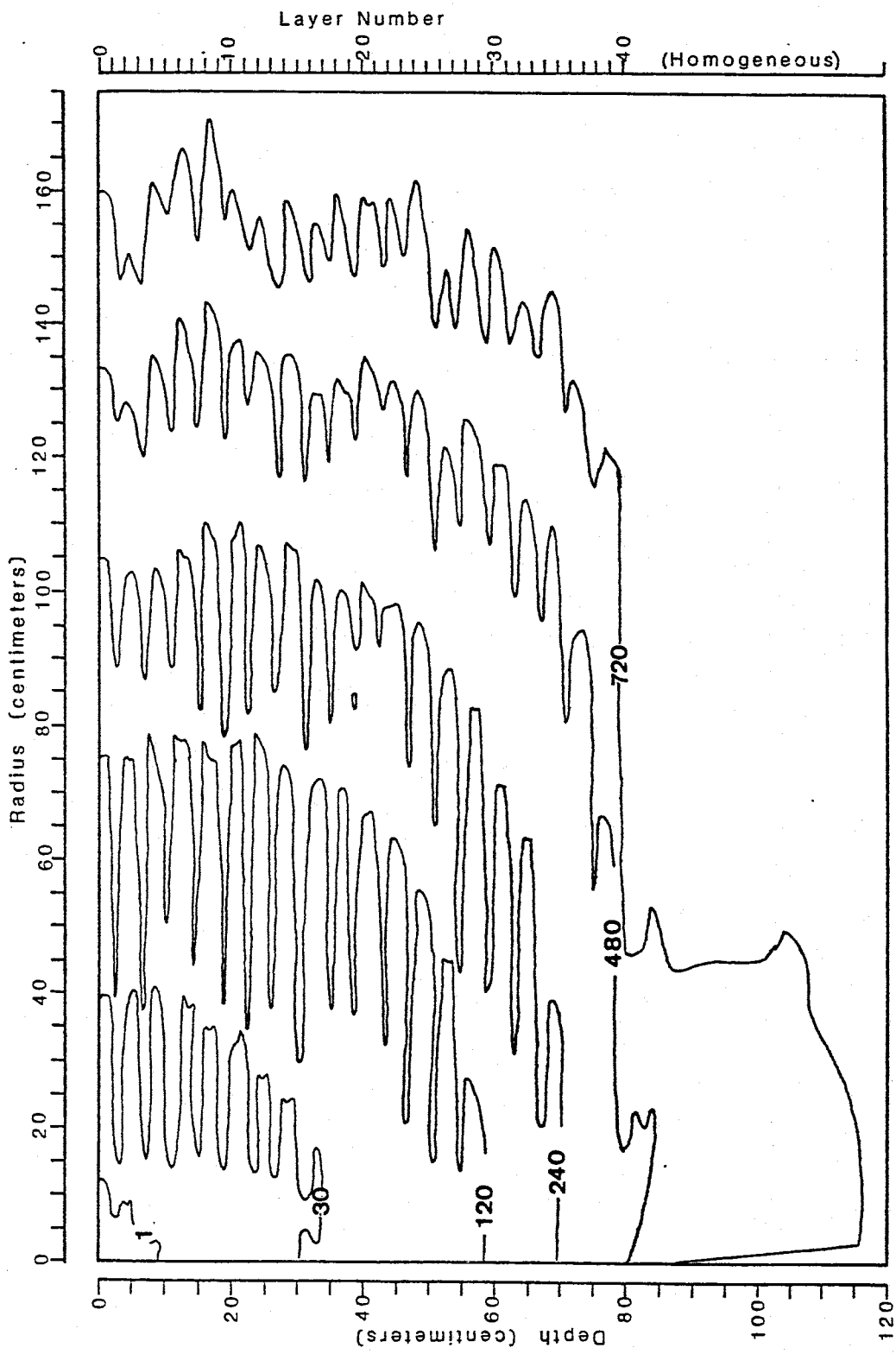

Figure 4.5 Wetting front profiles at shown times (in minutes) for experiment 3.

A small ponded region existed around the source extending to a radius of 3 cm and ponded to a height of approximately 0.2 cm. This somewhat increased the effective radius of the source.

The wetting front advanced in a manner similar to the previous experiments. One major difference was that lateral movement was noted in the coarse-grained layer near the source. The wetting front advanced radially at approximately the same rate as in the second experiment. The five-fold increase in flux was accommodated by a near five-fold increase in vertical movement.

At early time, from 0 to 60 minutes, before there was significant vertical movement from the fine-grained layers to the adjacent coarse-grained layers, two distinct wetting front profiles appeared. One profile consisted of the locus of wetting front positions in the fine-grained layer and the other consisted of the locus of wetting front positions in the coarse-grained layer. The profiles formed smooth parabolas suggesting that homogeneity existed between layers of the same soil type.

The wetting front profile within the basal Sevilleta dune sand layer displayed several irregularities, indicating that some heterogeneity exists within this layer. This may lead one to question whether all layers contain similar heterogeneities. This layer, however, is probably not

cm layers because it was not packed with the same care as the 2 cm layers.

4.1.4 Discussion

4.1.4.1 Infiltration behavior

Downward movement of the wetting front in all three experiments was characterized by erratic movement through the layers at very early time (less than 30 minutes) and by smooth movement through the layers at late time.

At early time, the wetting front moved downwards rapidly through the fine-grained layers and slowly through the coarse-grained layers. This is partially consistent with the observations of Miller and Gardner (1962) who observed a restriction in the downward advance of the wetting front from a fine-grained layer to a coarse-grained layer. Miller and Gardner (1962) also observed a surge of channelized water through the coarse-grained layer after the pressure of the wetting front immediately above that layer had increased to the water-entry value of the coarse material. This was not observed in any of the three experiments. Two main features differentiated these experiments from those of Miller and Gardner and probably explain the differences in behavior: 1) Present experiments were conducted in three-dimensions rather than one, and 2) water was introduced at a low rate of flow. In a

cannot build up immediately above a coarse-grained layer because the pressure is relieved by the lateral movement of water. As a result, the wetting front does not surge through the coarse-grained layer, but flows through slowly under a combination of matric and gravitational forces.

Philip (1975) provided evidence that wetting front instability would occur if the pressure gradients, at the wetting front, opposed the direction of flow. This commonly occurs in fine-grained layers overlying coarse-grained layers where pressure increases due to restricted advance of the wetting front. This could happen only if the downward component of flux was greater than the lateral component of flux. This would be the case in a column experiment in which there was no lateral flux component or in a three-dimensional infiltration experiment where water was introduced at a very high rate of flow. In all three sand tank experiments, lateral movement of water in the fine-grained layer was always greater than the vertical movement and thus there was no the buildup of pressure and formation of unstable wetting fronts. At late time during each of the experiments, the downward movement of the wetting front was smooth and displayed little change in velocity between the coarse-grained and fine-grained layers

For each experiment, two plots were made: one of the radial distance to the wetting front versus the square root of time and one of the vertical distance to the wettin

front versus the square root of time (Figure 4.6). In each experiment the wetting front advanced linearly with the square root of time in both the horizontal and vertical directions, showing some similarity to the theory described by Philip (1969a) for one-dimensional horizontal flow. A line was fit to each set of data by means of a least squares curve fit, the results of which are given in Table 4.1.

The slope of these lines is indicative of the relative rate of advance of the wetting fronts. The slopes of the lines corresponding to the radial advance of the wetting front are identical for the second and third experiments, indicating that wetting front behavior in the radial direction was identical for these two experiments. This similarity can be explained by the fact that the bulk hydraulic properties and boundary conditions controlling radial flow between experiments 2 and 3, namely the initial moisture content and moisture content at the source, were identical.

The intercepts of the fitted lines, designated as R_0 for radial flow and Z_0 for vertical flow, respectively, are consistently greater than 0 cm and increase with the flow rate. The existence of these intercepts reflects a steeper slope at early time which further reflects very rapid movement of the wetting front, both radially and vertically, at the initial stages of the experiments. As time progresses, the rate of advance of the wetting front

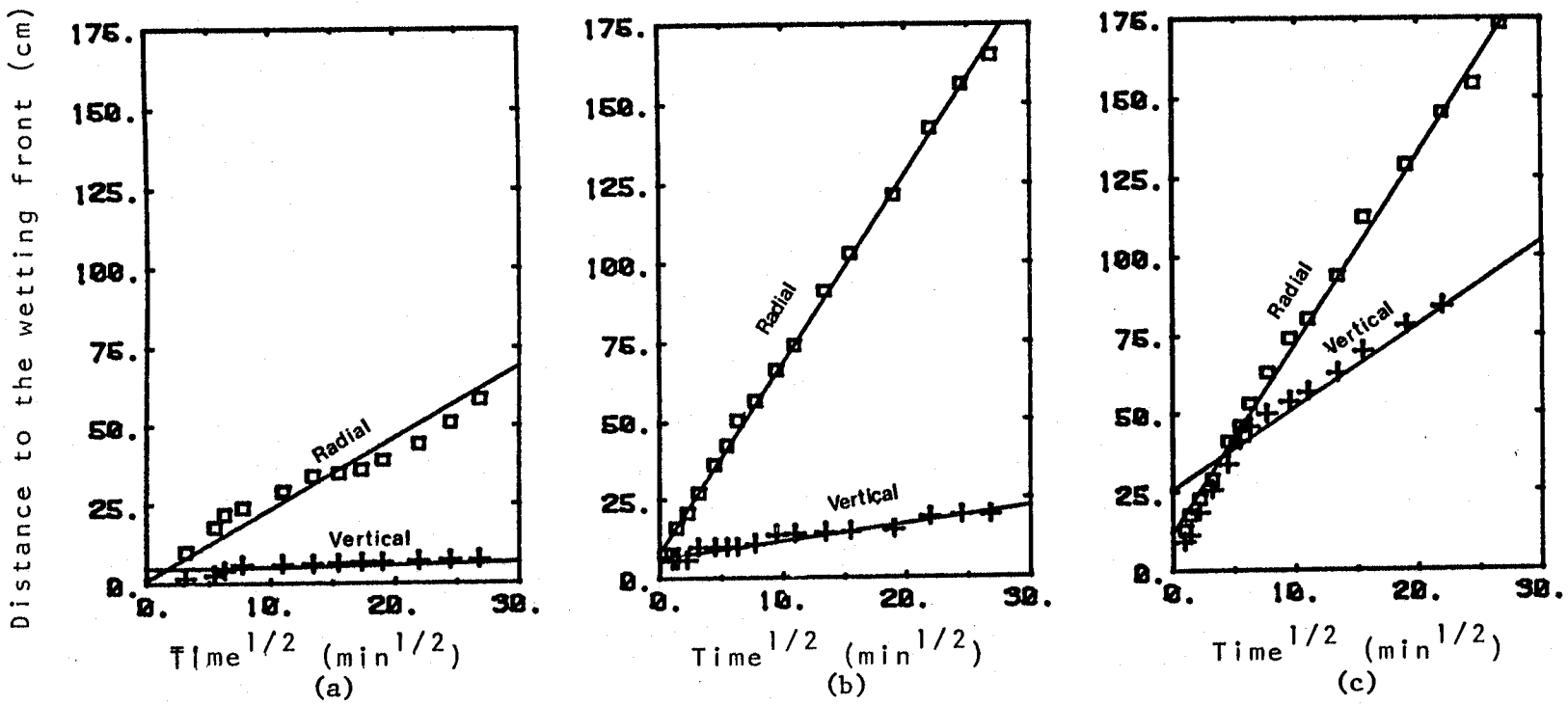

Figure 4.6 Maximum distance to the wetting front versus $t^{\frac{1}{2}}$ measured in the horizontal and vertical directions for (a) experiment 1, (b) experiment 2, and (c) experiment 3.

Table 4.1

Slopes, intercepts, and coefficients of determination (R^2) of lines fitted through the method of least squares to the distance to the wetting front versus time$^{1/2}$ data.

Experiment Number	Slope of line (cm/min$^{1/2}$)		Intercept of line (cm)		Coefficient of Determination	
	Radial Movement (m_r)	Vertical Movement (m_z)	Radial Movement (R_o)	Vertical Movement (Z_o)	Radial Movement	Vertical Movement
1	2.25	0.085	1.56	4.61	0.99	0.73
2	6.02	0.54	8.19	6.74	1.00	0.93
3	6.06	2.80	12.20	26.20	1.00	0.98

decreases with respect to the square root of time and eventually reaches a constant value.

Presently, it is not understood why there is such an abrupt change in the rate of advance of the wetting front at early time. The decrease in the rate of advance of the wetting front in the radial direction, relative to the square root of time, may be due to an increase in the flow of water from the fine-grained layers to the coarse-grained layers as the wetting front advances radially. This flow out of the fine-grained soil would reduce the flow of water to the wetting front and reduce the rate of advance of the wetting front.

Similarly, the decrease in the vertical rate of advance, relative to the square root of time, may be due to the increased lateral movement of water with time. Immediately below the source, water is initially forced downwards into the soil at a rate equal to or greater than the rate of lateral movement of the water. With increasing time and increasing distance to the wetting front, more layers are penetrated and more water flows laterally.

At a wetting front radius R_0, it appears that an equilibrium is reached between the amount of water flowing horizontally to the wetting front along the fine-grained layers and the amount of water flowing out of the fine-grained layers. At a wetting front radius Z_0, it

water towards the wetting front and the lateral movement of water away from the Z axis.

Although it is not presently understood why R_0 and Z_0 exist, these values appear to have a significant effect on the geometry of the wetting front. For the second and third experiments, R_0 and Z_0 appear to approximate the radii and depths of saturation. For the first experiment, there was no zone of saturation. These values also play a role in the analysis of wetting front geometry as a function of the flow rate. The lines fitted by the least squares method can be described by the equations

$$R = R_0 + m_r t^{1/2}$$

$$Z = Z_0 + m_z t^{1/2} \qquad (4.1)$$

where R and Z are the maximum distances to the wetting front, measured parallel to the radial and vertical axes respectively and measured from the origin at time t. The variables m_r and m_z are the slopes of the lines fitted to the radial and vertical wetting front data, respectively in Figure 4.6. From these equations, one can derive the relationship

$$(R - R_0)/(Z - Z_0) = m_r/m_z = \text{constant} \qquad (4.2)$$

Thus the ratio of the distances measured to the wetting

front in the radial and vertical directions is constant provided that either: 1) the effective source radius, R_0 and effective source depth, Z_0 are accounted for or 2) that R and Z are large enough that the values R_0 and Z_0 are negligible.

If $(R - R_0)/(Z - Z_0)$, as determined from the ratio m_r/m_z, is plotted as a function of the flow rate, a linear relationship is observed (Figure 4.7). This relationship can be described mathematically by the model

$$(R - R_0)/(Z - Z_0) = a - b \log Q \qquad (4.3)$$

where Q is the flow rate.

This model infers that at flow rates slightly greater than 100 ml/min, $(R - R_0)/(Z - Z_0)$, will fall below a value of 1. This is expected when gravity is significant. A greater flux would have little effect on the radial advance since the radial movement is controlled by the sorptivity of the soil which is dependent only on the soil type, the initial water content, and the water content at the source (Hillel, 1980b, pg.17). The sorptivity of the soil would not change with larger flow rates. The only effect on radial movement would occur in the form of a larger radius of saturation, which might be expressed in terms of a larger value of R_0. With only a small increase in radial flow, an increase in the flux would then have to be accomodated by an

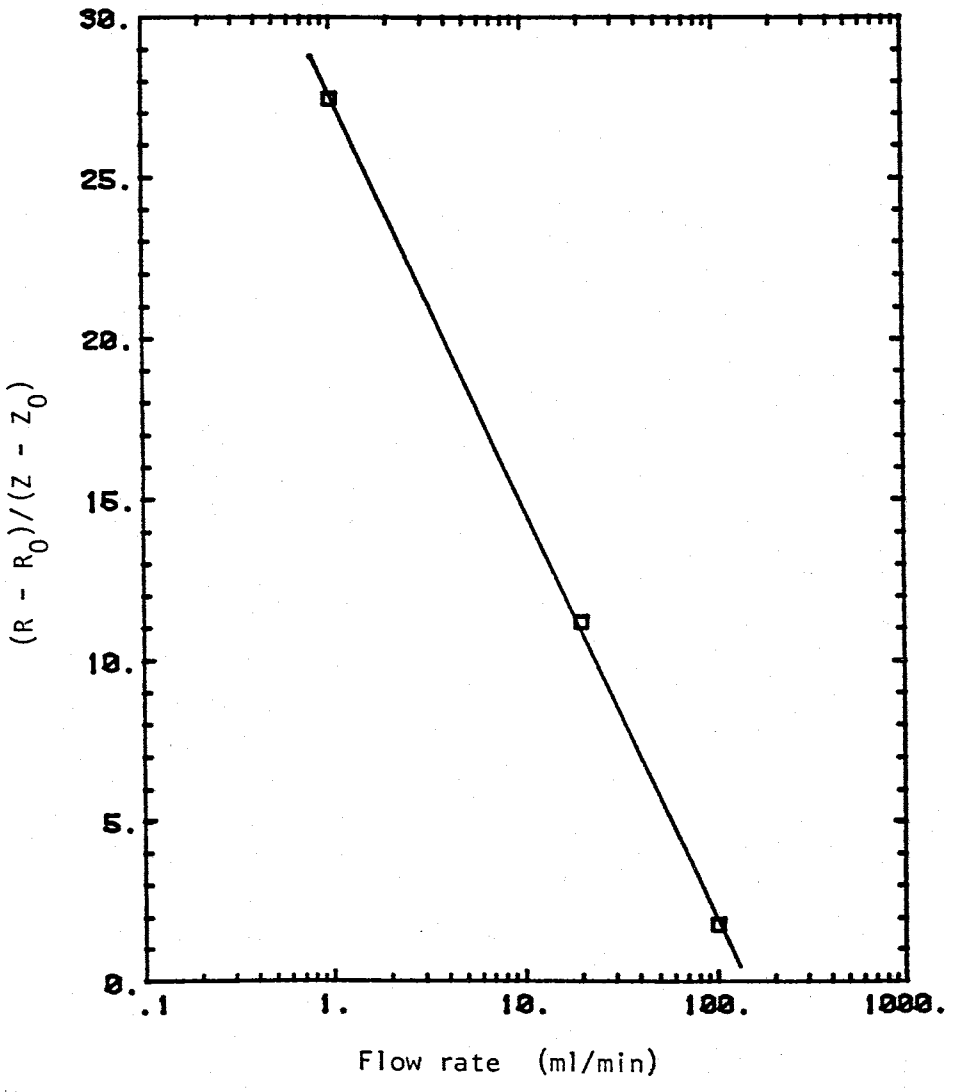

Figure 4.7 $R-R_o/Z-Z_o$ versus flow rate determined from the slopes and intercepts of lines fitted through the distance to the wetting front versus time$^{\frac{1}{2}}$ data for each of the experiments.

increase in flow in the vertical direction.

The model also predicts that the value of $(R - R_0)/(Z - Z_0)$ would fall below a value of 0 at large flow rates. This is physically impossible and shows that the model is limited to the range of flow rates used in the formulation of the model. Most likely, the ratio $(R - R_0)/(Z - Z_0)$ will assymptotically approach zero as the flow rate increases to infinity.

4.1.4.2 Effects of Soil Layering

For each of the three experiments, the ratio of the maximum distances to the wetting front, measured in the radial and vertical directions, R/Z, approached a constant value that was consistantly greater than unity. These observations are inconsistant with present infiltration theory constructed for homogeneous, isotropic soils. The discrepancies appear to be a result of layering in the soil

During infiltration into a homogeneous, isotropic soil the ratio R/Z is initially equal to unity and decreases with time. This can be explained in terms of the capillary and gravitational forces controlling the advance of the wetting front. Wetting front movement in the radial direction is driven by capillary forces while wetting front movement in the vertical direction is driven by a combination of capillary and gravitational forces. At early times capillary forces dominate and gravitational forces are

insignificant. In a homogeneous and isotropic soil, the capillary forces are uniform along the wetting front and so the front advances with spherical symmetry. At late time, however, the capillary forces diminish and gravitational forces become increasingly significant. As time progresses towards infinity, the radial advance of the wetting front approaches zero while the vertical advance of the wetting front approaches a constant value which is greater than zero. For this reason, the ratio R/Z decreases with time.

In each of the three experiments, the ratio R/Z did not decrease with time, but instead, increased towards what appeared to be a constant value. The initial values of the ratio R/Z were equal to the ratio R_0/Z_0, which were nearly equal to or less than unity for all experiments. The ratio R/Z increased, with time, and apprached m_r/m_z. The reason for this increase is not presently understood because the reasons for the existence of the values R_0 and Z_0 are not understood. It is hypothesized that this ratio would have eventually decreased, provided that the radial boundary of the sand tank was extended and the experiments were conducted for greater lengths of time

The relationship between the flow rate and the wetting front geometry shown in figure 4.7 suggests a direct correlation between the ratio $R-R_0/Z-Z_0$ and the average anisotropy of the flow system. This correlation would be based on the following line of reasoning: Figure 4.7 shows

that the ratio $R-R_0/Z-Z_0$ is inversely proportional the th flow rate. Since the flow rate, by nature, is directl proportional to the moisture content of the soil and th moisture content of the soil is, by theory, inversel proportional to the anisotropy of the flow system, i follows that the ratio $R-R_0/Z-Z_0$ should be directl proportional to the average anisotropy of the flow system It also follows that the average anisotropy should increas with a decrease in the flow rate. Care must be taken however, in relating the geometry of the wetting front t anisotropy in layered soils because little is known on ho this geometry varies with the flow rate in a homogeneous isotropic soil.

4.2 Steady-State Behavior

4.2.1 Tensiometers

The tensiometers functioned properly for the three experiments. Pressure heads measured by each of the tensiometers are plotted as a function of time in Appendix 3 for each of the experiments. The lengths of time it took for the tensiometers to equilibrate varied with the soil type, the degree of saturation, and the differences between the initial and equilibrated pressures within the tensiometers. The tensiometers equilibrated quickly in the Sevilleta dune sand, especially near the source where the hydraulic conductivities of the soil were highest. For the second and third experiments, the tensiometers placed into the Sevilleta dune sand equilibrated within one to two hours, depending upon their distance from the source and how accurately they were pre-set. As expected, the tensiometers responded slowly in the medium blasting sand, especially at distances far from the source where the hydraulic conductivities were at their lowest values. For the second and third experiments, the tensiometers placed into the medium blasting sand equilibrated within one to six hours also depending on the distance from the source and the accuracy to which they were preset. The tensiometers equilibrated much faster in the second and third experiments than in the first, because the moisture profiles were wetter and the hydraulic conductivities in turn were higher, and

because water levels in manometers were pre-set to their expected values. In the first experiment, tensiometers took as long as twelve hours to equilibrate in the Sevilleta dune sand, and as long as two days to equilibrate in the medium blasting sand.

The lack of change in tensiometer readings observed after the tensiometers were equilibrated with the soil suggests that steady-state conditions behind the wetting front were reached quickly.

4.2.2 Experiment I

Pressure head and total head profiles were constructed from tensiometer measurements taken at 4680 minutes (Figure 4.8). Pressure heads ranged from approximately -20 cm-H_2O near the source to less than -35 cm-H_2O near the wetting front. The total head profile shows that gradients were directed predominantly downwards.

Profiles of volumetric moisture content were constructed from cores taken at the end of the experiment (Figure 4.9). Because moisture content is highly discontinuous between layers, separate profiles were constructed for each soil type. Values ranged from 0.22 and 0.18 near the source to 0.13 and 0.05 near the wetting front for the Sevilleta dune sand and the medium blasting sand, respectively. The initial moisture content of the air-dry soil was determined, prior to the experiment, to be between

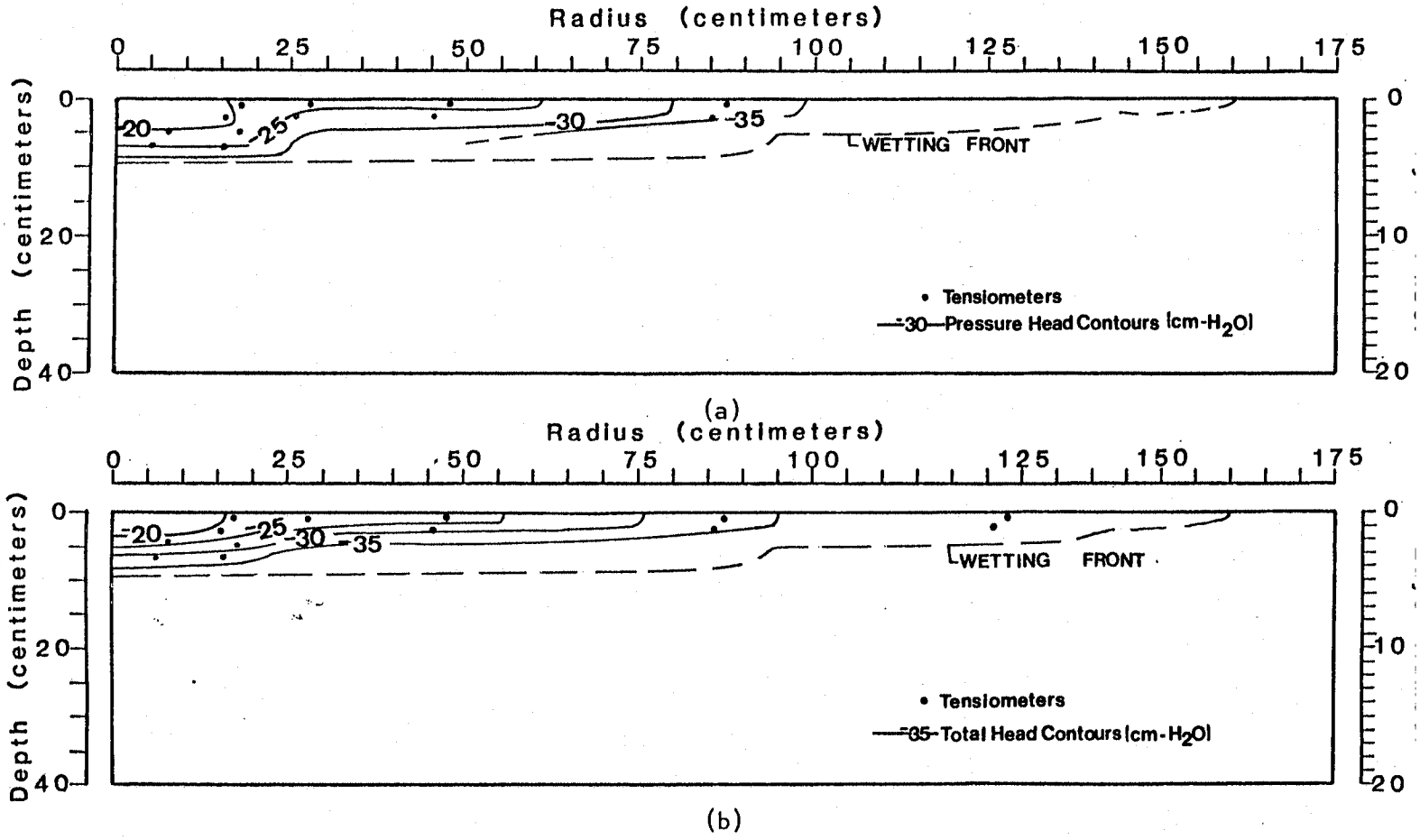

Figure 4.8 Pressure head profile (a) and total head profile (b) for experiment 1 at 4680 min.

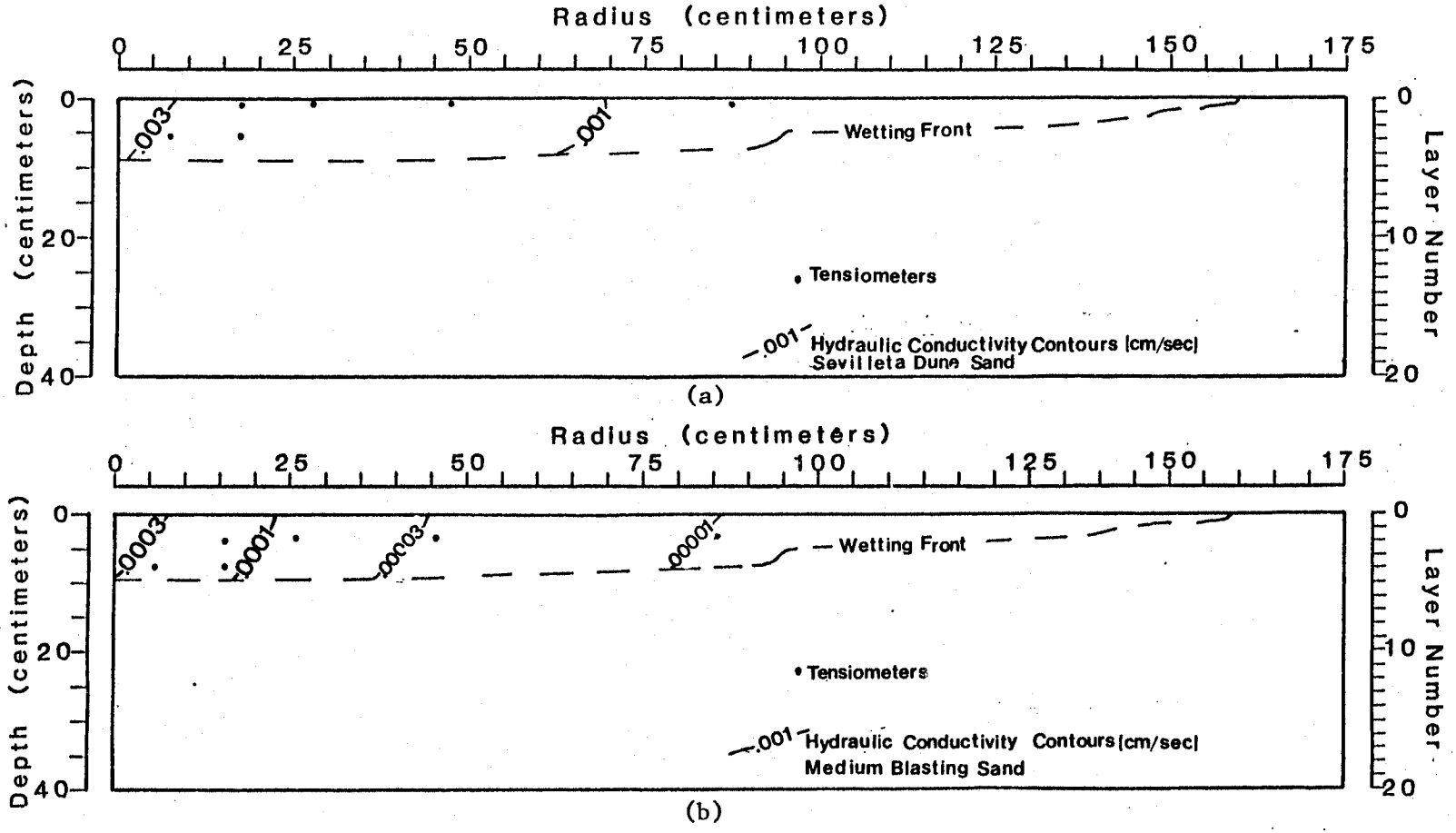

Figure 4.9 Volumetric moisture content profile computed separately for the Sevilleta dune sand (a) and the medium blasting sand (b) from tensiometer data collected in each of the two soils for the first experiment.

the values of 0.01 and 0.005.

Profiles of unsaturated hydraulic conductivity, at in-situ pressure heads (Figure 4.10), were constructed from the hydraulic conductivities of the individual soil layers (Figure 3.7). Values ranged from 3×10^{-2} cm/s to 3×10^{-3} cm/s for the Sevilleta dune sand and 2×10^{-4} cm/s to 2×10^{-5} cm/s for the medium blasting sand.

The pathlines followed by dyes injected at 4600 minutes are shown with respect to the total head profile (Figure 4.11a) and with respect to the ratio K_{sd}/K_{mb} (Figure 4.11b). Dyes injected into the fine-grained layer moved only in the radial direction, while dyes injected into the coarse-grained layers moved both downwards and upwards into the fine-grained layers, where they travelled radially towards the wetting front.

As shown in figure 4.11a, the pathlines of the dye were directed upward into the fine-grained layers, opposite to the total head gradients that were determined from tensiometer data. This is an apparent imposibility. One must realize, however, that the total head contours drawn represent an integration of highly variable potential fields and that gradients inferred from these contours represent only average gradients. Furthermore, the pressure heads and total heads determined at each tensiometer represent only an average of a range of pressures occuring within the volume of influence of the tensiometer. In reality, the region o

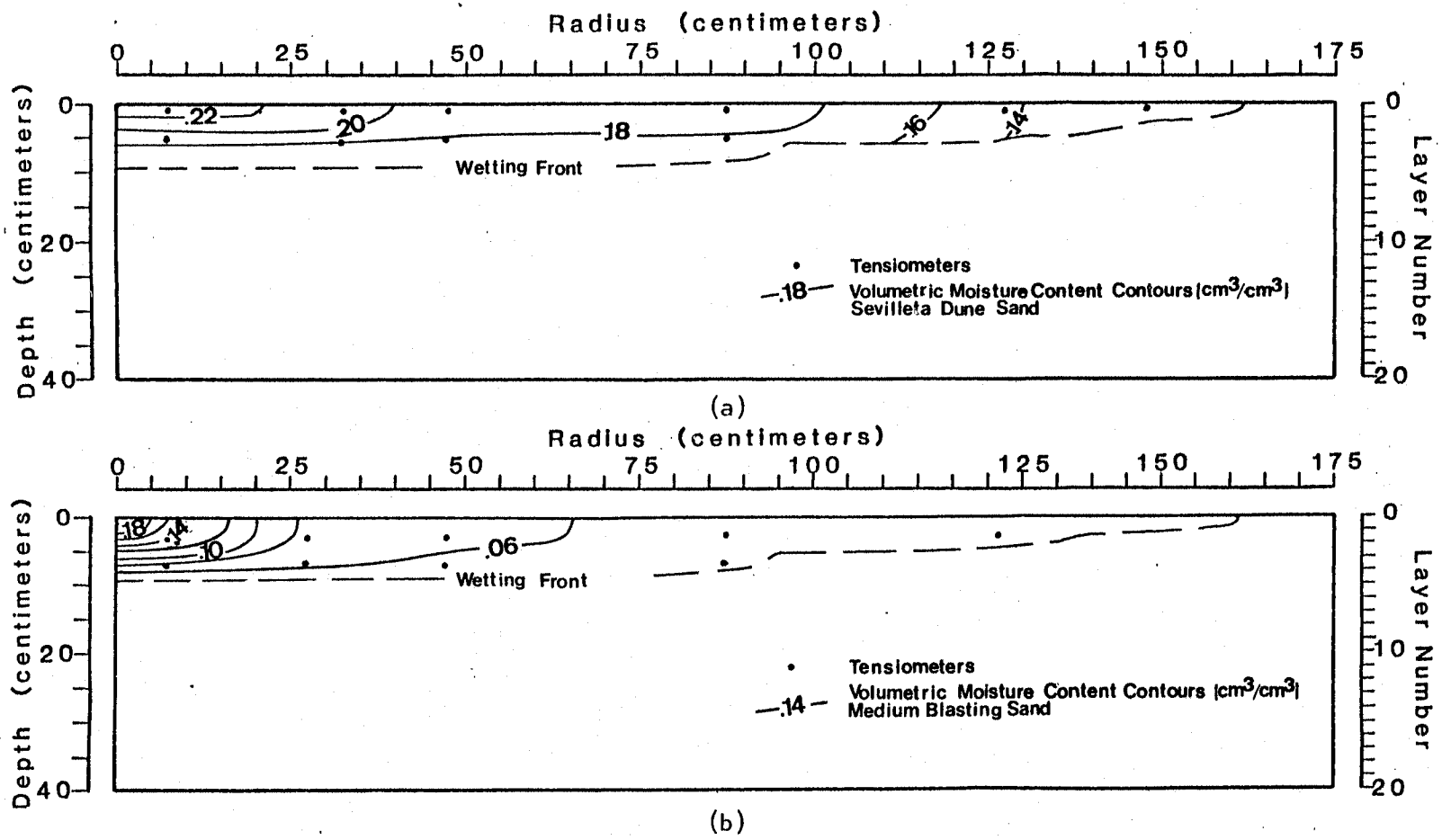

Figure 4.10 Hydraulic conductivity profiles computed separately for the Sevilleta dune sand (a), and the medium blasting sand (b) from tensiometer data collected in each of the two soils for the first experiment.

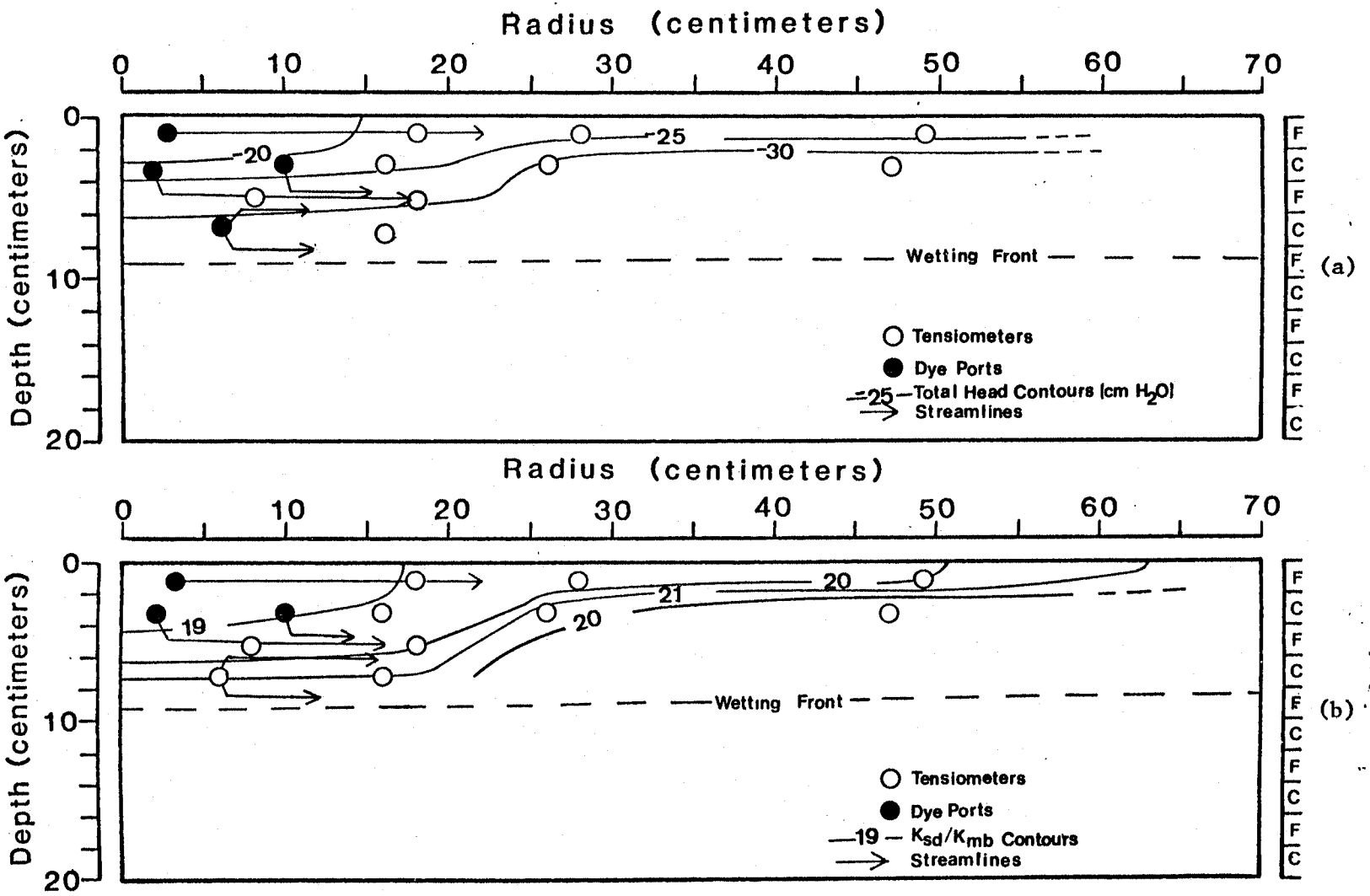

Figure 4.11 Pathlines of dye injected at 4600 minutes in relation to total head (a) and in relation to the ratio K_{sd}/K_{mb} (b) for the first experiment.

influence of a single tensiometer probably included the entire thickness of a layer and may have included several layers. The tensiometers were therefore not precise enough to map local changes in total head occurring within the individual soil layers.

One must also realize that the anisotropy is only an effective anisotropy that results only if flow occurs through a number of layers. In actuality, each layer is homogeneous and isotropic and flow through a given layer occurs only in the direction of the gradient at a given point within that layer. Based upon the idea that the dye moves parallel to the gradient within each layer, the total head profile in Figure 4.11a should look more like the hypothetical total head profile shown in Figure 4.12. This figure, constructed from the movement of dyes in conjunction with the pressure head values determined from tensiometric data, shows both upward and downward total head gradients within the coarse-grained layers. These gradients cause a convergence of pathlines into the fine-grained layers. This behavior is nearly identical to the convergence of pathlines into high-conductivity soil layers that is illustrated in Freeze and Cherry (1979, pg 397) for the flow of contaminants through saturated, layered soil.

Tensiometer data may have produced a total head profile similar to the hypothetical profile shown in Figure 4.12 if the soil layers were thicker and/or if the tensiometers were

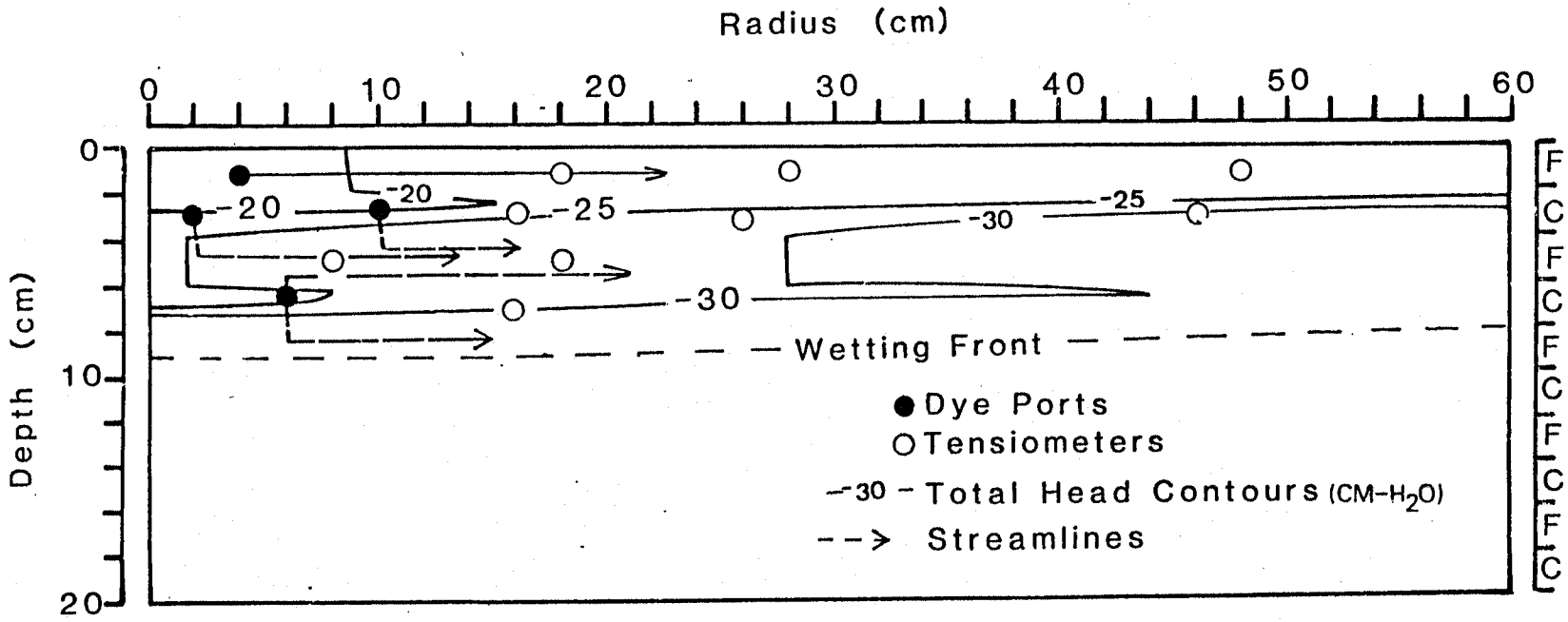

Figure 4.12 Pathlines of dye injected at 4600 minutes, experiment 1, in relation to a hypothetical total head profile constructed from dye movement and tensiometric data.

much smaller. If several tensiometers were placed within each layer and the region of influence for each tensiometer was reduced, the hydraulic gradients could have been mapped with greater precision. However, the purpose of the study was to produce an equivalent anisotropic soil from a layered soil and this could only be done if the total hydraulic gradient changes within layers and even between 2 or 3 layers were ignored.

The first experiment did not effectively produce an equivalent anisotropic system for the reason that only four complete layers were wetted and individual pathlines never crossed more than two layers. A flow system including many more layers would be needed to properly produce an equivalent anisotropic system.

4.2.3 Experiment II

Pressure head and total head profiles were constructed from tensiometer measurements collected at 720 minutes (Figure 4.13). Pressure heads ranged from 0 cm-H_2O at the source to less than -20 cm-H_2O near the wetting front. In most of the region, total head gradients were directed predominantly downwards, making an angle from the horizontal of 75 degrees to 80 degrees on the average.

Volumetric moisture content profiles were constructed from tensiometer data taken at 720 minutes (Figure 4.14). Again, several profiles were constructed for each soil type due to the discontinuities. Volumetric moisture contents ranged from the values of porosity at the source (approximately 0.36 for both soils) to 0.19 and 0.05 near the wetting front for the Sevilleta dune sand and medium blasting sand, respectively. As before, the initial moisture contents of both soils were less than 0.01 but greater than 0.005

Hydraulic conductivity profiles (Figure 4.15) were constructed from pressure head data taken at 720 minutes. Values ranged from 1.9×10^{-2} cm/s to 2×10^{-3} cm/s in the Sevilleta dune sand and 2.3×10^{-1} cm/s to less than 10^{-4} cm/s in the medium blasting sand.

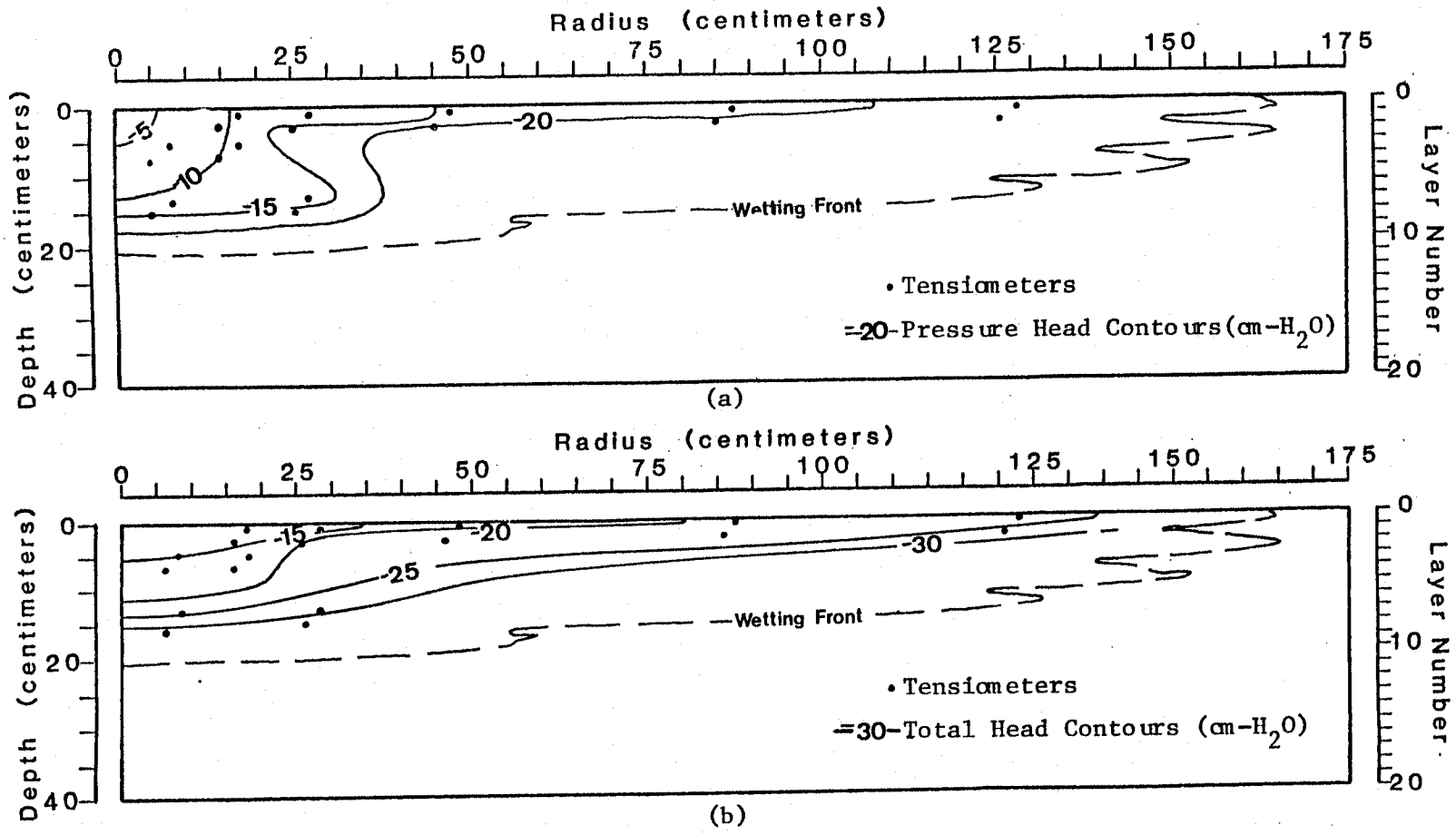

Figure 4.13 Pressure head (a) and total head (b) profiles at 720 minutes for experiment 2.

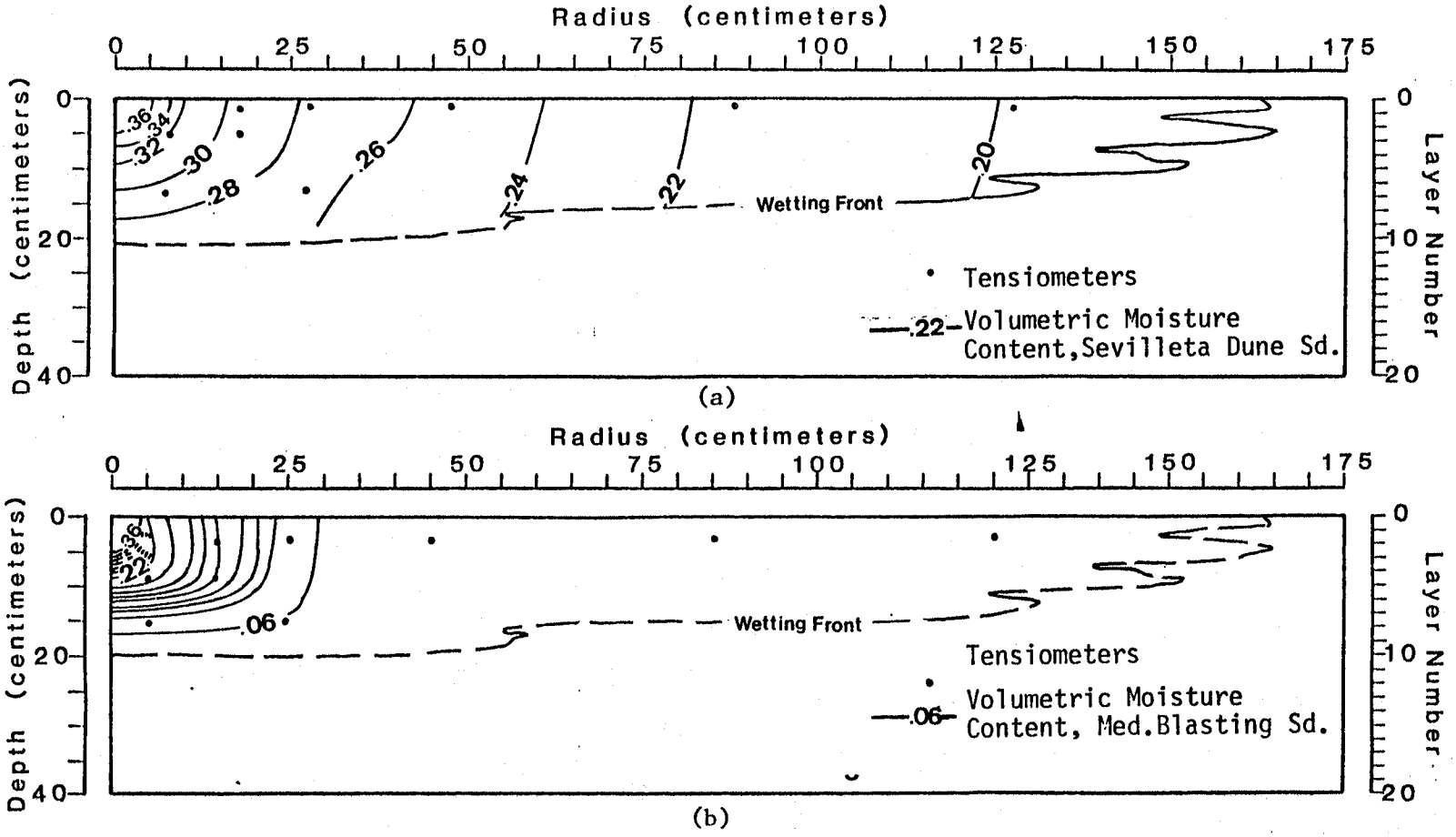

Figure 4.14 Volumetric moisture content profiles computed separately for the Sevilleta dune sand (a), and the medium blasting sand (b) from tensiometer data collected in each of the two soils at 720 minutes for experiment 2.

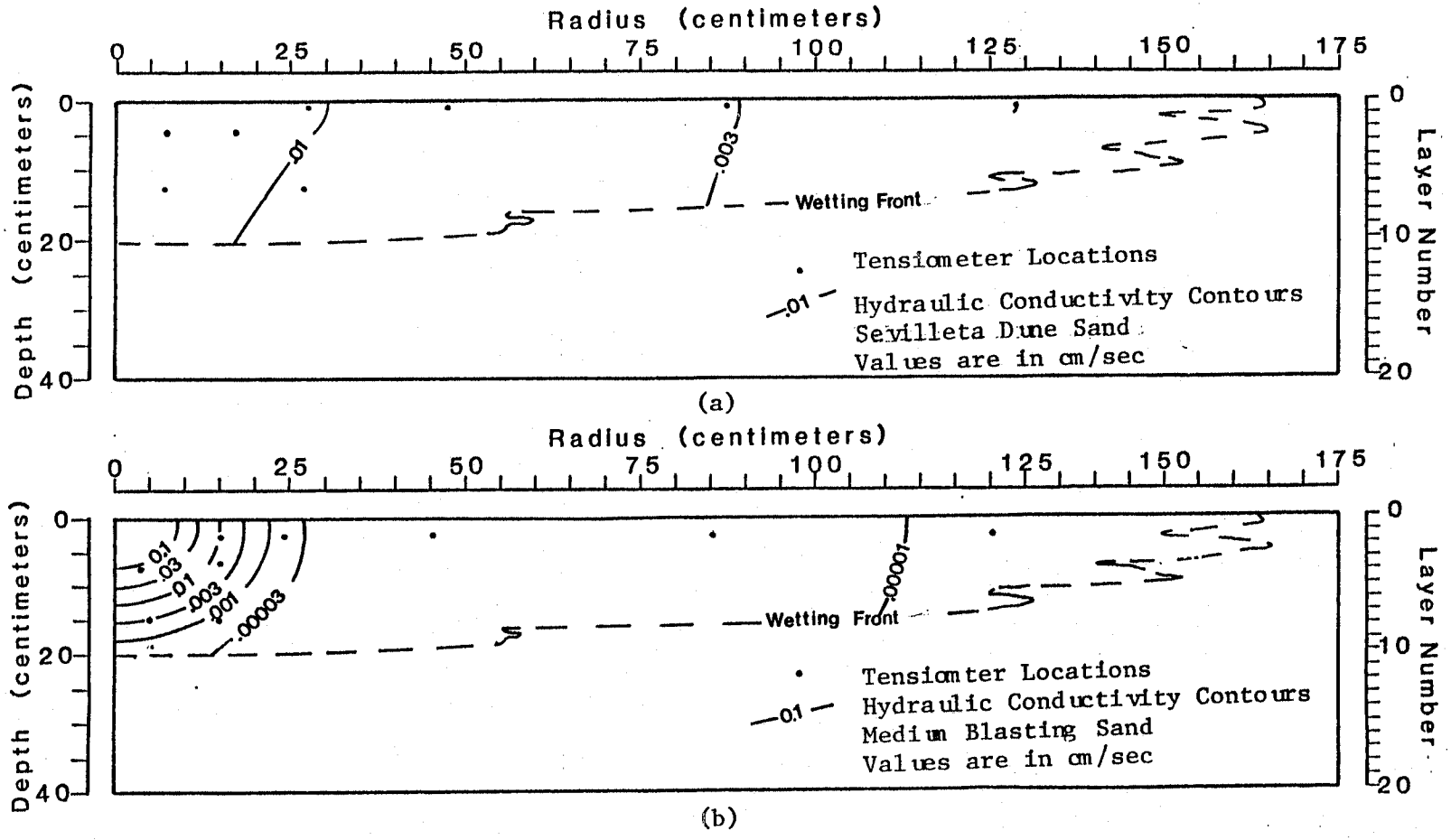

Figure 4.15 Hydraulic conductivity profile computed separately for the Sevilleta dune sand (a) and the medium blasting sand (b) for tensiometric data collected in each of the two soils for the second experiment.

At approximately 180 minutes, dye was injected into two coarse-grained layers at three locations. The outline of the dye movement and the pathlines that the dye followed are shown in relation to the total head profile determined at 720 minutes (Figure 4.16). From the nearly identical behavior of dye movement at 180, 360, and 650 minutes (Figures 4.16 to 4.19), it was assumed that steady-state conditions had been reached in the region shown in Figure 4.16 and that the total head profile within that region did not differ between 180 and 720 minutes. Under steady-state conditions, pathlines coincide with streamlines and are parallel to the specific flux vector.

Near the source, the dye moved in a direction close to that of the gradient. The pathlines increasingly diverged from the gradients as the soil became dryer and eventually were directed only in the radial direction.

The pathlines of the dye injected into the coarse-grained layer at a radius of 20 cm and a depth of 11 cm were directed both upwards and downwards. The upwards movement of the dye occurred in a direction opposite to the gradients inferred from the tensiometer data. At this location, at a very local scale, the dye movement suggests that there is an upwards component of the hydraulic gradient in upper part of the coarse-graine layer and this component is directed towards the overlying fine-grained layer ever though the tensiometer data show that the hydraulic gradient

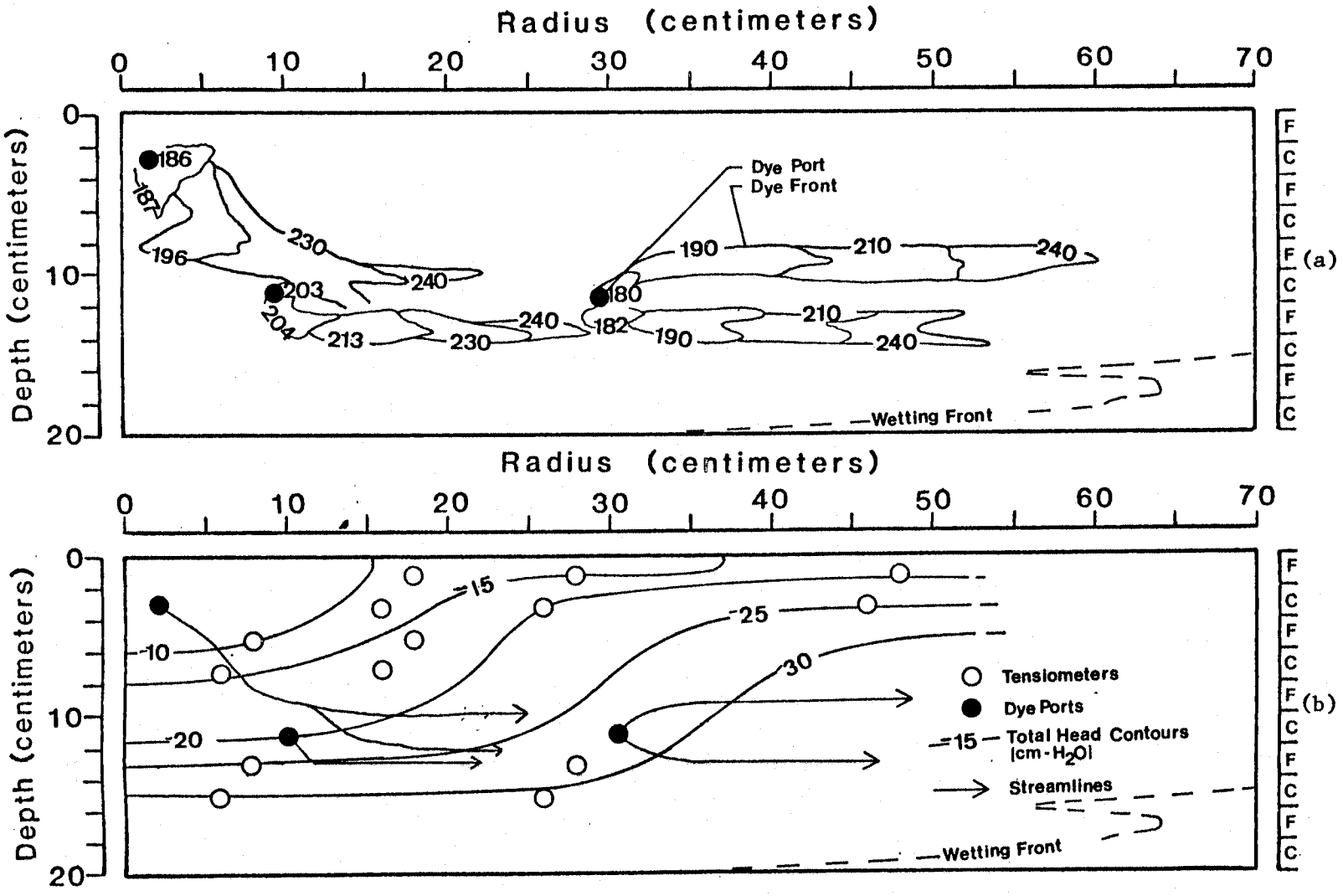

Figure 4.16 Outline of dye front movement (a), and pathlines of dye movement in relation to total head (b) for dye injected at 180 and 186 minutes for

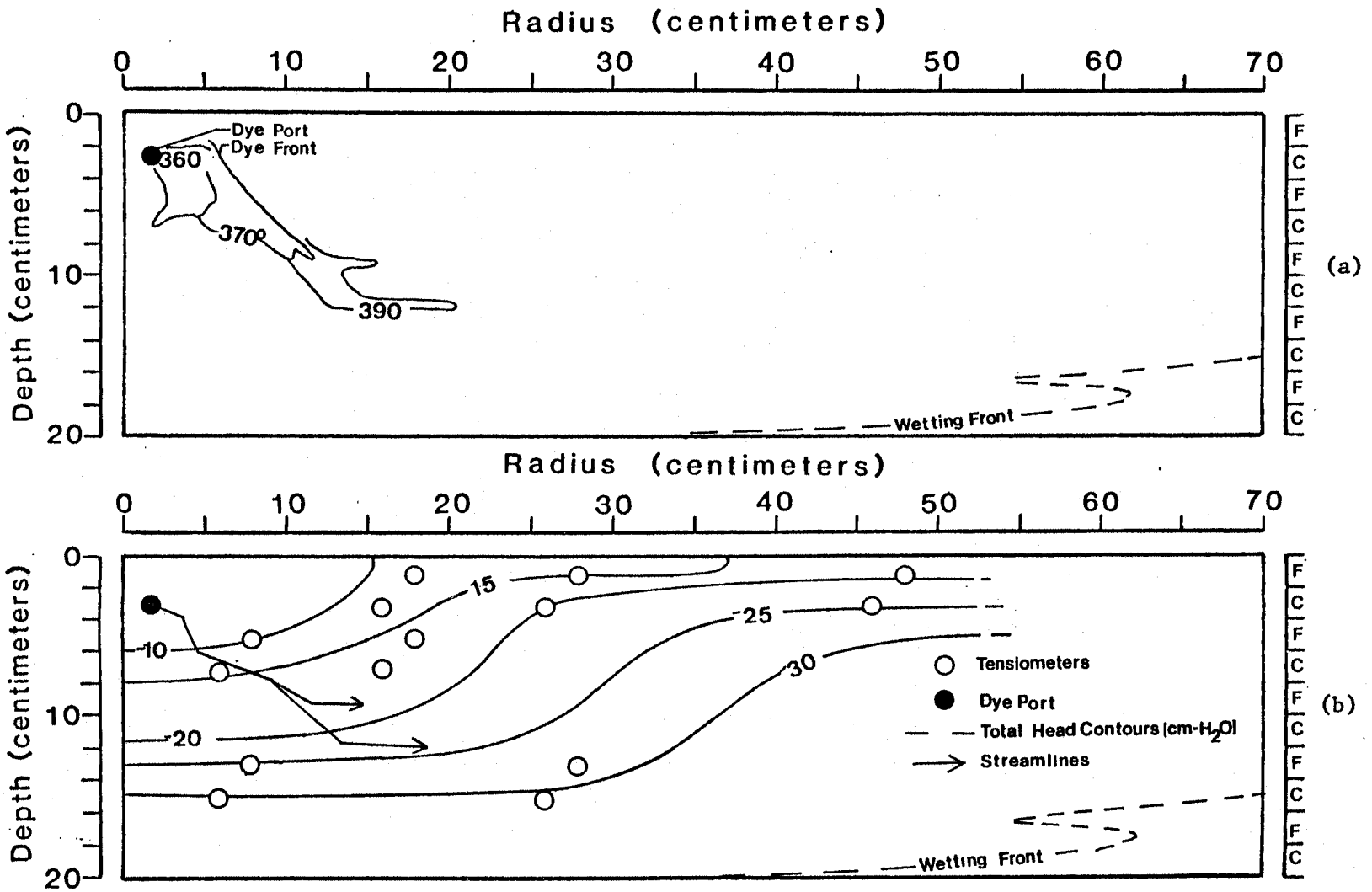

Figure 4.17 Outline of dye front movement (a) and pathlines of dye movement in relation to total head (b) for dye injected at 360 minutes for experiment

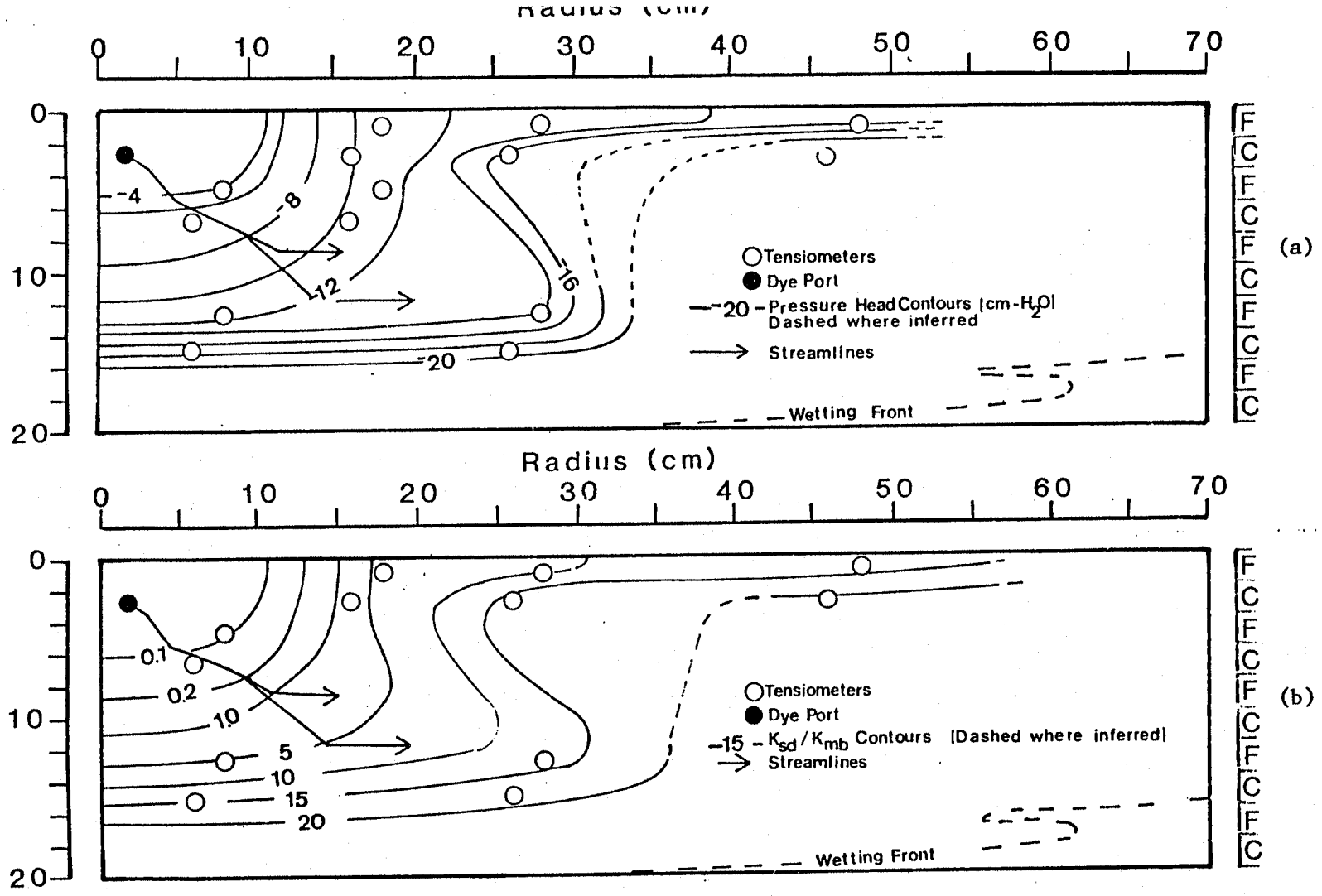

Figure 4.18 Pathlines of dye movement in relation to pressure head (a) and in relation to the ratio K_{sd}/K_{mb} (b) for dye injected at 360 minutes for experiment 2.

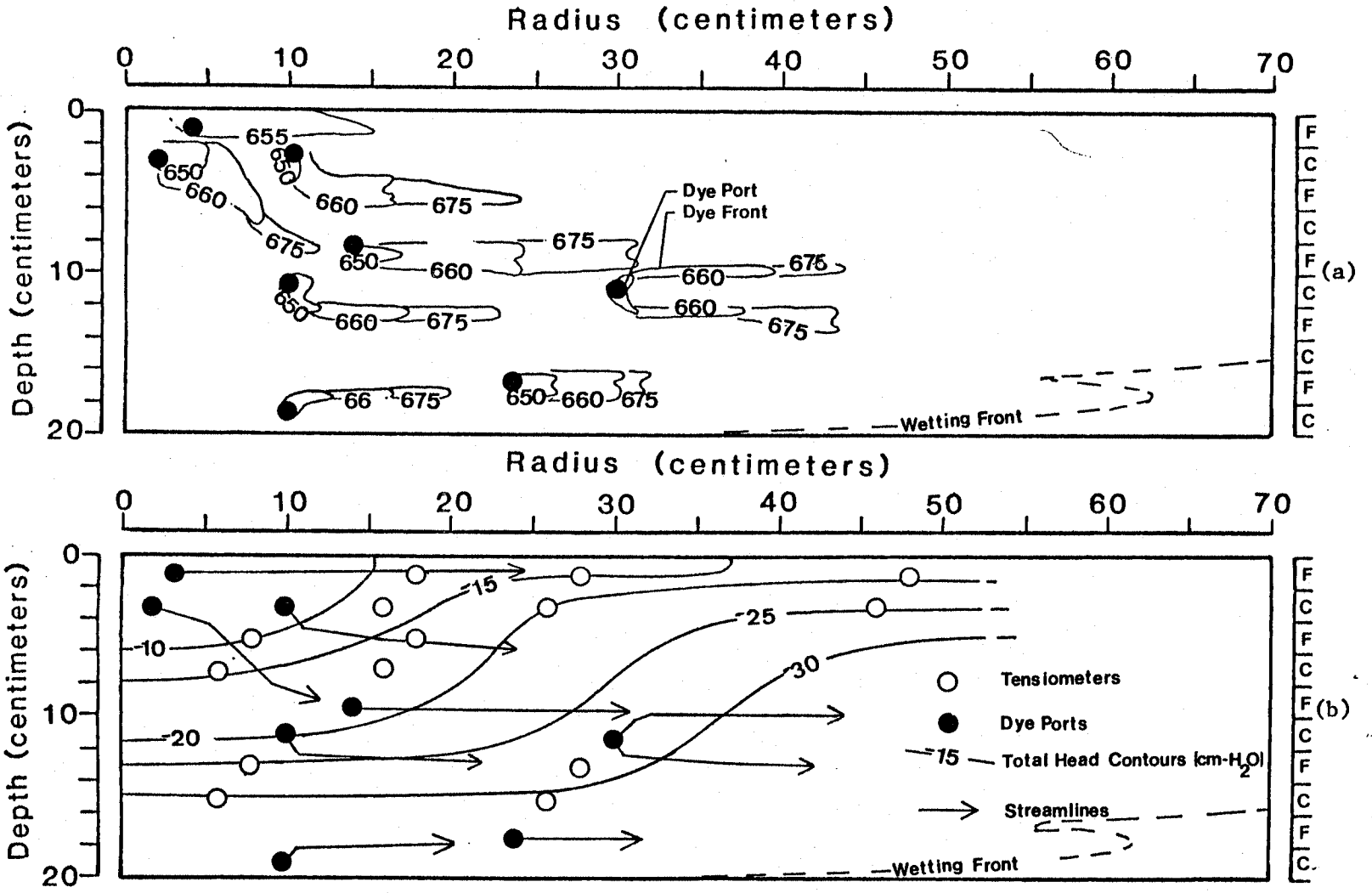

Figure 4.19 Outline of dye front movement (a) and pathlines of dye movement in relation to total head (b) for dye injected at 650 minutes for experiment 2.

is predominantly downwards. Again emphasis must be placed on the fact that the gradients inferred from the total head contours represent only an average of many different gradients.

At 360 minutes, dye was injected into the coarse-grained layer immediately below the source. The outline of its movement and the pathlines that it followed (Figure 4.17) are nearly identical to the outline of dye movement and the resulting pathlines shown for dye injected at the same location at 180 minutes. This similarity indicates that the system is at steady-state for the region shown. The pathlines are shown in relation to the pressure head profile and the profile of the ratio K_{sd}/K_{mb} (Figure 4.18). The pathlines become completely horizontal at a pressure head of -12 cm-H_2O and a K_{sd}/K_{mb} ratio of approximately 7.

At 650 minutes, dye was injected into both the fine-grained and coarse-grained sand at six locations (Figure 4.19). Dyes injected into the fine-grained layers remained in those layers, while dyes injected into the coarse-grained layers travelled immediately into the fine-grained layers. As before, there existed both upwards and downwards gradients in the coarse-grained layers on a local scale, owing to the contrast in hydraulic conductivities between these layers. Only in one case, near the source, did the dye travel through more than two layers

4.2.4 Experiment III

A pressure head profile was constructed from tensiometer data taken at 720 minutes (Figure 4.20a). Pressure heads ranged from 0 cm-H_2O at the source to approximately -22 cm-H_2O at the wetting front. Very little change was noted in pressure head in the vertical direction which suggests that downward flow resulted almost entirely from gravitational forces.

A total head profile (Figure 4.20b) shows a uniform gradient directed at an angle of 75 to 80 degrees from the horizontal.

Volumetric moisture content profiles were constructed from tensiometer data taken at 720 minutes (Figure 4.21). Moisture contents ranged from the value of porosity near the source to 0.20 and 0.05 near the wetting front for the Sevilleta dune sand and the medium blasting sand, respectively.

Hydraulic conductivities (Figure 4.22) also determined from pressure head data taken at the end of the experiment, range from 2×10^{-2} cm/s to 3×10^{-1} cm/s in the Sevilleta dune sand and from 2×10^{-2} cm/s to 10^{-4} cm/s in the medium blasting sand.

A profile of K_{sd}/K_{mb} was constructed from pressure head data also taken at 720 minutes (Figure 4.23). The ratio is less than 1 near the source where the pressure head is

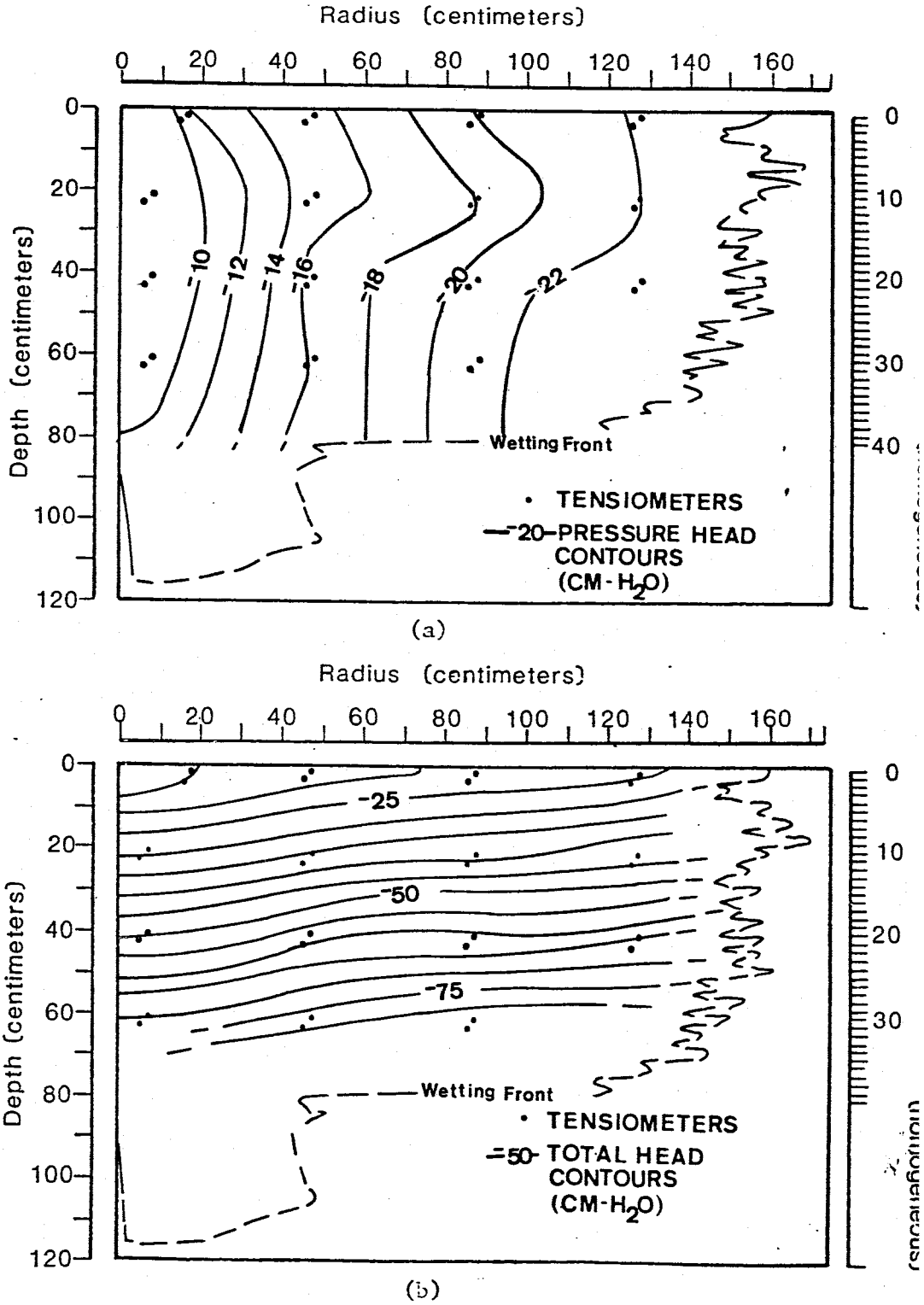

Figure 4.20 Pressure head (a) and total head (b) profiles for experiment 3 based on tensiometric data collected at 720 minutes.

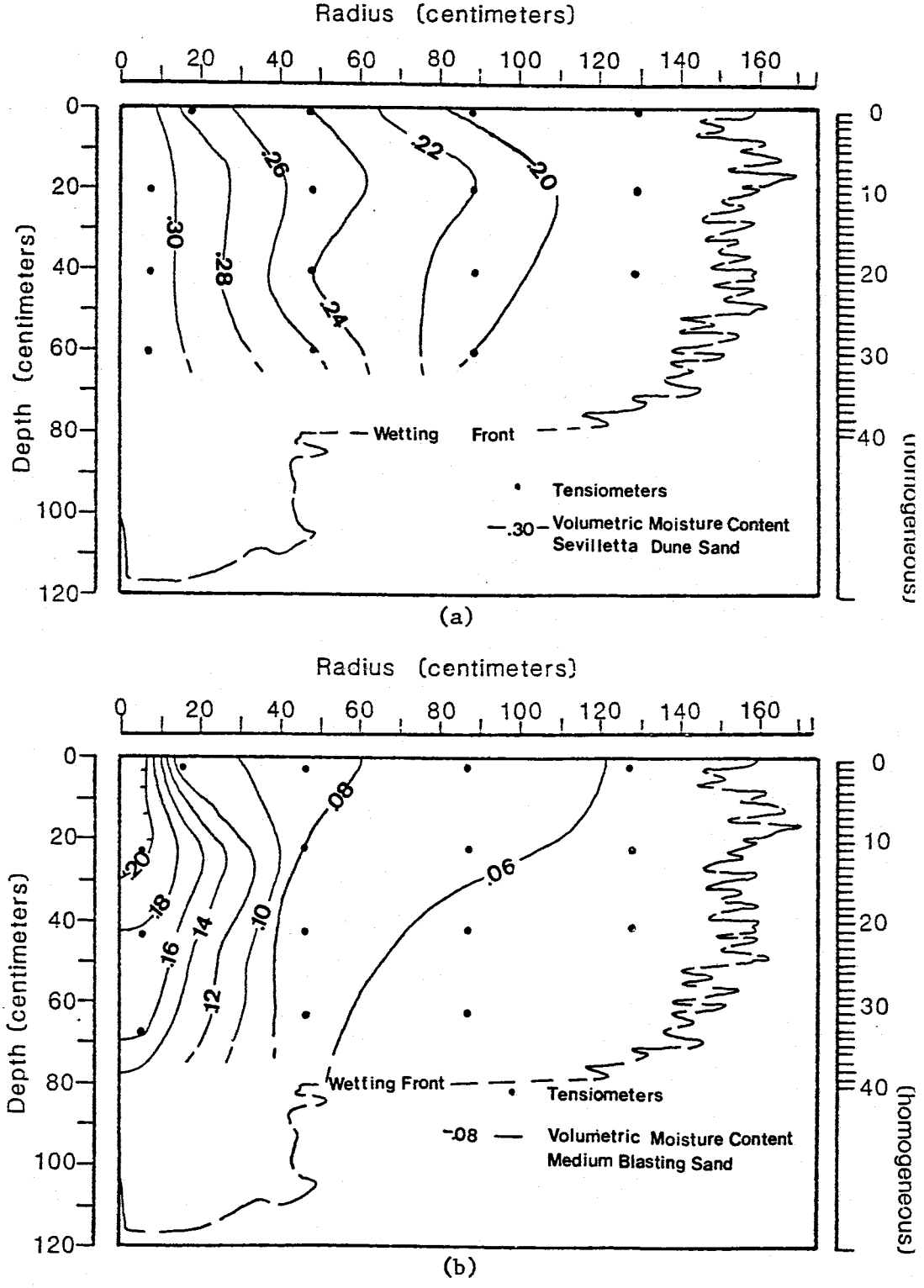

Figure 4.21 Volumetric moisture content profiles computed separately for the Sevilleta dune sand (a) and the medium blasting sand (b) from tensiometric data collected at 720 minutes for

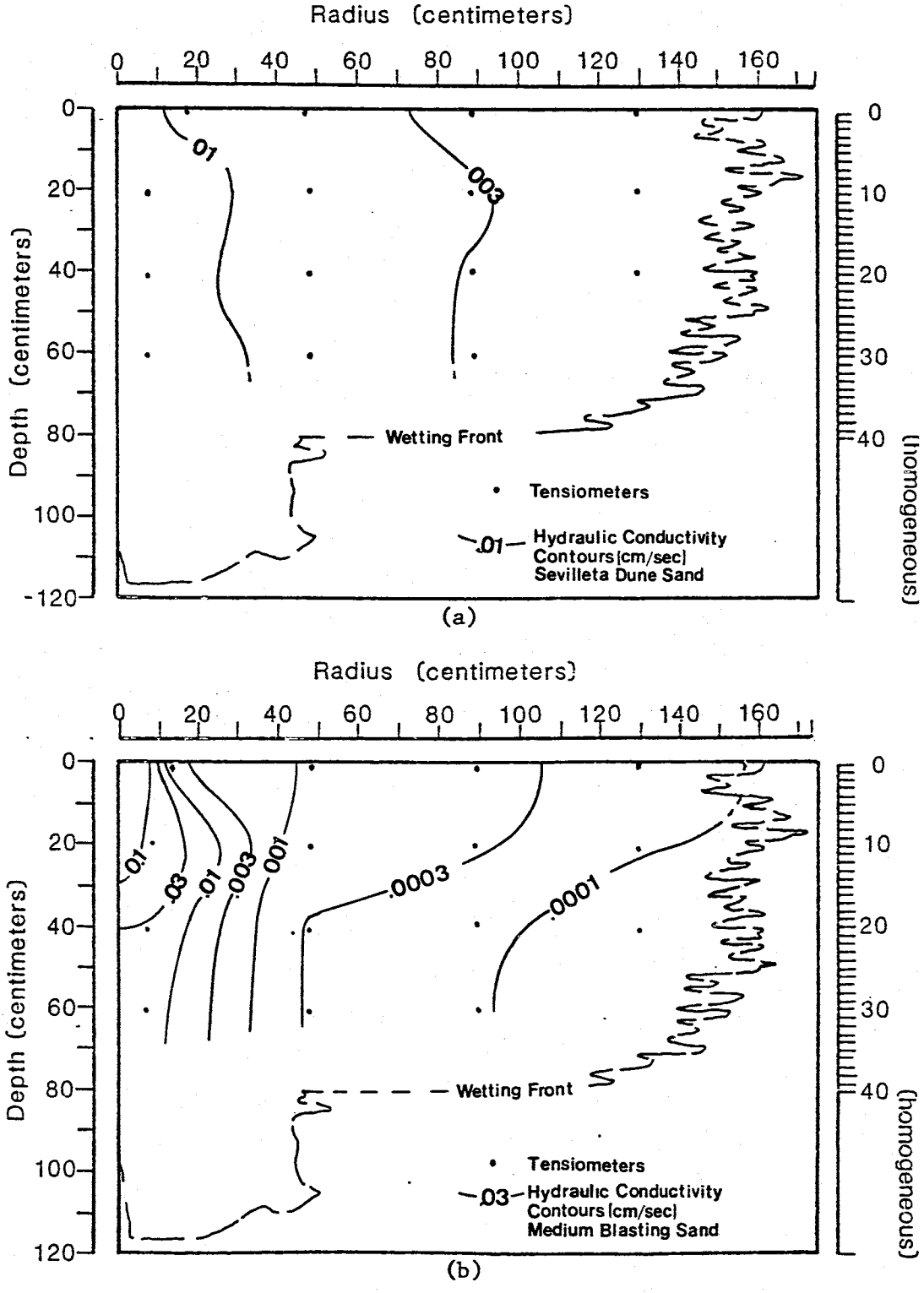

Figure 4.22 Hydraulic conductivity profiles computed separately for the Sevilleta dune sand (a) and the medium blasting sand (b) from tensiometric data collected at 720 minutes for

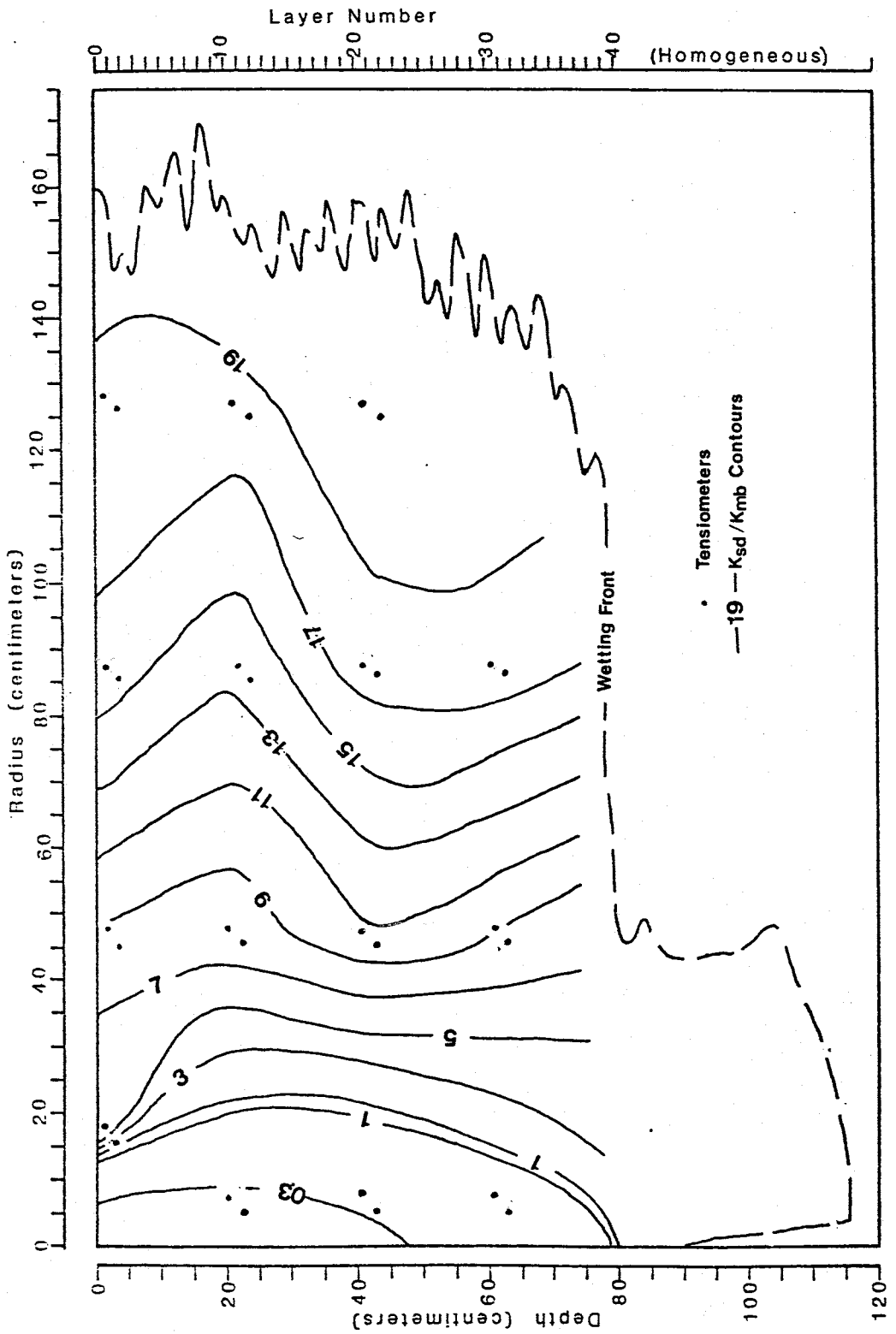

Figure 4.23 Profile of the ratio K_{sd}/K_{mb} determined from tensiometric data collected at 720 minutes for experiment 3.

greater than -10 cm h_2O and K_{mb} is greater than K_{sd}. The ratio increases to a maximum value of 19 near the wetting front.

Figure 4.24 shows the outline of the movement of the dye injected at 740 minutes. Figure 4.25 shows the pathlines that the dye followed in relation to the total head profile. Dyes injected near the source initially followed pathlines that were parallel to the gradients. But with increasing distance from the source, those pathlines diverged becoming more horizontal. In three instances, dyes injected into the coarse-grained layer travelled upward along pathlines that opposed the gradients inferred from the total head profile. This once again demonstrates that the potentials were distributed in a much more complex manner than smoothed contours of the tensiometer data show.

From the pathline labeled A-A', gradient and pathline angles were measured from the vertical axis at the intersections of the pathlines and the total head contour lines. These were plotted as a function of distance along the pathline (Figure 4.26). The pathline diverges gradually from the gradient vector from a distance of 0 to 50 cm along A-A', but then quickly diverges from 50 to 60 cm where the pathline makes a full 90 degree angle from the vertical axis and a 70 degree angle from the gradient.

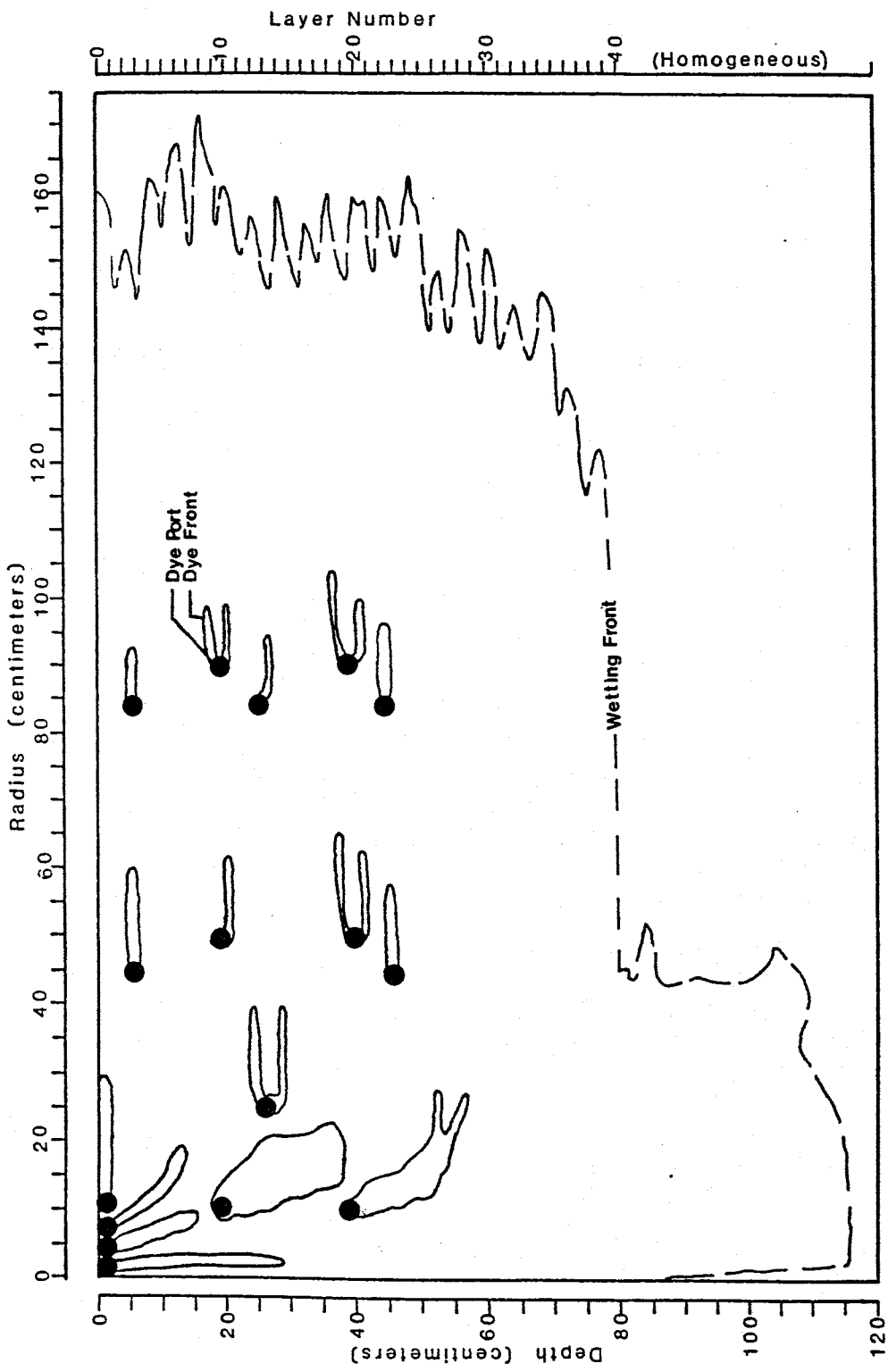

Figure 4.24 Outline of dye front movement for dye injected at 740 minutes for the third experiment.

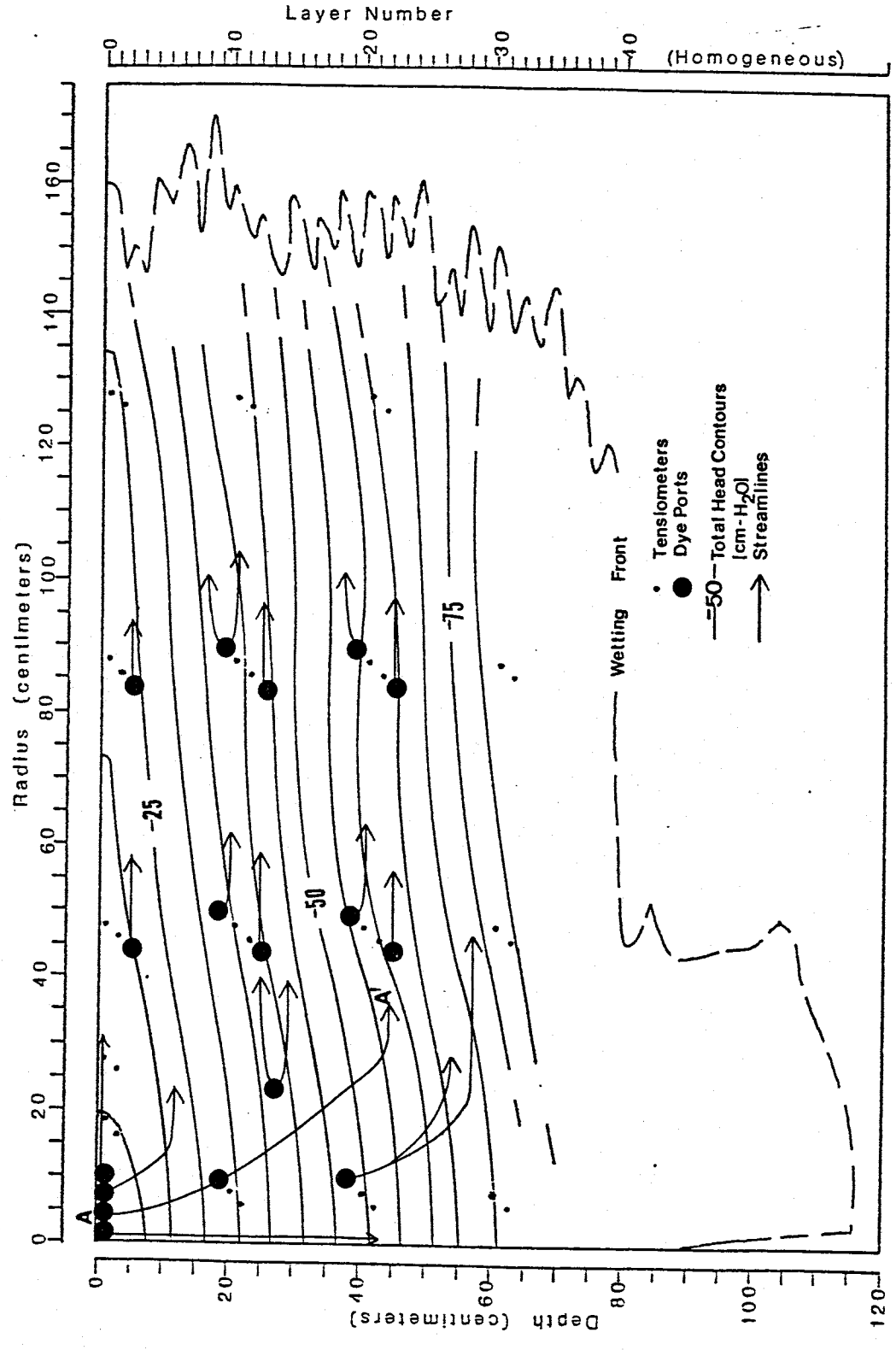

Figure 4.25 Pathlines of dye injected at 740 minutes for experiment 3 in relation to the total head profile.

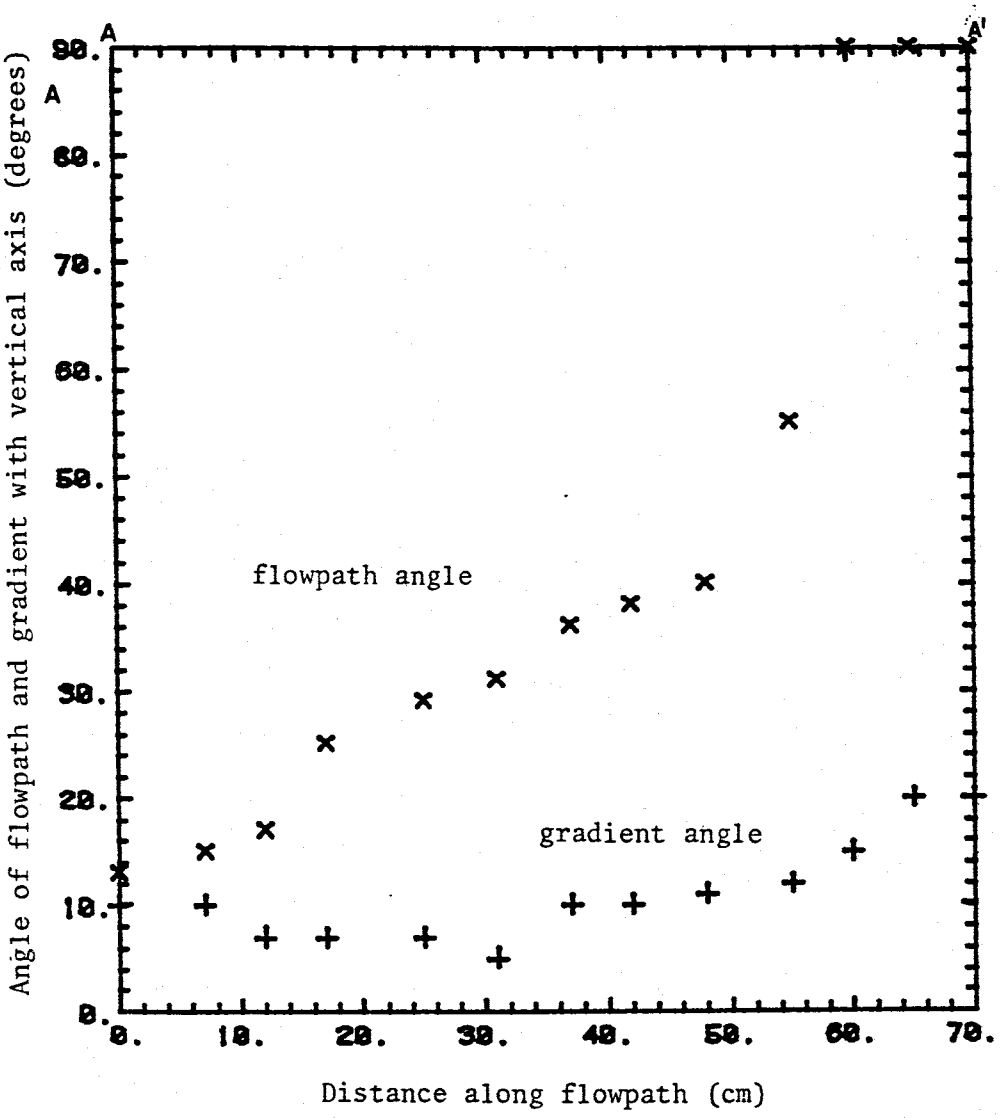

Figure 4.26 Pathline and gradient angles (measured from the vertical axis) versus distance along pathline A-A' of Figure 4.25.

Figure 4.27 shows the outline of dye front movement for dye injected near the source at 578 minutes. Streamlines constructed from the dye movement are shown in Figure 4.28 in relation to the total head profile near the source. Along the numbered intervals, between the points shown, gradient and streamline angles were measured graphically. K_r/K_z was determined using equation 2.7

This was also done for the numbered points in Figure 4.29. The values of K_r/K_z determined from these angles were plotted as a function of the pressure head determined for each point of measurement (Figure 4.30). For comparison, the predicted relationship between anisotropy and pressure head, shown previously in Figure 3.10, and represented by Equation 2.4 is plotted.

From Figure 4.30, it is obvious that Equation 2.4 underpredicted the anisotropies of the system. The reason why the anisotropies were underpredicted is not presently understood. In one-dimensional column studies where flow is directed parallel and normal to layering, the anisotropy predicted by the theoretical model of Mualem may have produced better agreement. But in the axisymmetrical unsaturated flow model, the pressure head distribution which reacted to the varying hydraulic conductivities caused a convergence of the streamlines into the fine-grained layers. This magnified the components of flow in the radial direction and increased the effectiv

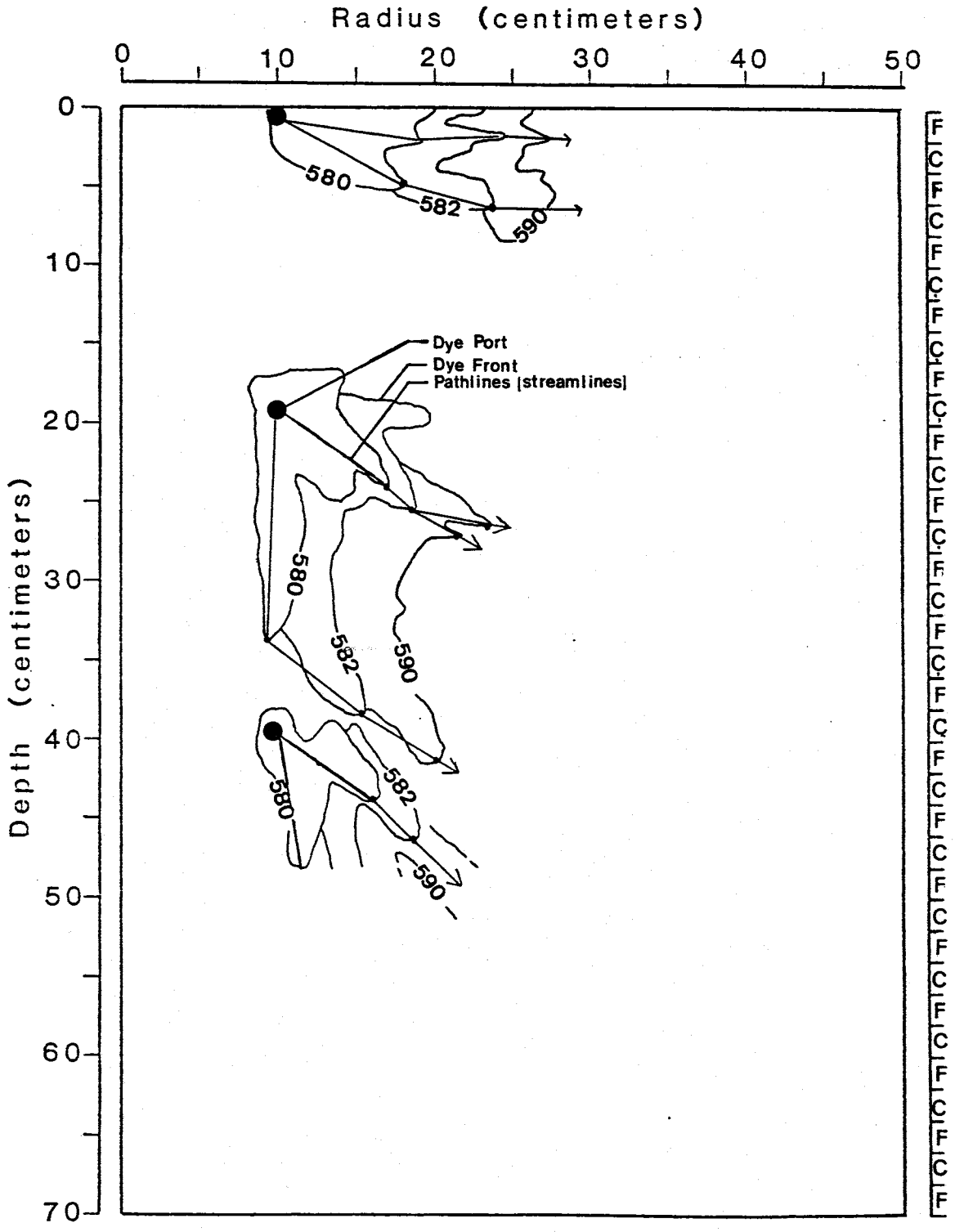

Figure 4.27 Outline of dye front movement near the source for dye injected at 578 minutes for experiment 3.

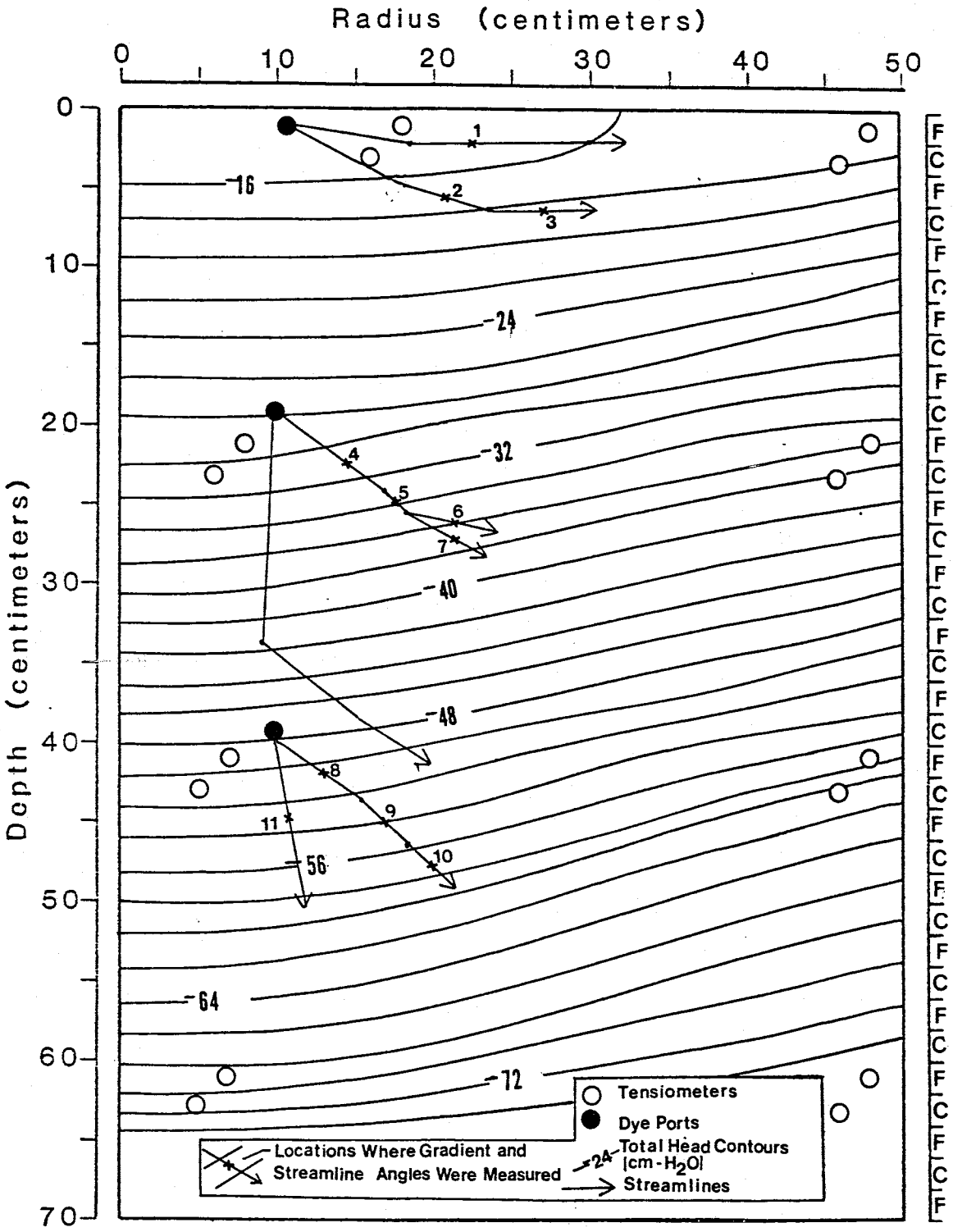

Figure 4.28 Pathlines of dye injected at 578 minutes for experiment 3 in relation to total head. Numbers 1 through 11 refer to locations where gradient and pathline angles were measured.

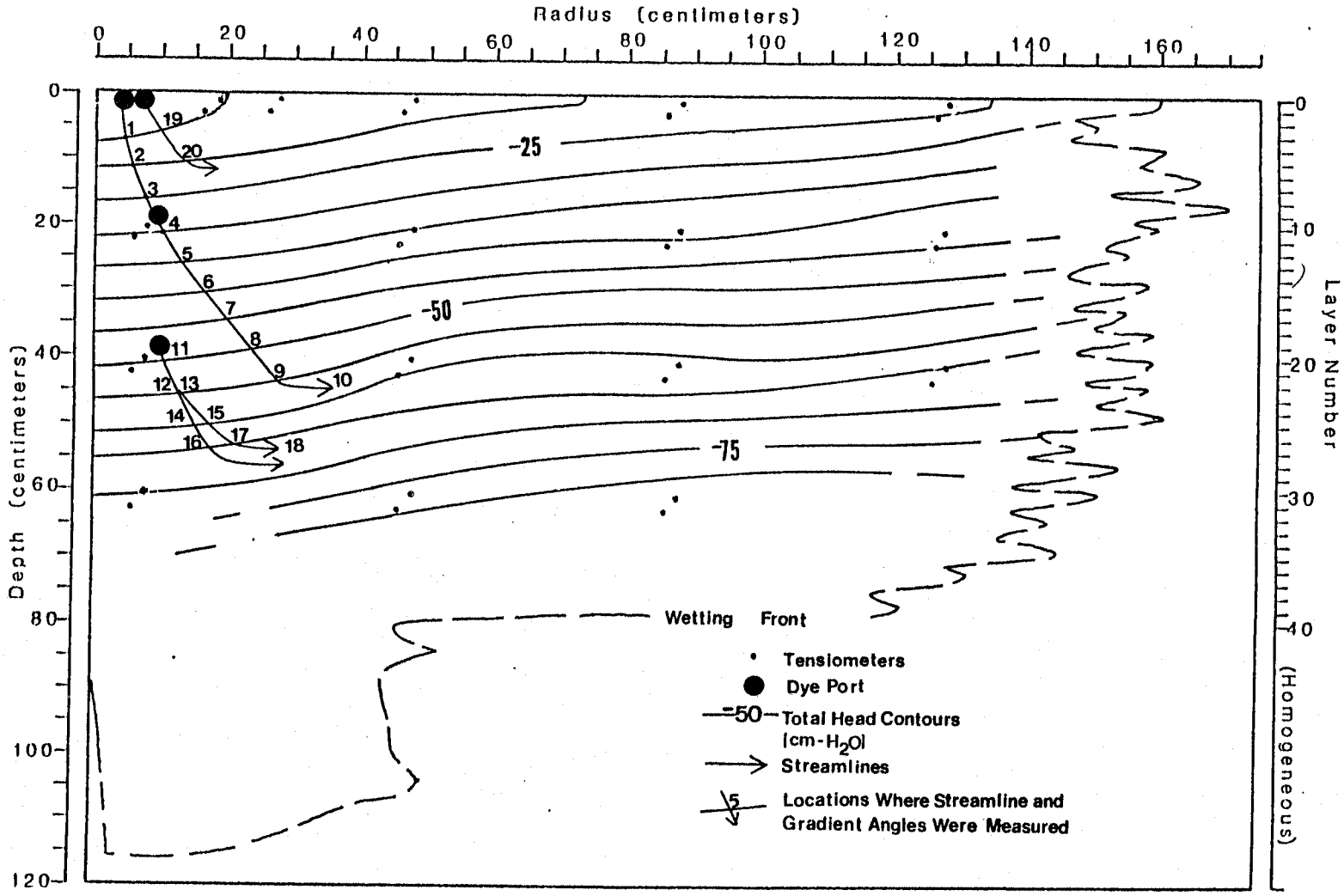

Figure 4.29 Streamlines determined from the movement of dye injected at 740 minutes in relation to total head for experiment 3. Numbers 1 through 19 refer to

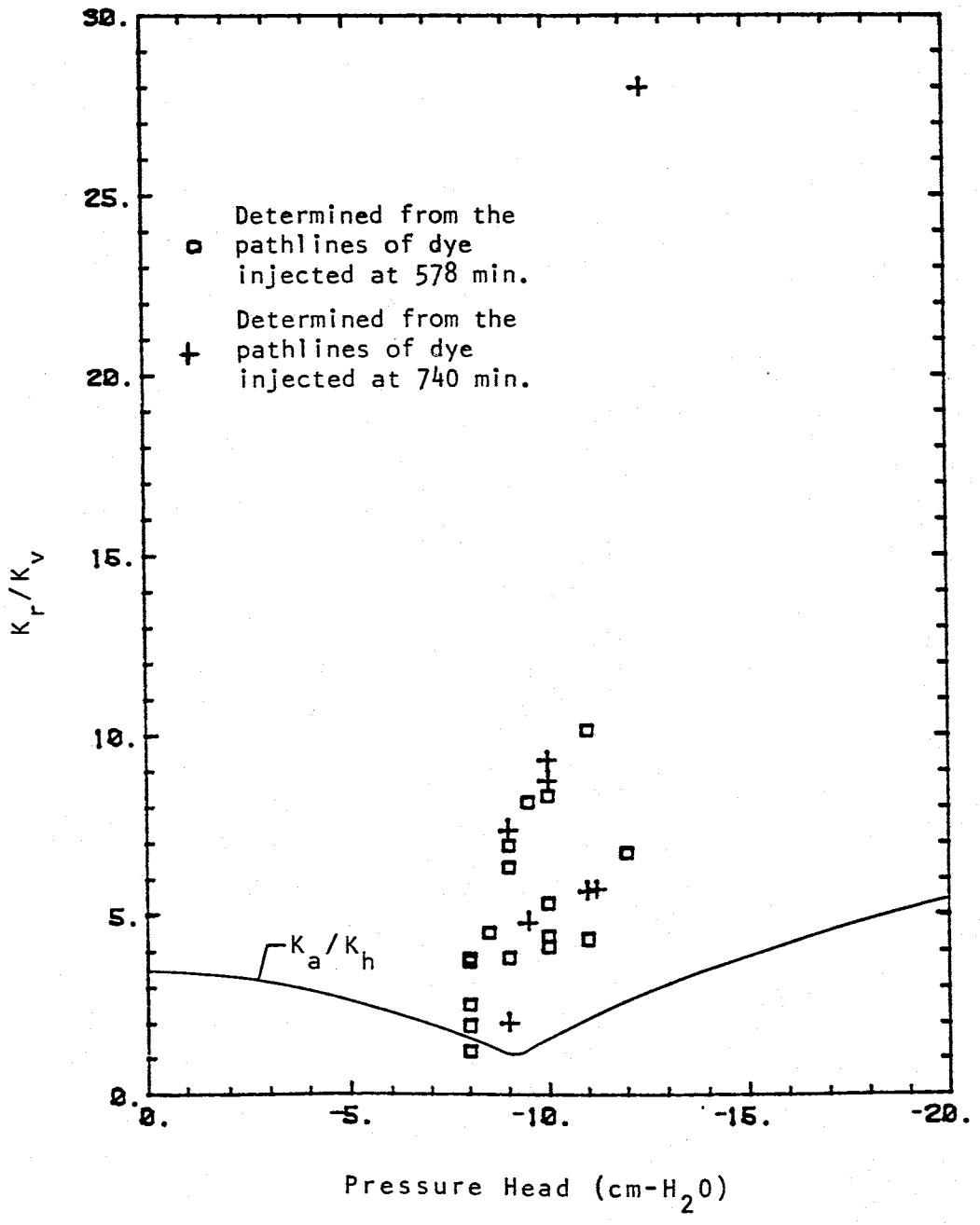

Figure 4.30 K_r/K_z versus pressure head determined from gradient and streamline angles and as determined from equation 2.4.

anisotropies of the flow system to values many times greate than those predicted by Equation 4.12

4.2.5 Discussion

The relationships between pathlines, gradients, a pressure head in each of the three experiments ha demonstrated that anisotropy increases as pressure he decreases in an unsaturated, layered soil. The anisotro is in actuality an effective anisotropy resulting from t variability of the gradient vectors found between and with the individual layers.

Near saturation, there was relatively little variati between gradient vectors within a given volume of soil a as a result, the effective anisotropy was small. But wi increasing soil dryness, the gradients in the fine-grain layers (with greater hydraulic conductivities) increasing became directed parallel to the layers while the gradien in the coarse-grained layers increasingly became direct normal to the layers. The result of this was an increase flow parallel to the layers even through the avera gradient was predominantly downwards. This further result in an increase in the effective anisotrop

As soil dryness increased further, the gradients with the coarse-grained layer became directed both upwards a downwards towards the adjacent fine- grained layers as sh in Figure 4.12. Under this gradient geometry, streamlin

converged into the fine-grained layers and water became essentially trapped within the fine-grained layers and could move only in the radial direction. The result of this was an anisotropy apparently near to infinity

Pathline data from all three experiments showed that flow within the fine-grained layers became virtually horizontal at a pressure head of -13 cm-H_2O and a K_{sd}/K_{mb} ratio of approximately 10. It was also found, from the pathlines of dye movement, that the total hydraulic gradients within the coarse-grained layers changed from downwards to both downwards and upwards at a pressure head of approximately -17 cm-H_2O, which was associated with a K_{sd}/K_{mb} ratio of approximately 15.

Contrasts in hydraulic conductivities that resulted in horizontal flow within the unsaturated region did not appear to cause the same degree of horizontal flow within the saturated region. Where pressure heads were greater than - cm-H_2O, the soil was saturated and the ratio of the hydraulic conductivities of the two soils was approximately equal to 12. (The medium blasting sand had the greatest hydraulic conductivity at saturation) Within this region very little divergence of the streamlines from the gradient was observed. In the unsaturated region, the pressure head associated with this same hydraulic conductivity ratio was -15 cm-H_2O. At this pressure head, all flow was directed horizontally. In light of this, it seems that the reaction

of the flow system to yield very high effective anisotropies may be inherent to unsaturated flow conditions.

4.3 Comparison of Experimental and Steady-State Analytical Results

Profiles of total head determined from the steady-state analytical solution of Raats (1971) are compared to observed profiles for experiments 1 and 2 (Figure 4.31) and experiment 3 (Figure 4.32). For the first two experiments, there is little correlation between the observed and predicted profiles. This may be due to the inaccuracy of the equation used, the inaccuracy of the parameters used in the equation, an insufficient number of layers wetted so that an equivalent anisotropic system was not produced, or the observed total head profile was inaccurately constructed due to an insufficient number of data points. In the third experiment the observed and predicted total head profiles coincide immediately below the source. These profiles, however, become increasingly different as the radial distance from the source increased. This is probably because anisotropy increases with decreasing pressure head, whereas the analytical model assumed a fixed anisotropy

The effect of anisotropy on an unsaturated axisymmetric flow system is two-fold. First, the total head profile is

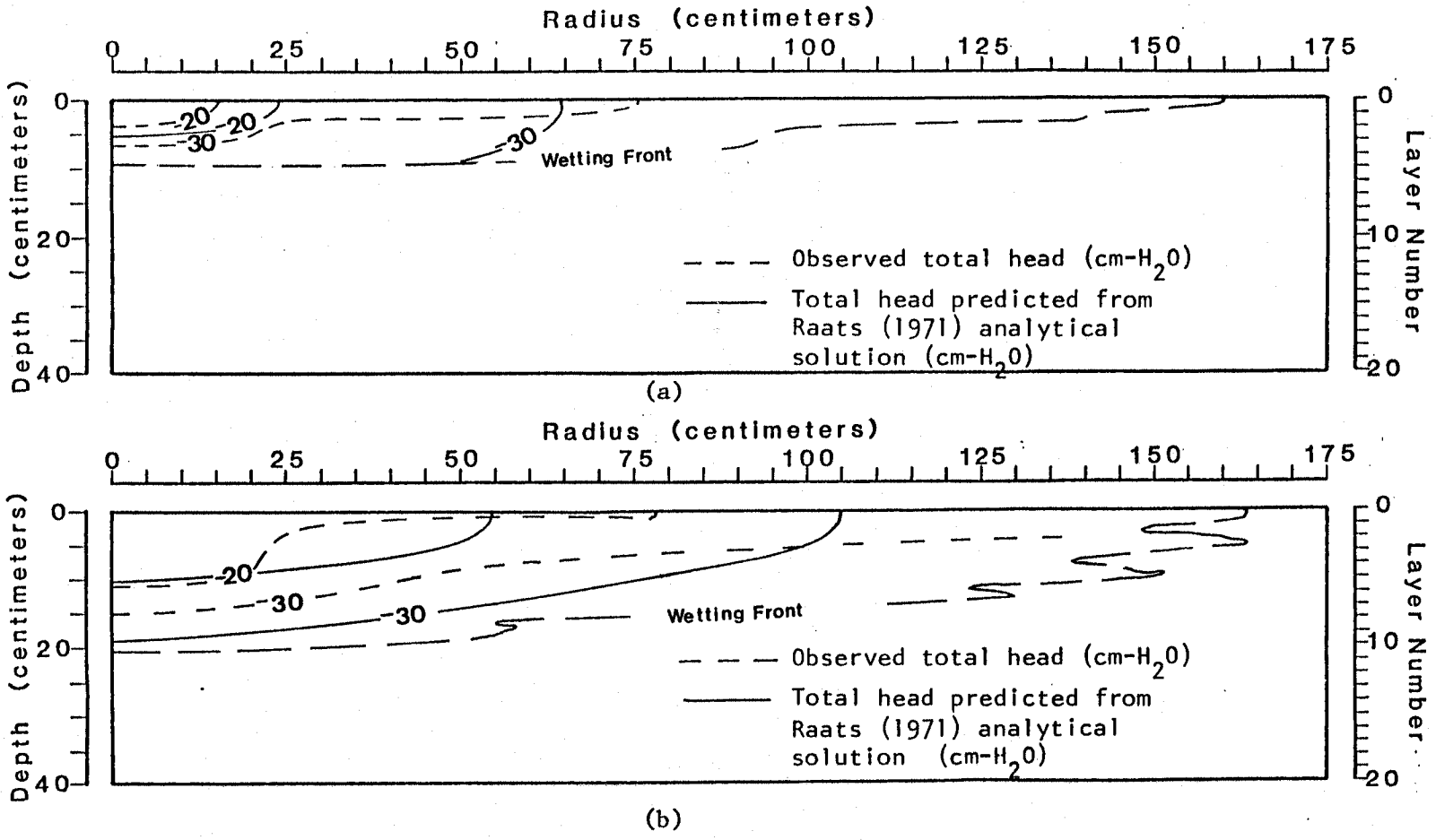

Figure 4.31 Observed total head profiles in relation to profiles predicted from Raats (1971) analytical solution using a scaling factor of 3.5. (a) Experiment 1 values, (b) experiment 2 values.

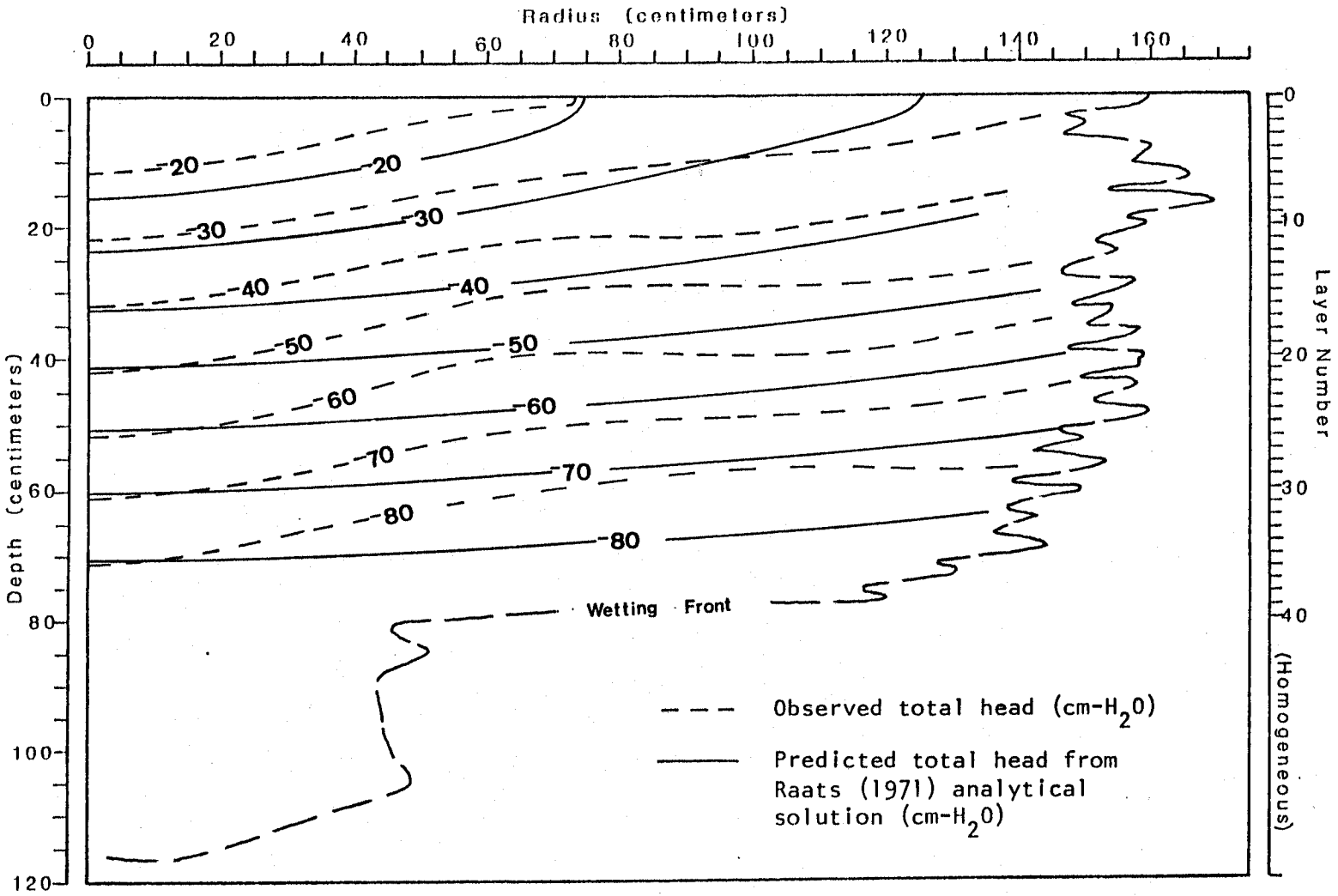

Figure 4.32 Observed total head profile in relation to profiles predicted by Raats (1971) analytical solution, scaled by a factor of 3.5 for

unity. Secondly, streamlines diverge from the gradients which are defined by total head profile.

The total head profiles shown in Figures 4.31 and 4.32 suggest that the anisotropies controlling the distribution of total head may be smaller than the anisotropies determined from the analysis of the streamline and gradient data and may in fact be much closer to the values of anisotropy predicted using Equation 2.4. This is suggested by the reasonable correlation in experiment 3 between the observed total head profile and the total head profile that was predicted by scaling the analytical solution of Raats (1971) (equation 2.12) by a constant value of 3.5. If indeed, the anisotropies that controlled the distribution of total head approached infinity (as did the anisotropies observed from the streamline and gradient data), then one would expect the total head contours, mapped in the three experiments, to be scaled radially by values that approached infinity. The intersection of the -20 cm-H_2O total head contour lines with the radial axis in Figures 4.31 and 4.32 demonstrates that these contour lines were not scaled by a value that approached infinity.

It appears that the distribution of total head is influenced by anisotropies that vary less with pressure head than do the anisotopies that influence the divergence of streamlines from total head gradients. The reason for this discrepancy is not presently understood because it is not

presently understood why the anisotropies measured from the streamline and gradient data are so much greater than those predicted using equation 2.4. It can only be speculated that the reason for this discrepancy may lie in the fact that the soil is not a truly anisotropic soil, but a heterogeneous soil and that the anisotropies observed in this soil are only effective anisotropies.

CHAPTER 5

CONCLUSIONS

Observations of the anisotropic behavior of axisymmetrical infiltration from a point source through a layered soil support the conceptual models of Mualem (1984) and Yeh (1985) that anisotropy increases with decreasing pressure head in an unsaturated, layered soil. Observations were made of the behavior of streamlines, which were mapped from the movement of dyes, and which were found to diverge from the average total hydraulic gradients as the distance from the point source increased and as the pressure head of the soil decreased.

Measurements of anisotropy, based upon the divergence of streamlines from average total hydraulic gradients, showed that anisotropy increased much more with decreasing pressure head than was predicted from the unsaturated hydraulic conductivities of the individual soil layers. Below pressure head values of -13 cm-H_2O, the dye movement was virtually horizontal, even though the average total hydraulic gradients were predominantly downwards. This suggested that anisotropy approached an infinite value at a pressure head of -13 cm-H_2O. This is in high contrast to the predicted anisotropy value of 3 at pressure head of -13 cm-H_2O.

Pathline data from all three experiments showed that at pressure heads less than -16 cm-H_2O, flow within the coarse-grained layers became directed both upwards and downwards towards the adjacent fine-grained layers of greater hydraulic conductivity, even though the tensiometer data showed that the hydraulic gradients were predominantly downwards. This suggested that there existed very localized upward components of the hydraulic gradient in the upper part of the coarse-grained layers.

The use of an analytical solution (Raats, 1971) for infiltration from a point source into a homogeneous, isotropic soil was found to be ineffective in predicting flow behavior in a layered soil. The analytical solution was ineffective because it could not be properly scaled due to the varying anisotropy of the soil and therefore could not properly predict the distribution of total hydraulic head within the soil. The analytical solution was also ineffective because it could not predict the orientations of the streamlines since the streamlines were not parallel to the total hydraulic gradients, but instead occured at highly variable angles to these gradients.

Anisotropic behavior was also observed from the movement of the wetting front. Radial movement of the wetting front was found to be consistantly greater than vertical movement in all three experiments. This is in contrast to the wetting front behavior in homogeneous, isotropic soils where wetting

fronts advance faster in the vertical direction than in the radial direction.

It was found that the ratio of the radial and vertical distances to the wetting front, measured from the point source, remained relatively constant during each of the experiments. It was also found that this ratio increased, between experiments, as the flow rate decreased. This suggested that the ratio of the radial and vertical distances to the wetting front increased as a result of an increase in the anisotropy of the flow system. This further suggests that the anisotropy of the flow system is dependent on the rate of flow at the source. However, because the ratio of the radial and vertical distances to the wetting front may vary with flow rate in homogeneous, isotropic soils, the observed change in this ratio could not be related solely to anisotropic behavior.

Observations of wetting front movement revealed that the moisture moved through the fine-grained layers horizontally and that moisture moved into the coarse-grained layers vertically from both the underlying and overlying fine-grained layers. No wetting front instability was observed in any of the three experiments. This suggests that wetting front instability may not be as significant at low flow rates and under three-dimensional or axisymmetrical flow conditions as it is for one-dimensional flow conditions.

Chapter 6

FUTURE WORK

This study demonstrated many concepts of flow in unsaturated soils. It also raised many questions concerning unsaturated flow through layered soils. For instance, what are the effects of the layer thicknesses? If the layers were thinner with respect to the flow system, would changes in the behavior of streamlines and gradients result? What were the actual changes in pressure head within the layers? What would be the effect of a higher flow rate? Would a higher flow rate show a linear trend between the ratio of the horizontal and vertical distances to the wetting front and the log of the flow rate? Would a higher flow rate cause wetting front instabilities to occur?

In a future laboratory study, the soil layers could be made thicker so that several tensiometers may be placed in each layer so that pressure head profiles could be determined within the layers.

The flow system could also be studied using a numerical flow model. Employing sensitivity analyses, one could study the effects on the unsaturated flow system resulting from changes in numerous boundary conditions such as flow rate, layer thickness, and the hydraulic conductivities of the layers. One could write a numerical model for unsaturated

flow in a homgeneous, anisotropic soil and compare results from that model to results from a model of unsaturated flow through a layered soil. Finally one could use a numerical model to study the pressure head distribution within each layer of a layered profile. One would then obtain a better understanding of the flow system and be better able to predict unsaturated anisotropy in a layered soil.

Chapter 7

REFERENCES

Abramowitz M., and I.A. Stegum, Handbook of mathematical functions, Nat Bur. Stad. Appl Math. Ser., Vol 55 U.S. Government Printing Office, Washington D.C., 1964.

Bear, J., Dynamics of fluids in porous media, 746 pp., Elsevier, New York, 1972.

Bruce, R. R. and A. Klute, The measurement of soil moisture diffusivity, Soil Sci. Soc. Proc.,20, 458-462, 1956.

Crosby, J. W., D. C. Johnstone, C. H. Drake, and R. L. Fenston, Migration of pollutants in a glacial outwash environment, Water Resourc. Res., 4 (5), 1095-1113, 1968.

Diment, G. A. and K. K. Watson, Stability analysis of water movemment in unsaturated porous materials 3. experimental studies, Water Resourc. Res., 21(7), 979-984, 1985.

Freeze, R. A. and J. A. Cherry, Groundwater, 604 pp., Prentice Hall, Englewood Cliffs, 1979.

Hill, D. E. and J. Y. Parlange, Wetting front instability in layered soils, Soil Science Soc. Amer. Proc., 36, 697-702, 1972.

Hillel, D., Fundamentals of Soil Physics, 385 pp., Academic Press. New York, 1980a.

Hillel, D., Applications of Soil Physics., 385 pp., Academic Press, New York, 1980b.

McKee, C. R., J. T. Laman, T. L. Dehsler, and R. H. Jacobsen, Use of a Competer Model to Select Monitoring Locations in the Vadose Zone, in Proceedings of the NWWA/U.S. EPA Conference on Characterization and Monitoring of the Vadose (Unsaturated) Zone, National Water Well Association, Worthington, Ohio, 133-165 (1983).

Miller, D. E. and W. H. Gardner, Water infiltration into stratified soil, Soil Science Soc. Amer. J., 26,

Mualem, Y., Anisotropy of unsaturated soils, Soil Sci. Soc. Am. J., 48, 505-509, 1984.

Palmquist, W. N. and A. I. Johnson, Vadose flow in layered and non-layered materials, U.S. Geological Survey Prof. Paper 450-C, c142-c143, 1962.

Philip, J. R., Theory of infiltration, Adv. Hydrosci., 5, 215-290, 1969.

Philip, J. R., Stability analysis of infiltration, Soil Sci. Soc. Amer.Proc., 39, 1042-1049, 1975a.

Philip, J. R., The growth of disturbances in unstable infiltration flows, Soil Sci. Soc. Amer. Proc., 39, 1049-1053, 1975b.

Raats, P. A. C., Steady infiltration from point sources, cavities, and basins, Soil Sci. Amer. Proc., 35, 689-694, 1971.

Raats, P. A. C., Unstable wetting fronts in uniform and nonuniform soils, Soil Sci. Amer. Proc., 37, 681-685, 1973.

Routson, R. C.; W. H. Price, D. J. Brown, and K. R. Fecht, "High-level waste leakage from the 241-T-106 Tank at Hanford", Earth Sciences Research Group, Rockwell International, RHO-ST-14, 1979.

Wygal, R. J., Construction of models that simulate oil reservoirs, Society of Petroleum Engineers Journal, 281-286, 1963.

Yeh, Jim, Lynn Gelhar, and A. L. Gutjahr, Stochastic analysis of unsaturated flow in heterogeneous soils: Part I. statistically isotropic media, Part II. statistically anisotropic media with variable alpha, Part III. observations and applications, Water Res. Resourc. Res.,21, 447-471, 1985.

Zavlavsky, D. and G. Sinai, Surface Hydrology: IV-Flow in sloping layered soil, J. Hydr. Div., Amer. Soc. Civil Eng., 53-64, 107 (HY1), 1981.

APPENDIX 1

DETERMINING SOIL DIFFUSIVITY

This section provides a detailed outline of th procedures used to determine the soil diffusivity of th Sevilleta dune sand and the medium blasting sand. Th procedures used in the analysis were based on the method c Bruce and Klute, (1956).

The column, shown in Figure A1.1, was filled in manner similar to the filling of the sand tank. Soils wer introduced to the column by slowly pouring the sand throug a stack of two seives (No.8 and No.10 standard seives). Th seives did not retain the sand, but bounced the grain around producing a homogeneous soil with a bulk density tha was much higher than would exist if the soil was simpl poured in. This method of filling is similar to the metho of Wygal (1961). Before and after being filled, the colur was weighed so that the dry bulk density of the soil coul be determined.

The apparatus was set up as shown in Figure A1.1. marriot apparatus, consisting of a burrette and a bubbl tube, provided a constant head source. The base of th bubble tube was placed at an elevation equal to that of th center of the soil column so that the pressure head would l equal to zero at point A shown in Figure A1.1.. Tube B wa

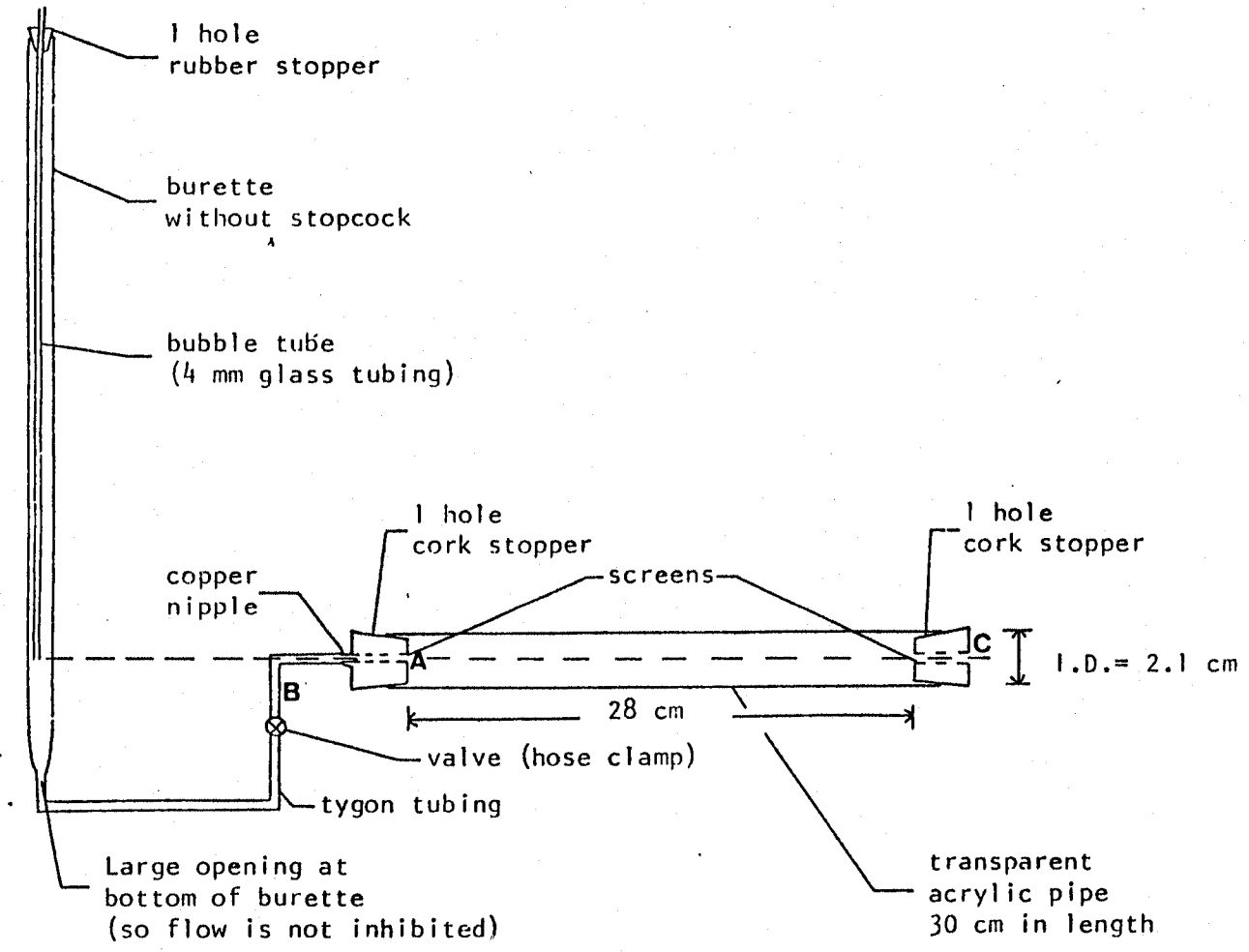

Figure A1.1. Apparatus used in the determination of soil diffusivity.

left disconnected to the nipple located at point A.

Water was drained from the burette through tube B until bubbles were emmited from the bubble tube. Tube B was clamped shut and attached to the brass nipple at point A.

The experiment was started by disconnecting the clamp on tube B and applying a short, instantaneous suction to the nipple located at point C. Suction was applied by attaching a hose to the nipple at point C and sucking on the hose for approximately one half of a second.

Water was allowed to infiltrate for a selected length of time. At the end of that time period, the experiment was stopped by placing a hose clamp on tube B. The tube was disconnected from the nipple at point A and the column was weighed.

Soil was extracted from the column by using a 30 cm length of thin-walled vinyl pipe which had an outside diameter equal to the inside diameter of the soil column. The vinyl pipe was lubricated slightly with petroleum jelly. The pipe was inserted a distance of 1 cm into the column at point A. The tube was twisted and pulled out removing a 1 cm section of soil. This was repeated until the wetting front had been cored.

Volumetric moisture contents were determined individually for each 1 cm sample by weighing each sample while wet, drying the samples at 105^{o}C for 24 hours and

reweighing the samples dry. The volume of each 1 cm section was computed by dividing the dry weight of the soil section by dry bulk density of determined previously for the entire column.

Volumetric moisture content values were assigned to the midpoint of each soil section. The distances to these points, from point A, were converted to the Boltzman variable, λ, using Equation 3.3.

Values of moisture content, θ, were plotted as a function of the Boltzman variable, λ, and a hand-drawn curve was fit through the data as shown in Figure 3.5 of the text. Values of λ were taken from this curve for each integer value of the moisture content. These values were used in Equation 3.4.

Equation 3.4 was solved numerically using the program DFSVTY listed on the following pages. This program solves the integral using both the Simpsons and the Trapezoidal rule. The differential is solved using a three-point centered differencing scheme for all but the initial and final values of moisture content. A three-point backward differencing and three-point forwards differencing schemes are used at the endpoints. The program creates a file of soil diffusivity values for values of moisture content ranging from 0.01 to the saturated value. These values are plotted in Figure 3.6 of the text.

The only major problem encountered in the Bruce and Klute method involved a loss in the hydraulic connection between the burette and the soil that occurred during the testing of the medium blasting sand. The sorptivity of this soil was so high that the throat of the burette would not allow water to be delivered fast enough to the soil. This problem was corrected by constructing a burette that had no throat or other narrow sections that might impede flow.

The method of Bruce and Klute required a high degree of accuracy in weighing the soil samples. Due to the small size of the 1 cm samples, small errors in weighing resulted in large errors in the moisture content. Use of the triple beam balance did not yield sufficient accuracy so a highly precise and accurate electronic balance was used

```
      PROGRAM DFSVTY
C     ******************************************
C
C     CALCULATES DIFFUSIVITY AS A FUNCTION OF
C     MOISTURE CONTENT USING THE METHOD OF
C     BRUCE AND KLUTE.
C
C     ******************************************
C
C     THIS VERSION OF THE PROGRAM WAS MODIFIED
C     SO THAT LAMBDA COULD BE USED INSTEAD OF X.
C     IN THE PROGRAM, THE VARIABLE X REPRESENTS
C     THE VARIABLE LAMBDA. TO USE THE PROGRAM,
C     ONE CREATES A DATA FILE IN THE FORM :
C
C        FILENAME.DAT
C
C     INPUT VALUES CONSIST OF THETA (MOISTURE
C     CONTENT) AND LAMBDA (BOLTZMAN VARIABLE).
C     THESE ARE PLACED IN TWO COLUMNS, UNFORMAT-
C     TED WITH ANY NUMBER OF SPACES BETWEEN THE
C     COLUMNS. THE PROGRAM PROMPTS THE USER FOR
C     THE NAME OF THE DATA FILE AND CREATES AN
C     OUTPUT FILE NAMED BY THE USER. THE OUTPUT
C     FILE CONSISTS OF MOISTURE CONTENTS AND
C     DIFFUSIVITY VALUES.
C
C     ******************************************
C
C     THETAD=VOLUMETRIC MOISTURE CONTENT (ML/ML)
C      X(I) =BOLTZMAN VARIABLE (CM/(SEC)**1/2)
C
C     ******************************************
      DOUBLE PRECISION DATA,OUTFL,SLTYP
      INTEGER THETA
      REAL INTGL
      DIMENSION THETA(0:45), X(0:45)
C     ******************************************
      WRITE(5,*) 'ENTER THE NAME OF THE DATA FILE'
 10   FORMAT(A10)
      READ (5,10)DATA
      WRITE(5,*)'ENTER THE NAME OF THE OUTPUT FILE'
      READ(5,10)  OUTFL
      WRITE(5,*)'ENTER THE NUMBER OF DATA POINTS'
      READ(5,*) NUMB
      OPEN (UNIT=21,FILE=DATA)
      OPEN (UNIT=22,FILE=OUTFL)
      DO 100 I=0,NUMB-1
        READ(21,*)THETAD,X(I)
        THETA(I)=THETAD*100
 100  CONTINUE
 11   FORMAT(10X,'THETA (%)',5X,'DIFFUSIVITY (CM*CM/SEC)',/)
 12   FORMAT(5X,F10.2,10X,1P,E10.4)
 14   FORMAT(///,3X,'DIFFUSIVITY VALUES FROM THE HORIZONTAL
```

```
15    FORMAT(3X,'INPUT  FILE:',A10)
16    FORMAT(3X,'OUTPUT FILE:',A10)
      WRITE(22,14)
      WRITE(22,15)DATA
      WRITE(22,16)OUTFL
      WRITE(22,11)
      DO 101 J=0,NUMB-1
           JJ=J
        IF (J.EQ.0) THEN
          INTGL=0
        ELSE
             IF (MOD(J,2).EQ.0) THEN
            CALL SIMPSN(THETA,X,INTGL,JJ)
             ELSE
            INTGL=INTGL*100+(X(J)+X(J-1))/2
          END IF
        END IF

        CALL THRPT(X,THETA,DXDTH,NUMB,JJ)
        INTGL=INTGL/100
        THETOP=FLOAT(THETA(J))/100.
        DIFF=-(DXDTH*INTGL/2)
        WRITE(22,12)THETOP,DIFF
101   CONTINUE
      CLOSE(UNIT=21)
      CLOSE(UNIT=22)
      END
C     ****************************************

C     ****************************************
      SUBROUTINE SIMPSN (THETA,X,INTGL,J)
      INTEGER THETA
      REAL INTGL,M
      DIMENSION THETA(0:45),X(0:45)
      M=(THETA(J)-THETA(0))/2
      THETA0=X(0)+X(J)
      THETA1=0
      THETA2=0
      DO 100 K=1,2*M-1
        IF(MOD(K,2).EQ.0) THEN
             THETA2=THETA2+X(K)
        ELSE
             THETA1=THETA1+X(K)
        END IF
100   CONTINUE
      INTGL=(THETA0+2*THETA2+4*THETA1)/3

      RETURN
      END
```

```
C     ********************************************
      SUBROUTINE THRPT(X,THETA,DXDTH,NUMB,J)
      INTEGER THETA
      DIMENSION X(0:45),THETA(0:45)
      IF(J.EQ.0) THEN
        DXDTH=(X(1)-X(0))*100
      ELSE IF ((J.GT.0).AND.(J.LT.(NUMB-1))) THEN
        DXDTH=((-X(J-1)+X(J+1))/2)*100
      ELSE
        DXDTH=(X(J)-X(J-1))*100
      END IF
      RETURN
      END
C     ********************************************
```

APPENDIX 2

Wetting Front Profiles

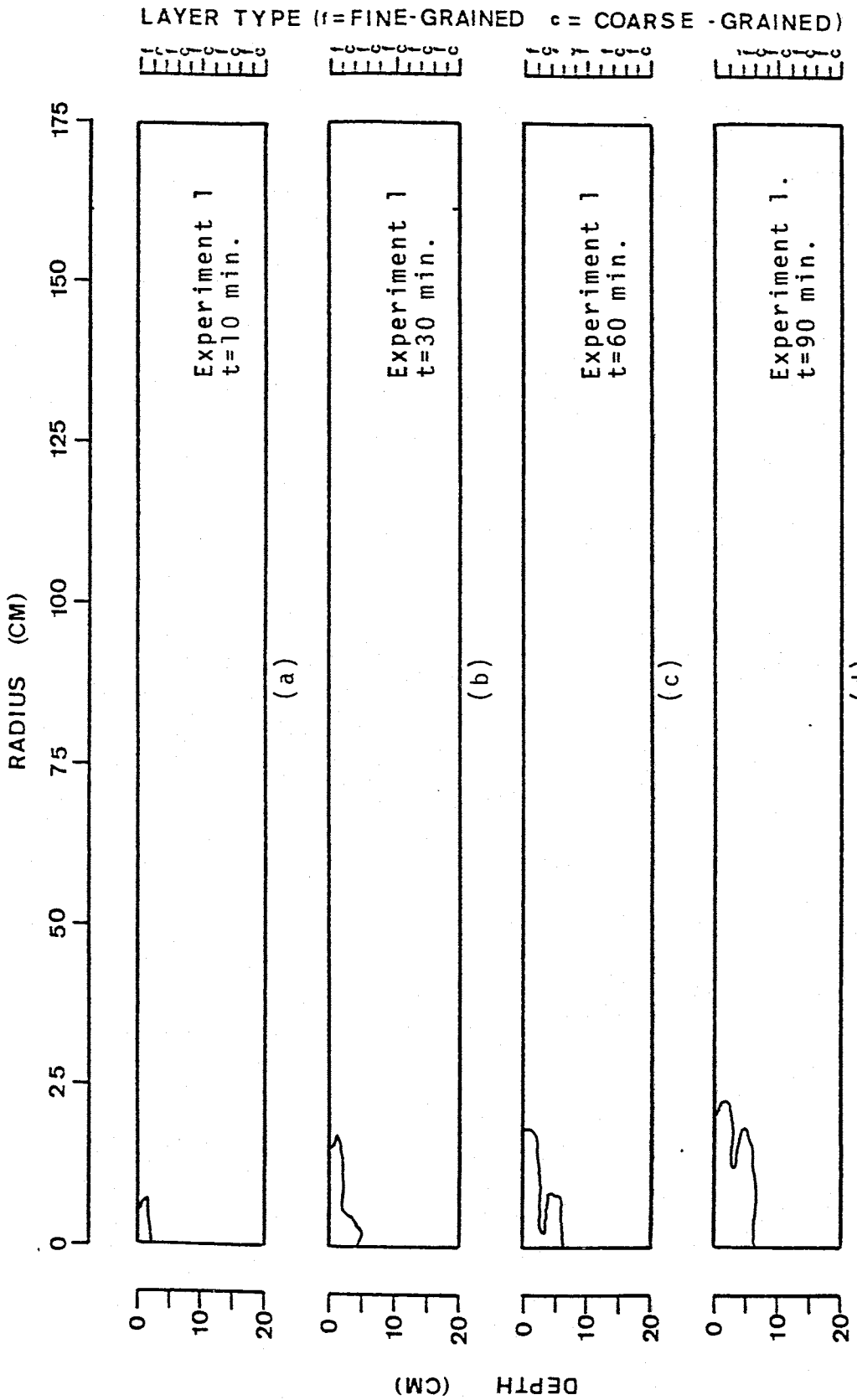

Figure A2.1. Wetting front profile for experiment 1 at (a) 10 min., (b) 30 min., (c) 60 min., and (d) 90 min.

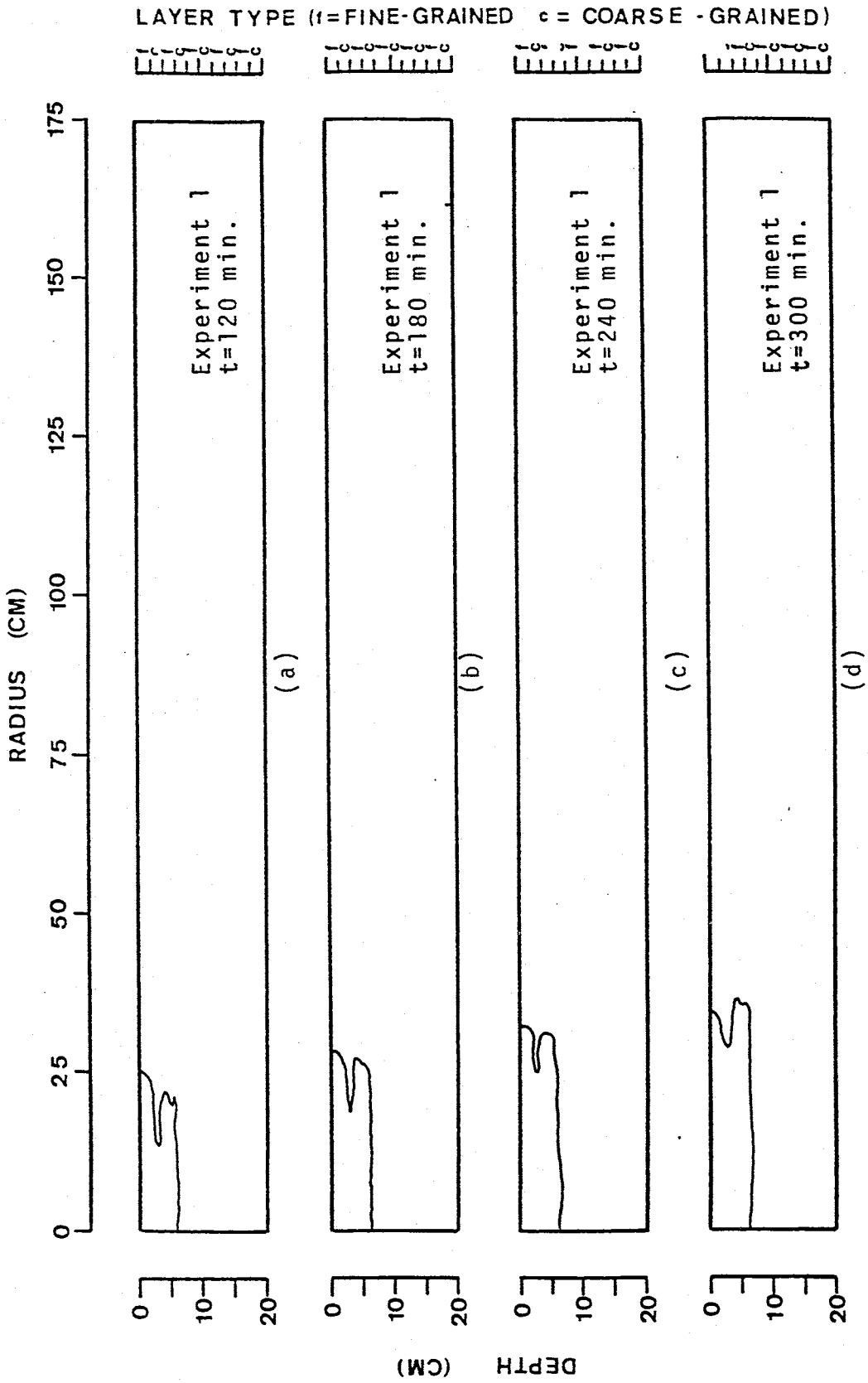

Figure A2.2. Wetting front profiles for experiment 1 at (a) 120 min., (b)180 min., (c)240 min., and (d) 300 min.

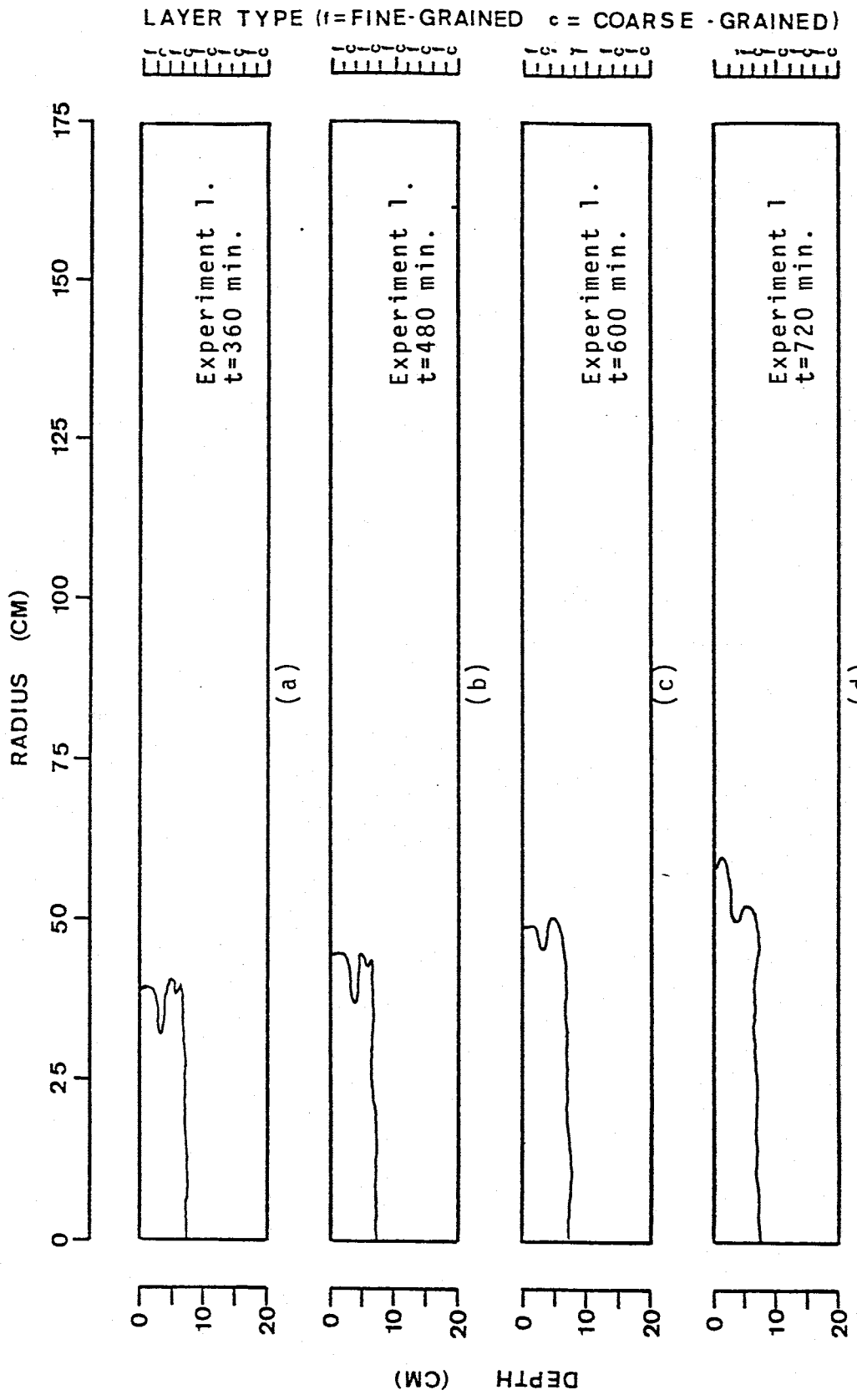

Figure A2.3. Wetting front profiles for experiment 1 at (a) 360 min., (b) 480 min., (c) 600 min., and (d) 720 min.

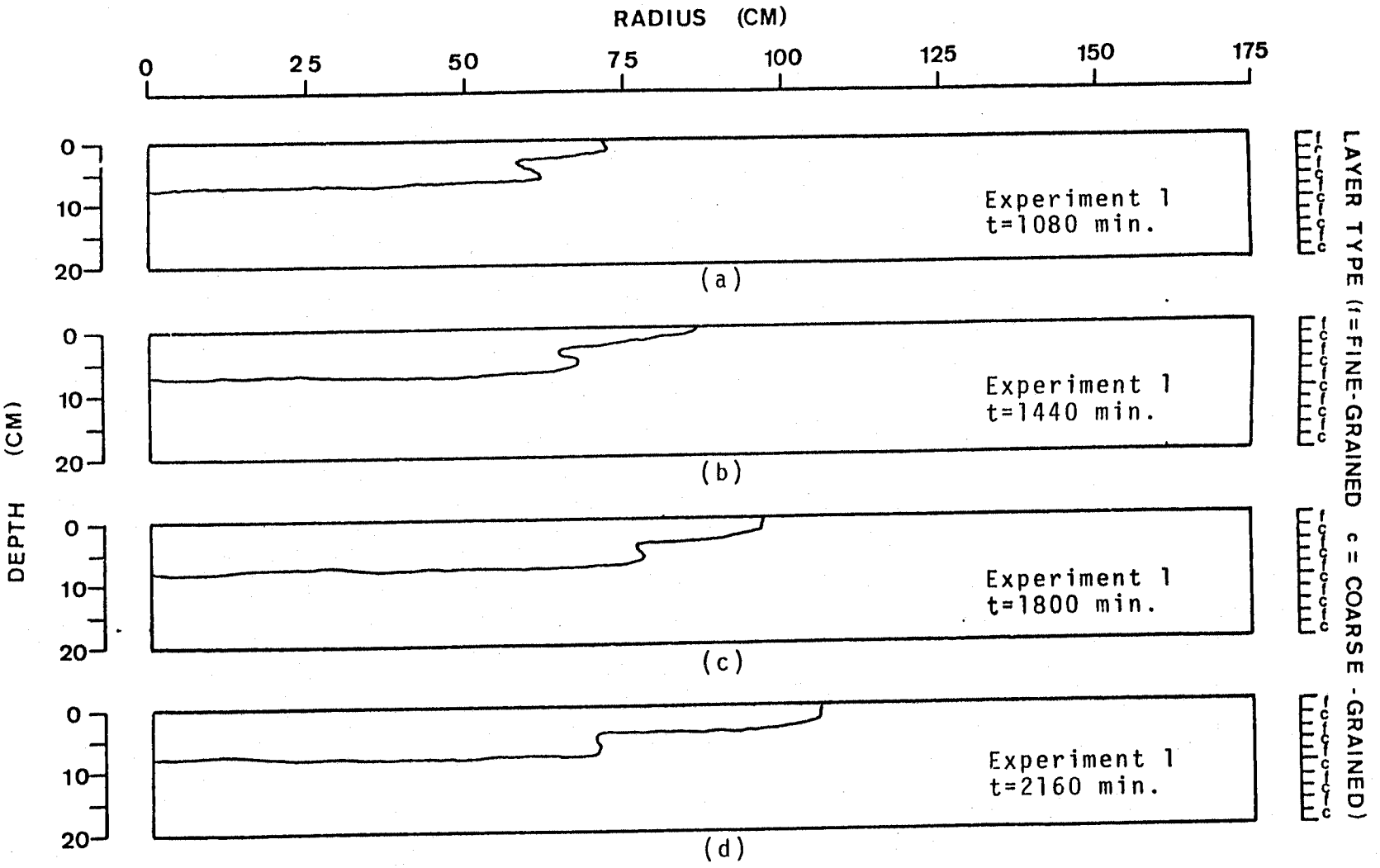

Figure A2.4. Wetting front profiles for experiment 1 at (a) 1080 min., (b) 1440 min., (c) 1800 min. and (d) 2160 min.

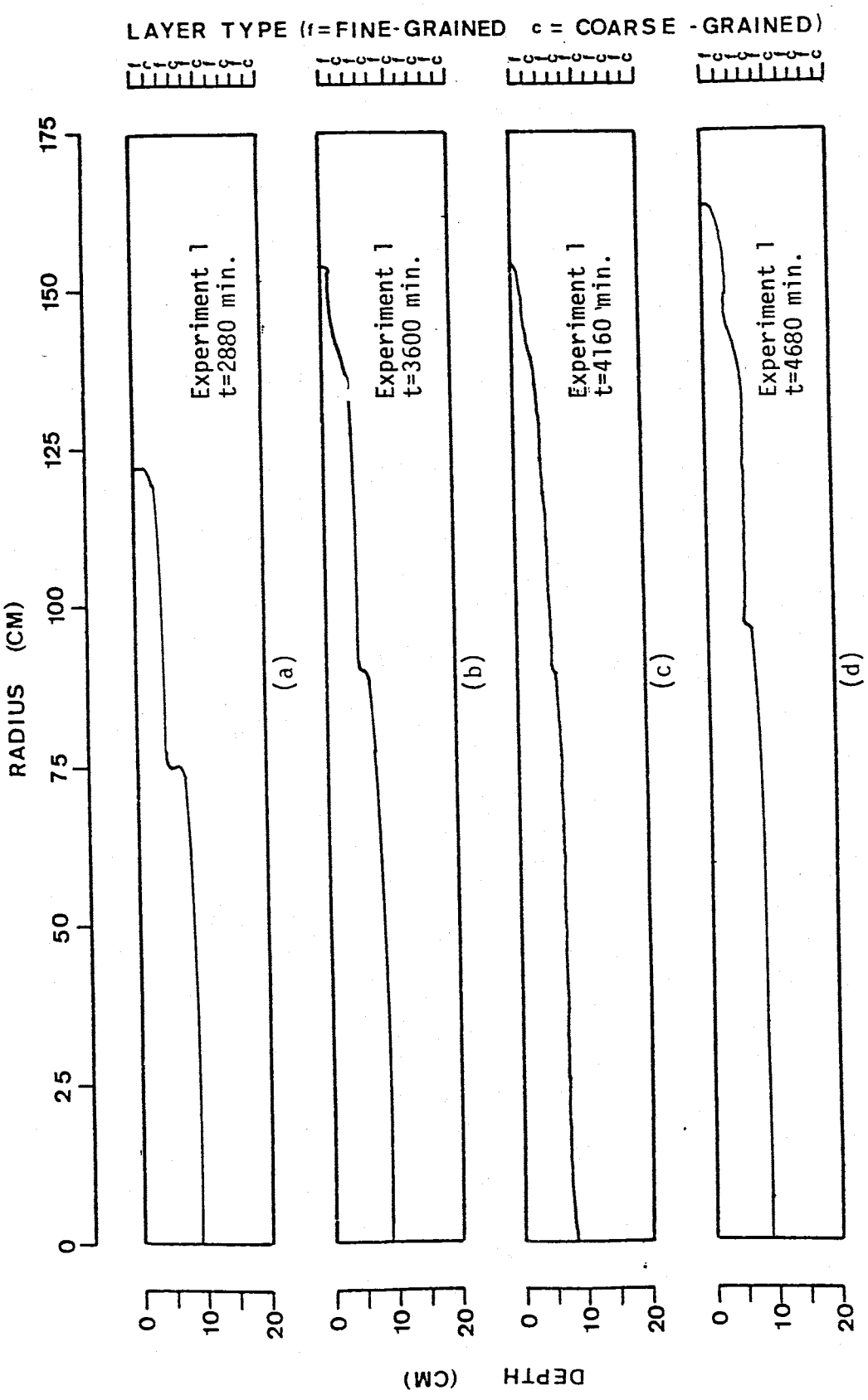

Figure A2.5. Wetting front profiles for experiment 1 at (a) 2880 min.,(b)3600 min., (c)4160 min. and (d) 4680 min.

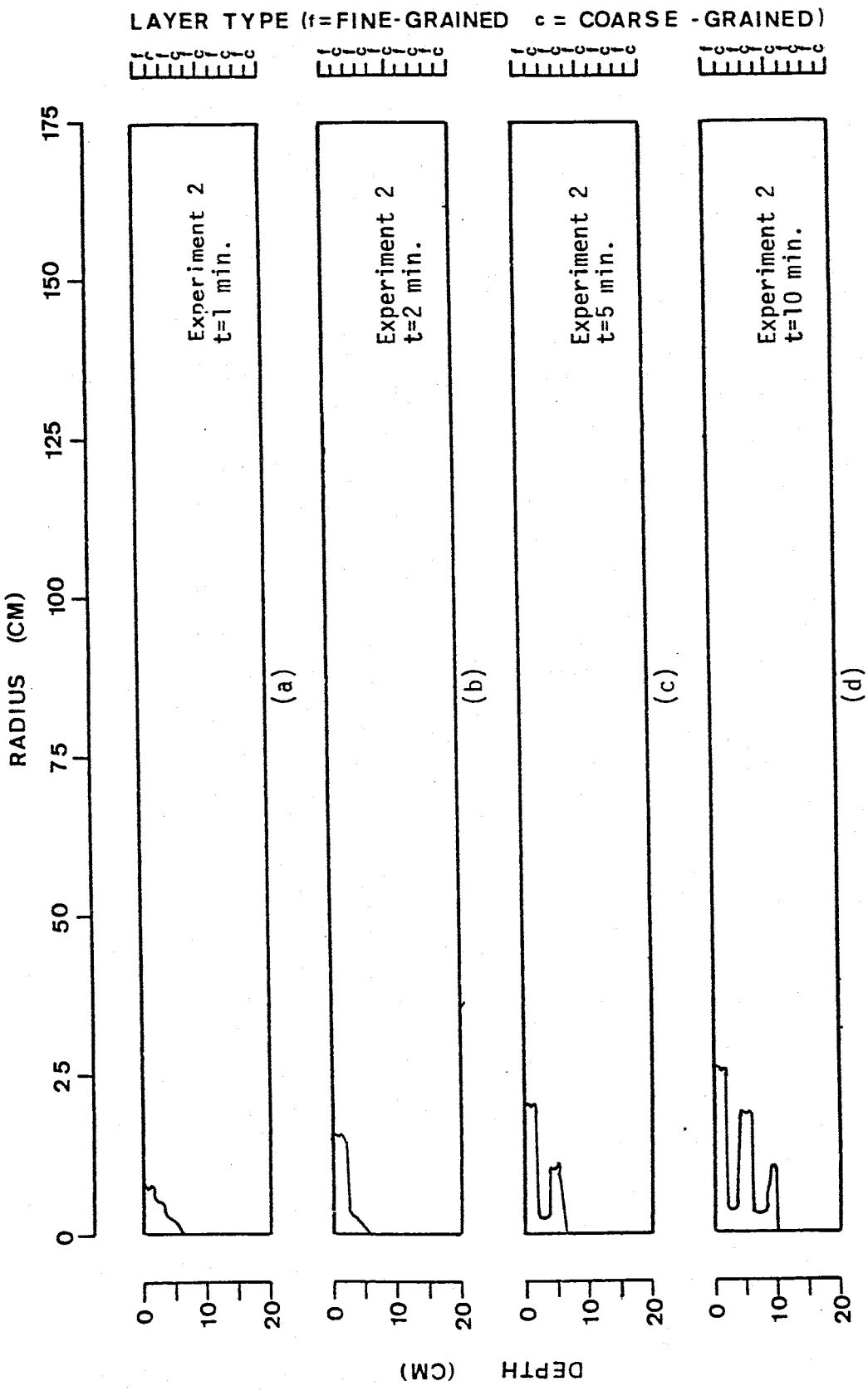

Figure A2.6. Wetting front profiles for experiment 2 at (a) 1 min., (b) 2 min., (c) 5 min., and (d) 10 min.

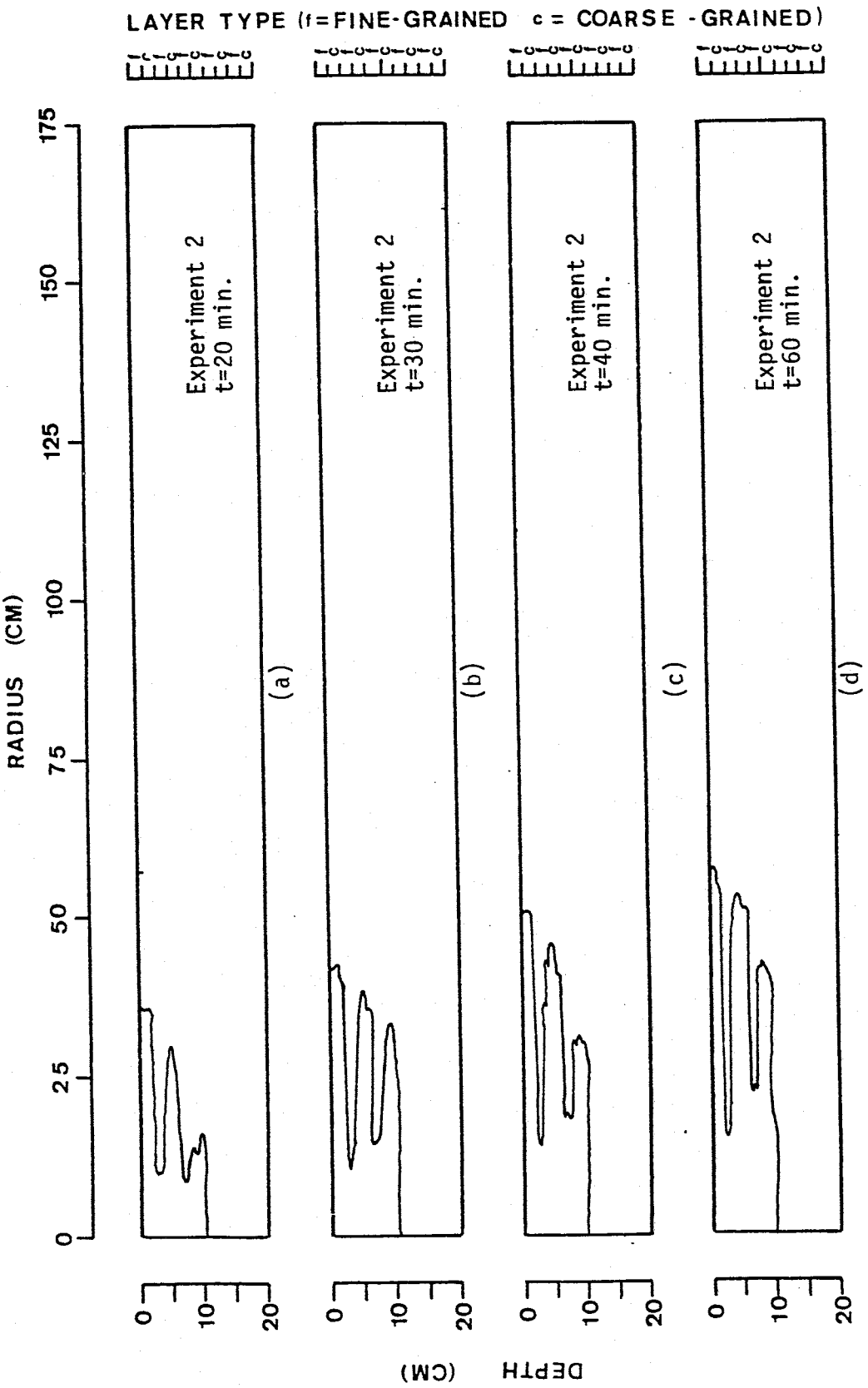

Figure A2.7 Wetting front profiles for experiment 2 at (a) 20 min., (b) 30 min., (c) 40 min., and (d) 60 min.

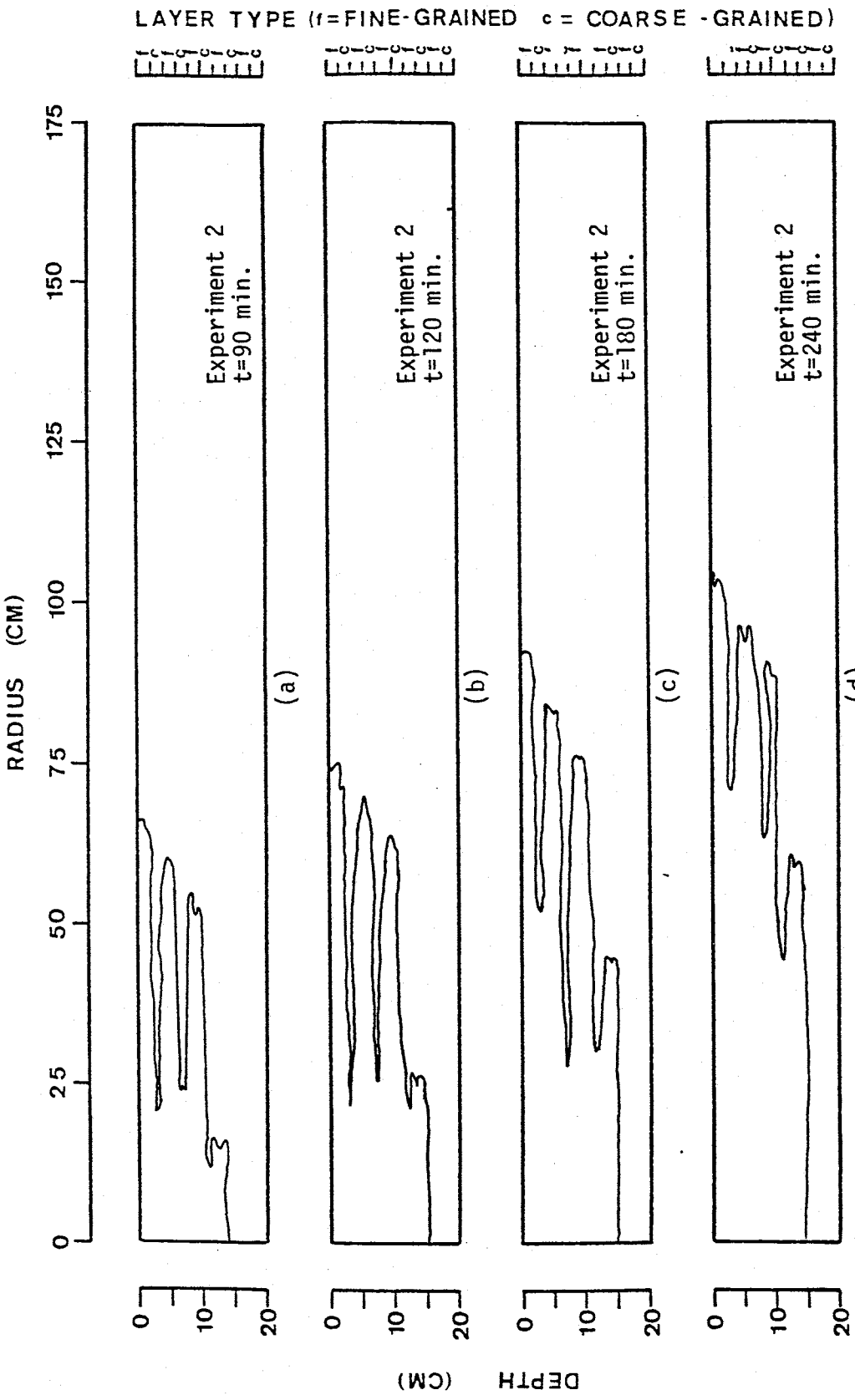

Figure A2.8 Wetting front profiles for experiment 2 at (a) 90 min., (b) 120 min., (c)180 min., and (d) 240 min.

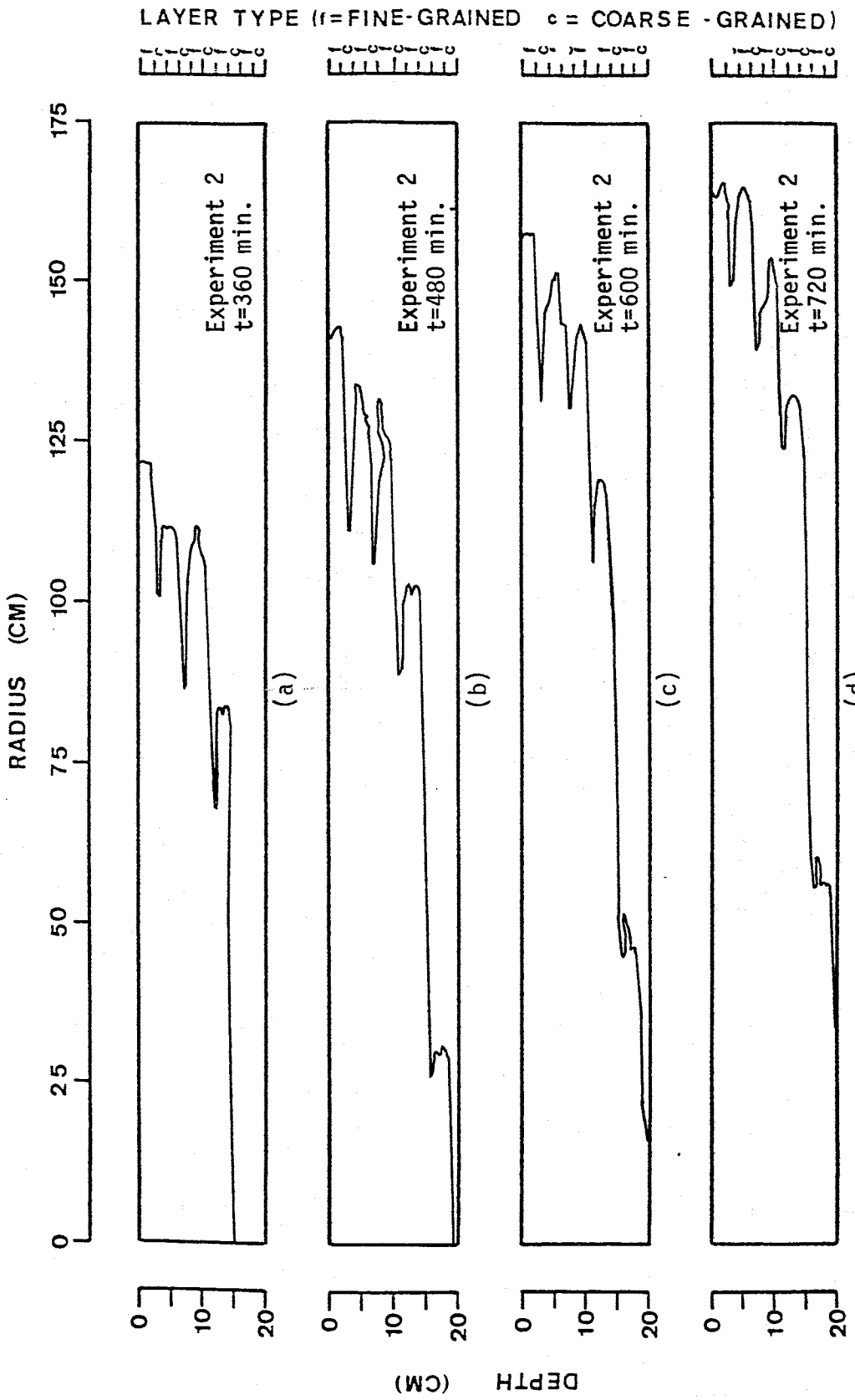

Figure A2.9 Wetting front profiles for experiment 2 at (a) t=360 min, (b) t=480 min., (c) t=600 min., and (d) t=720 min.

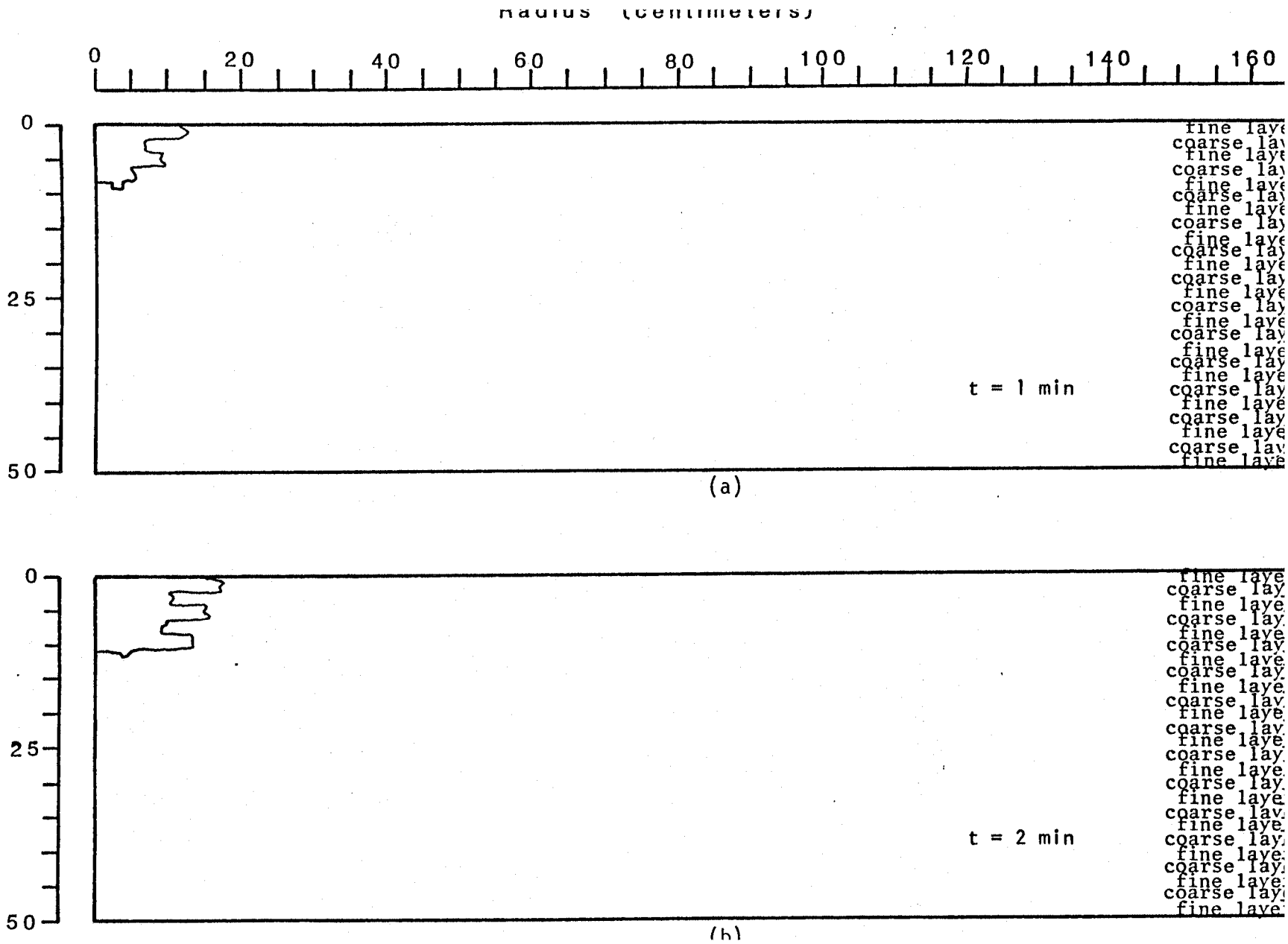
Radius (centimeters)
0
20
40
60
80
100
120
140
160
0
25
50
t = 1 min
(a)
t = 2 min
(b)

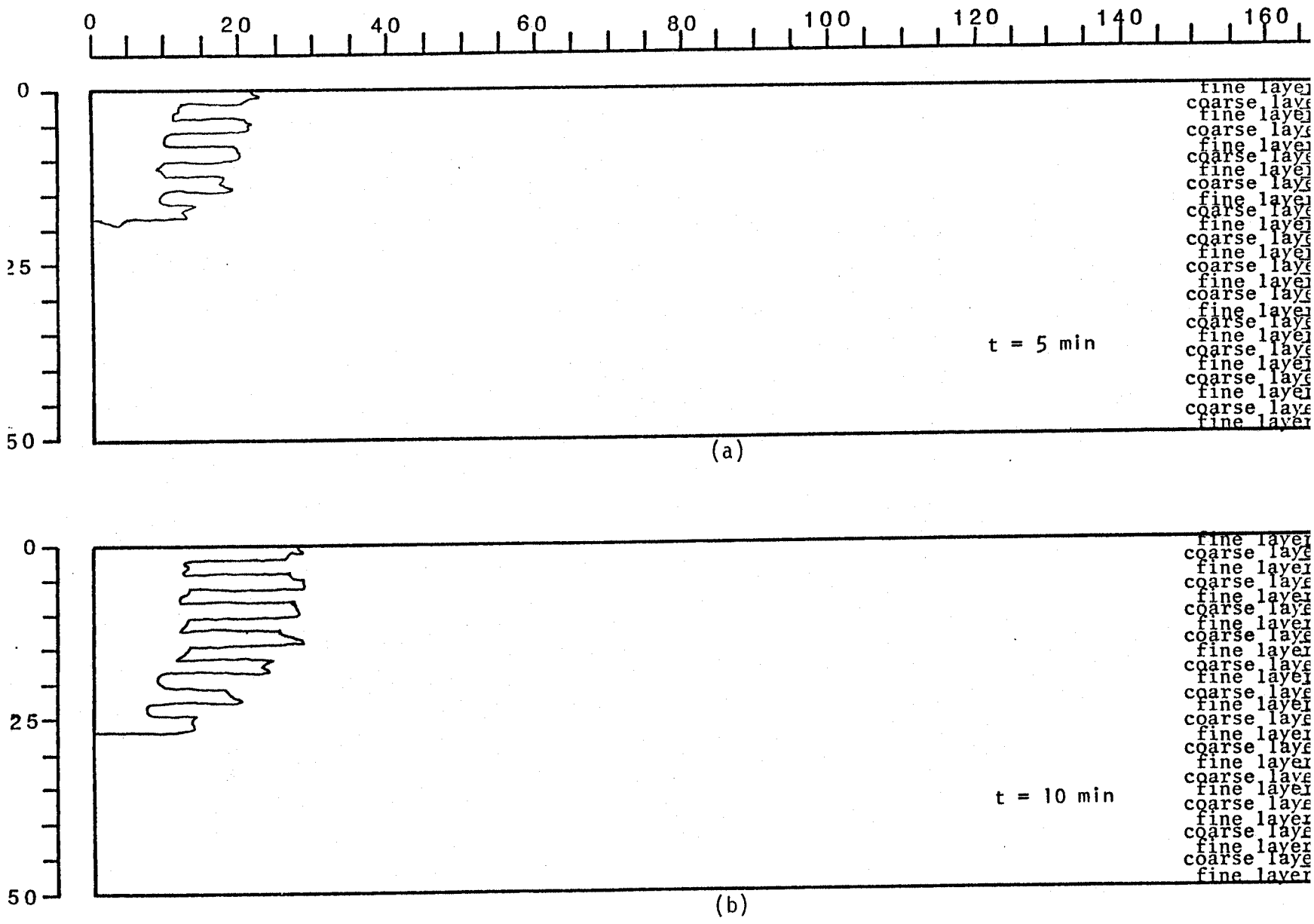
0
20
40
60
80
100
120
140
160
0
25
50
fine layer
coarse layer
t = 5 min
(a)
t = 10 min
(b)

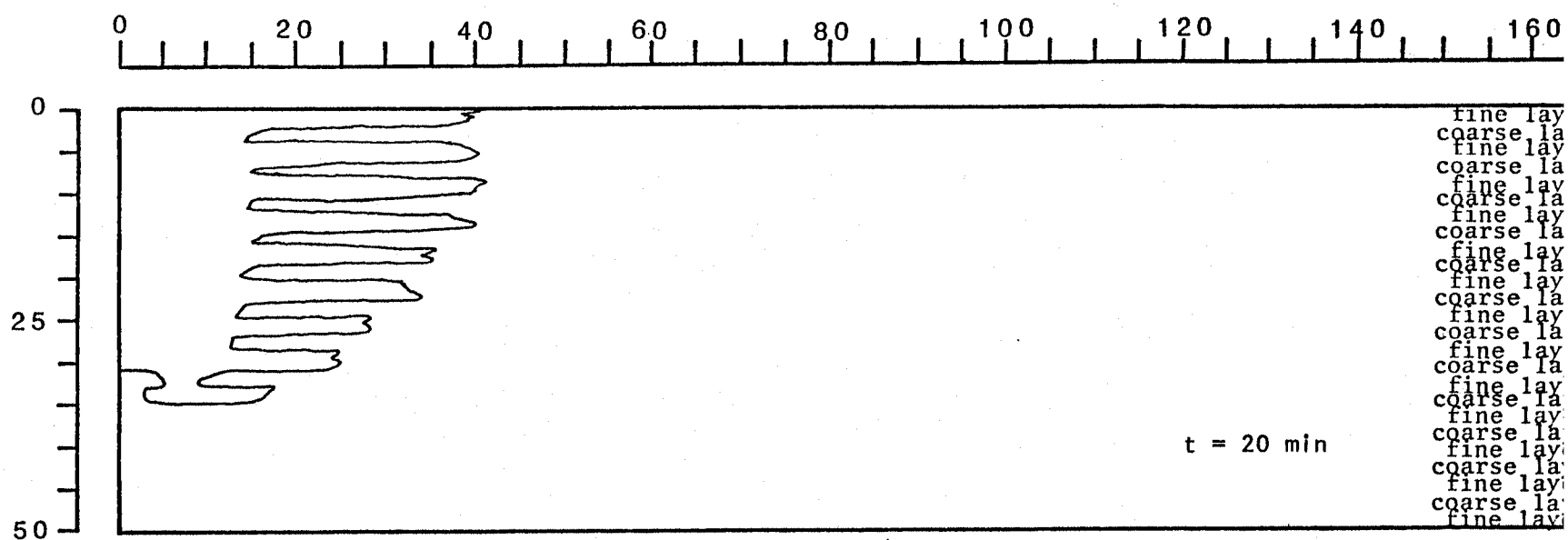

(a)

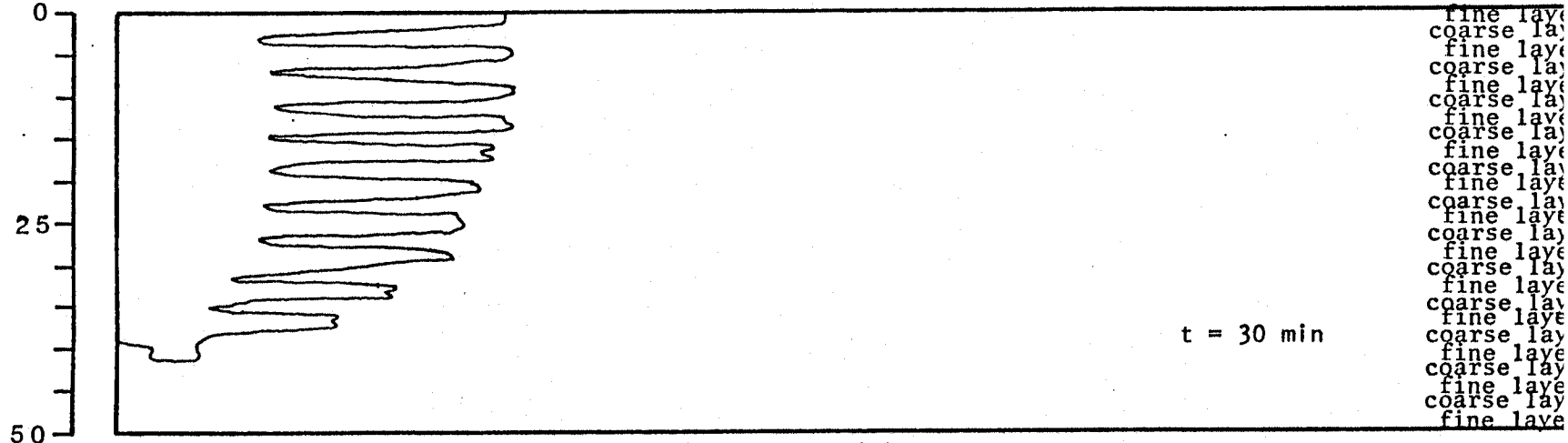

(b)

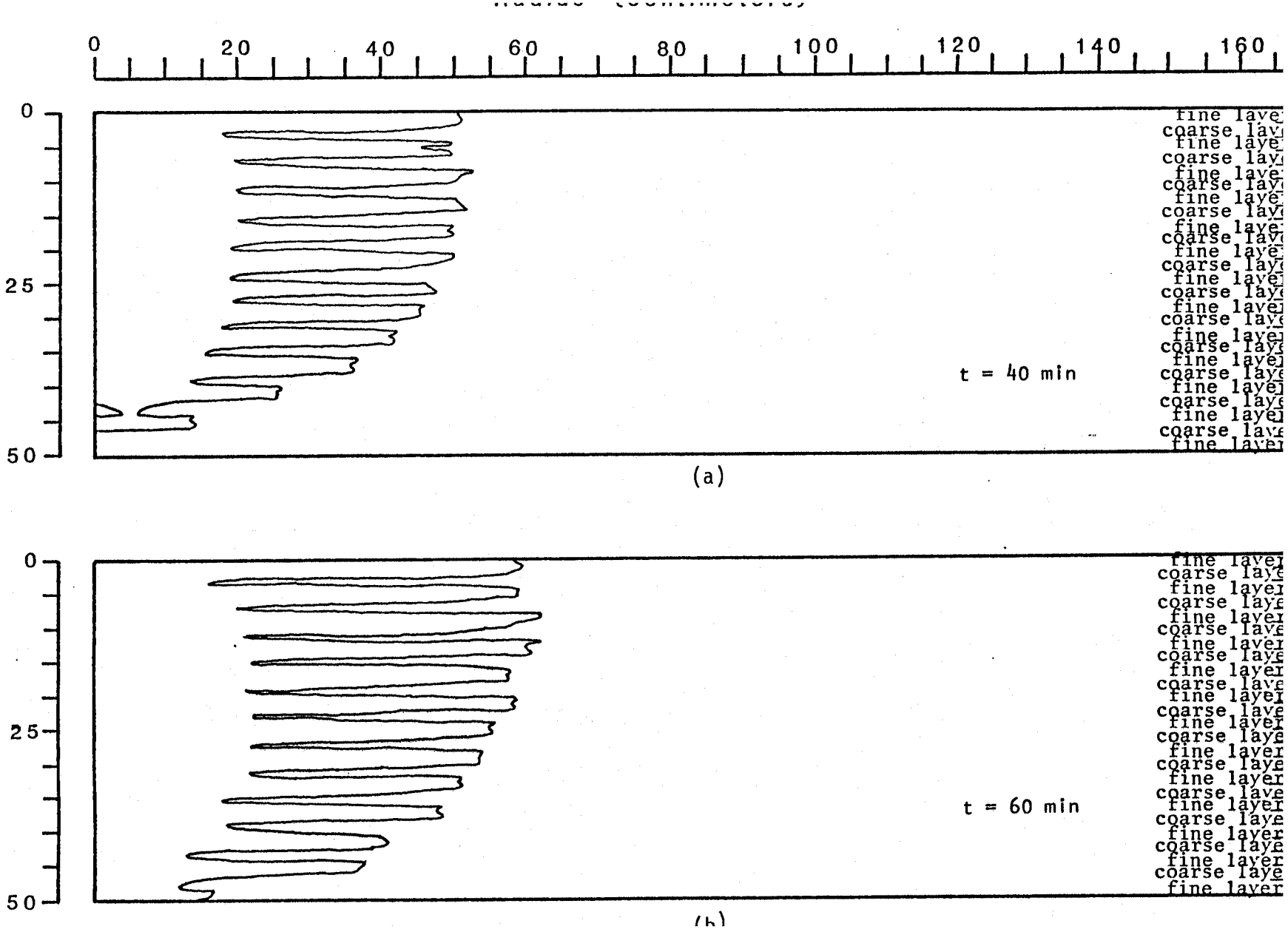
0
20
40
60
80
100
120
140
160
0
25
50
t = 40 min
(a)
t = 60 min

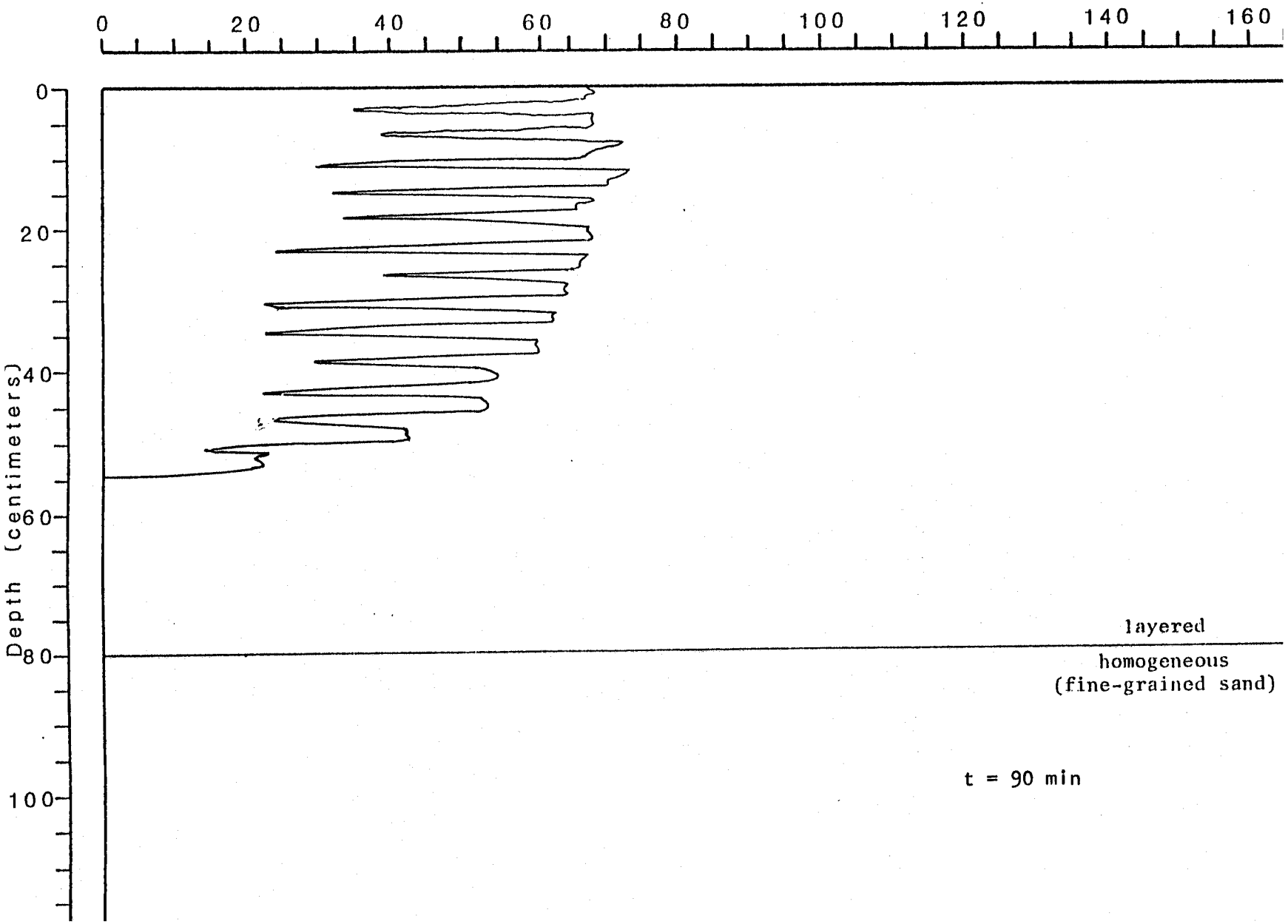
0
20
40
60
80
100
120
140
160
Depth (centimeters)
0
20
40
60
80
100
layered
homogeneous
(fine-grained sand)
t = 90 min

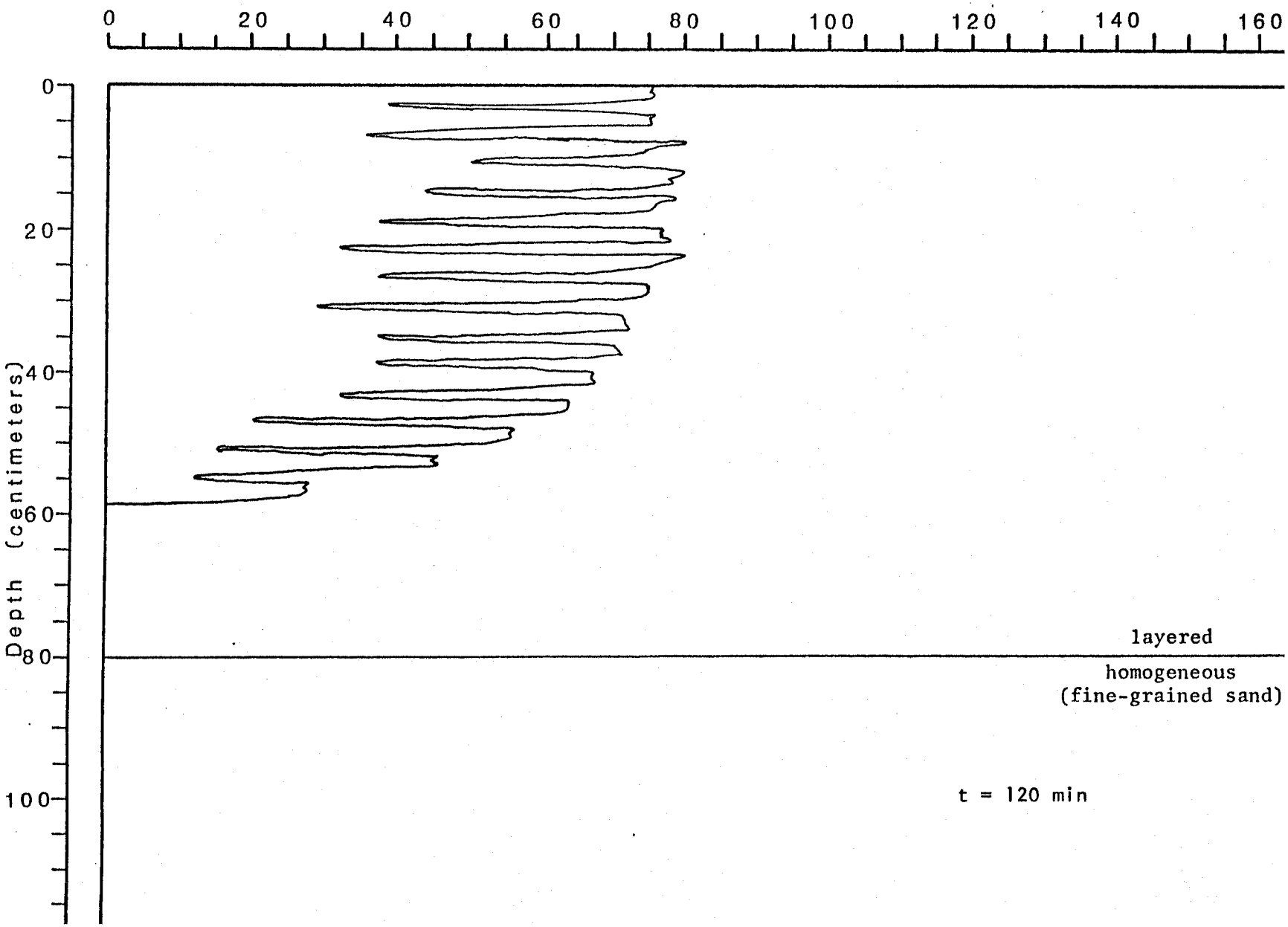
0
20
40
60
80
100
120
140
160
Depth (centimeters)
0
20
40
60
80
100
layered
homogeneous
(fine-grained sand)
t = 120 min

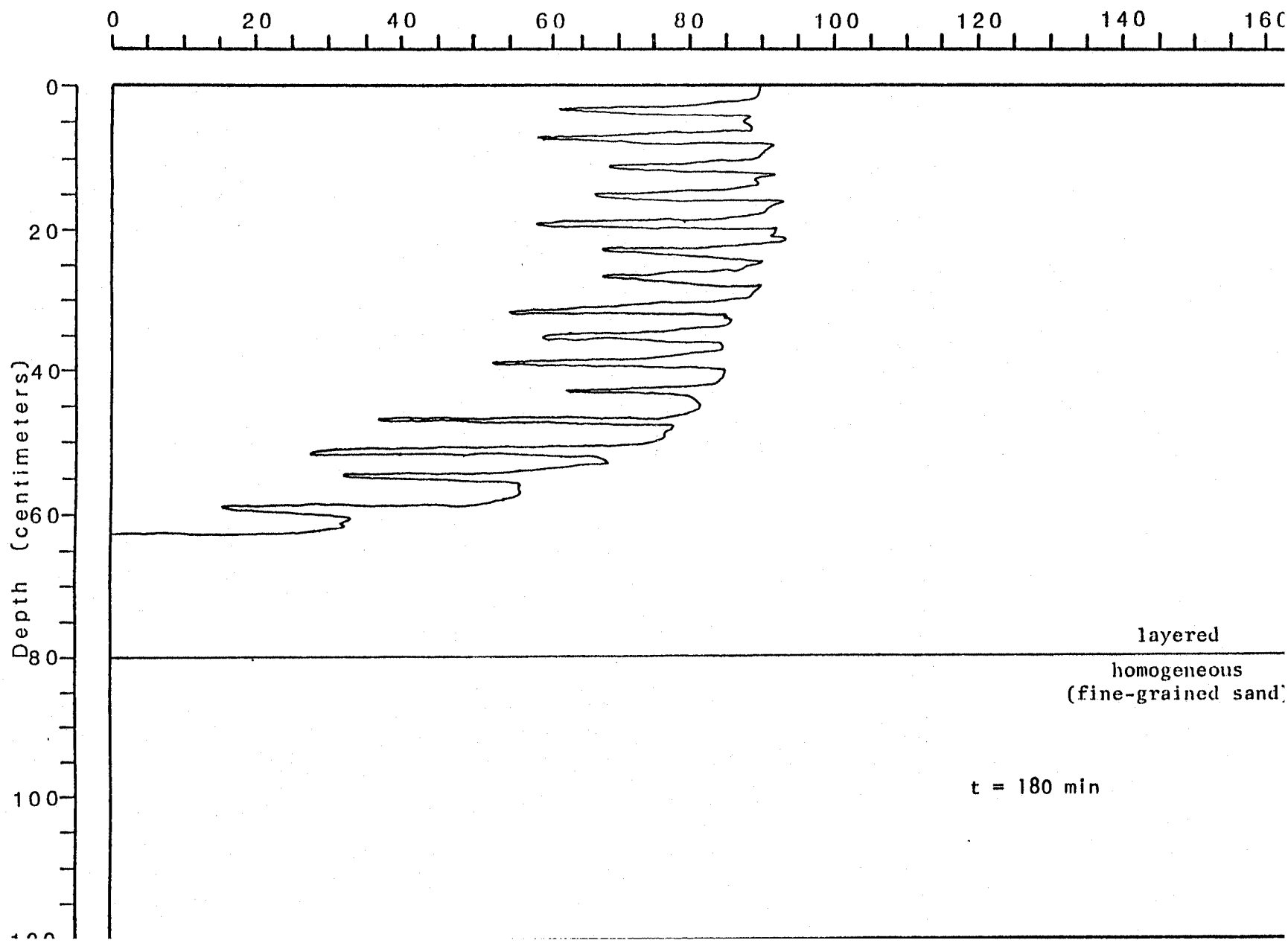
0
20
40
60
80
100
120
140
160
Depth (centimeters)
0
20
40
60
80
100
layered
homogeneous
(fine-grained sand)
t = 180 min

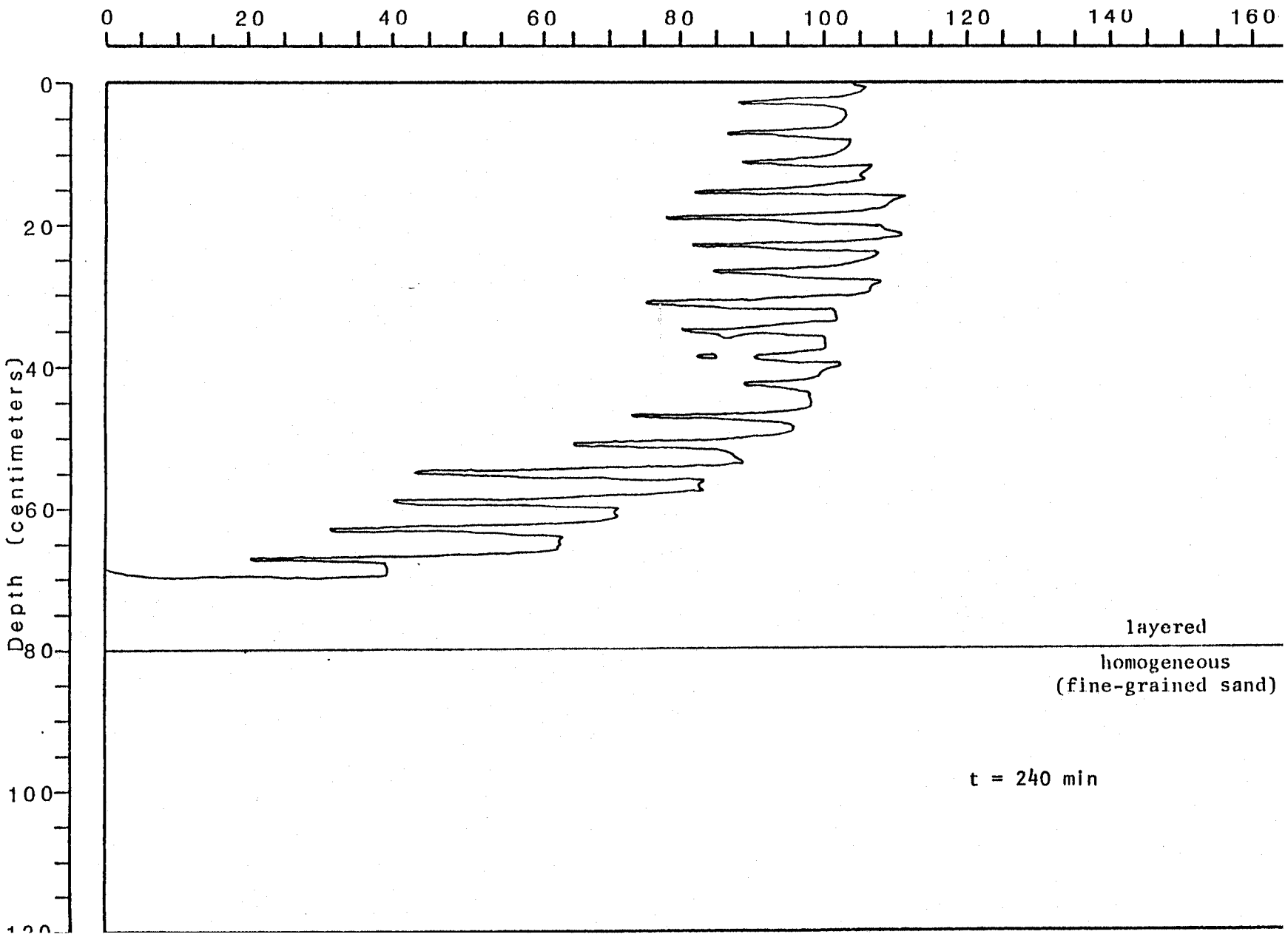
0
20
40
60
80
100
120
140
160
Depth (centimeters)
0
20
40
60
80
100
layered
homogeneous
(fine-grained sand)
t = 240 min

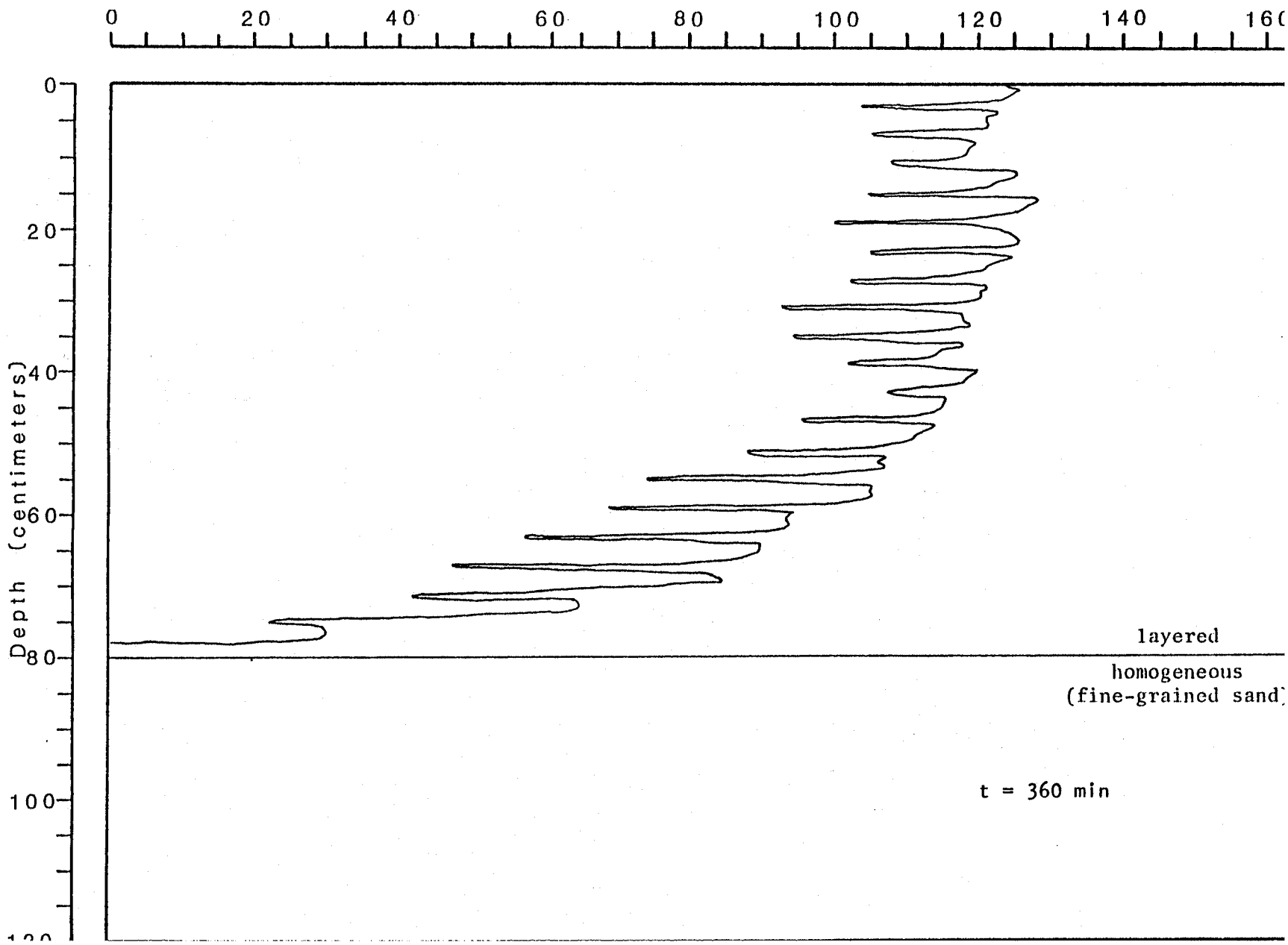
0
20
40
60
80
100
120
140
160
Depth (centimeters)
0
20
40
60
80
100
layered
homogeneous
(fine-grained sand)
t = 360 min

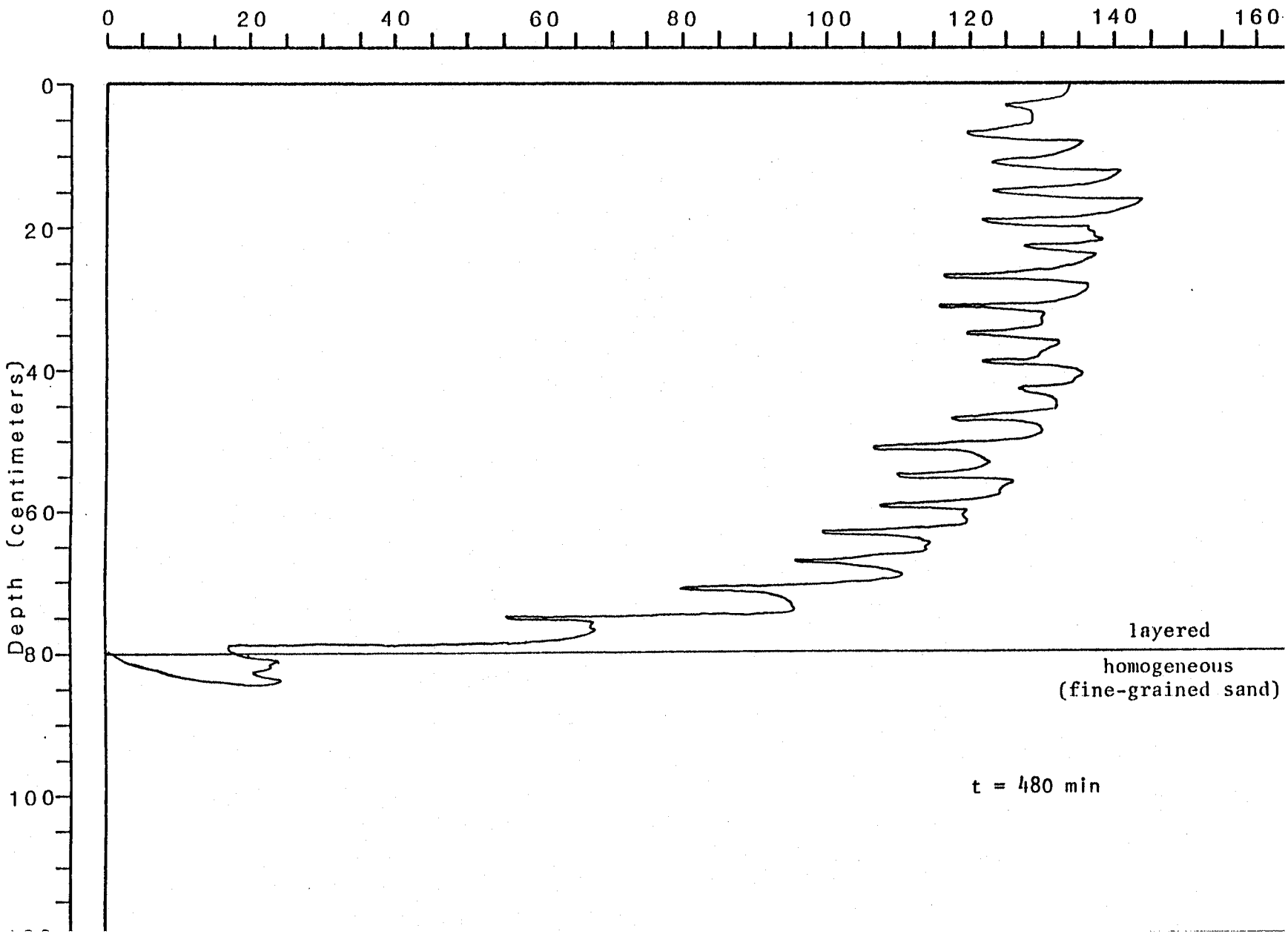
0
20
40
60
80
100
120
140
160
Depth (centimeters)
0
20
40
60
80
100
layered
homogeneous
(fine-grained sand)
t = 480 min

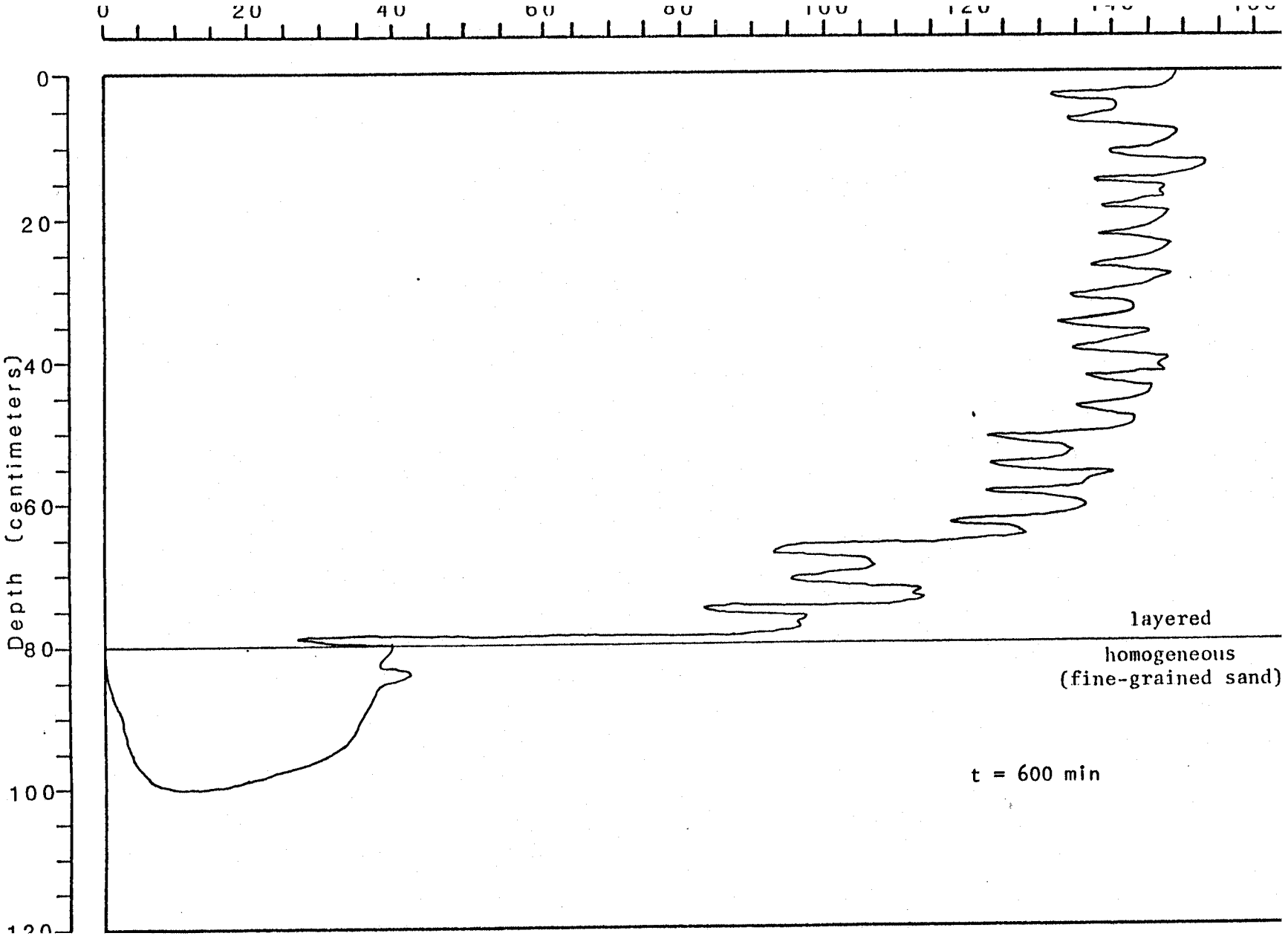
0
20
40
60
80
100
120
Depth (centimeters)
layered
homogeneous
(fine-grained sand)
t = 600 min

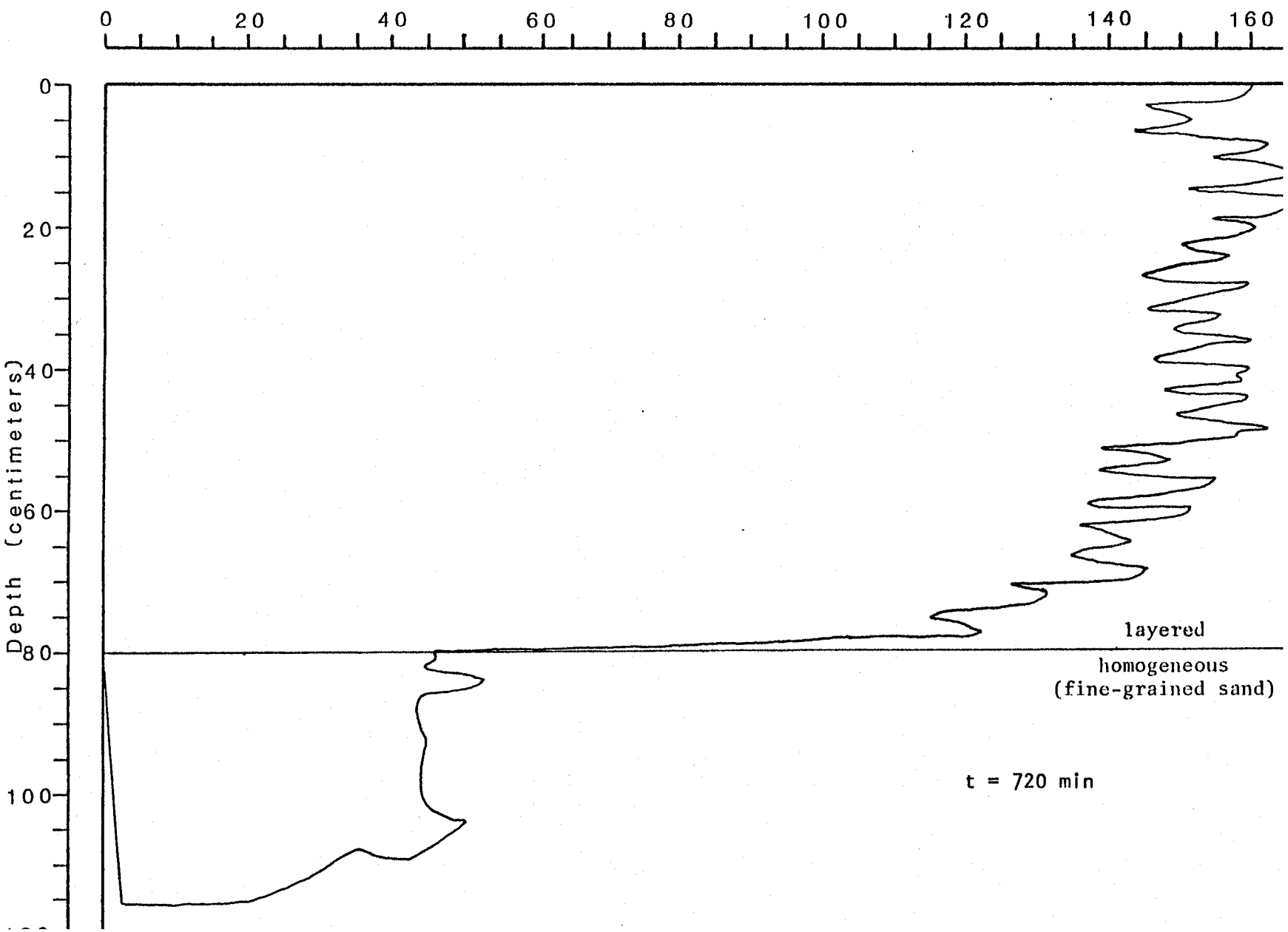
0
20
40
60
80
100
120
140
160
Depth (centimeters)
layered
homogeneous
(fine-grained sand)
t = 720 min

APPENDIX 3

Tensiometer Data

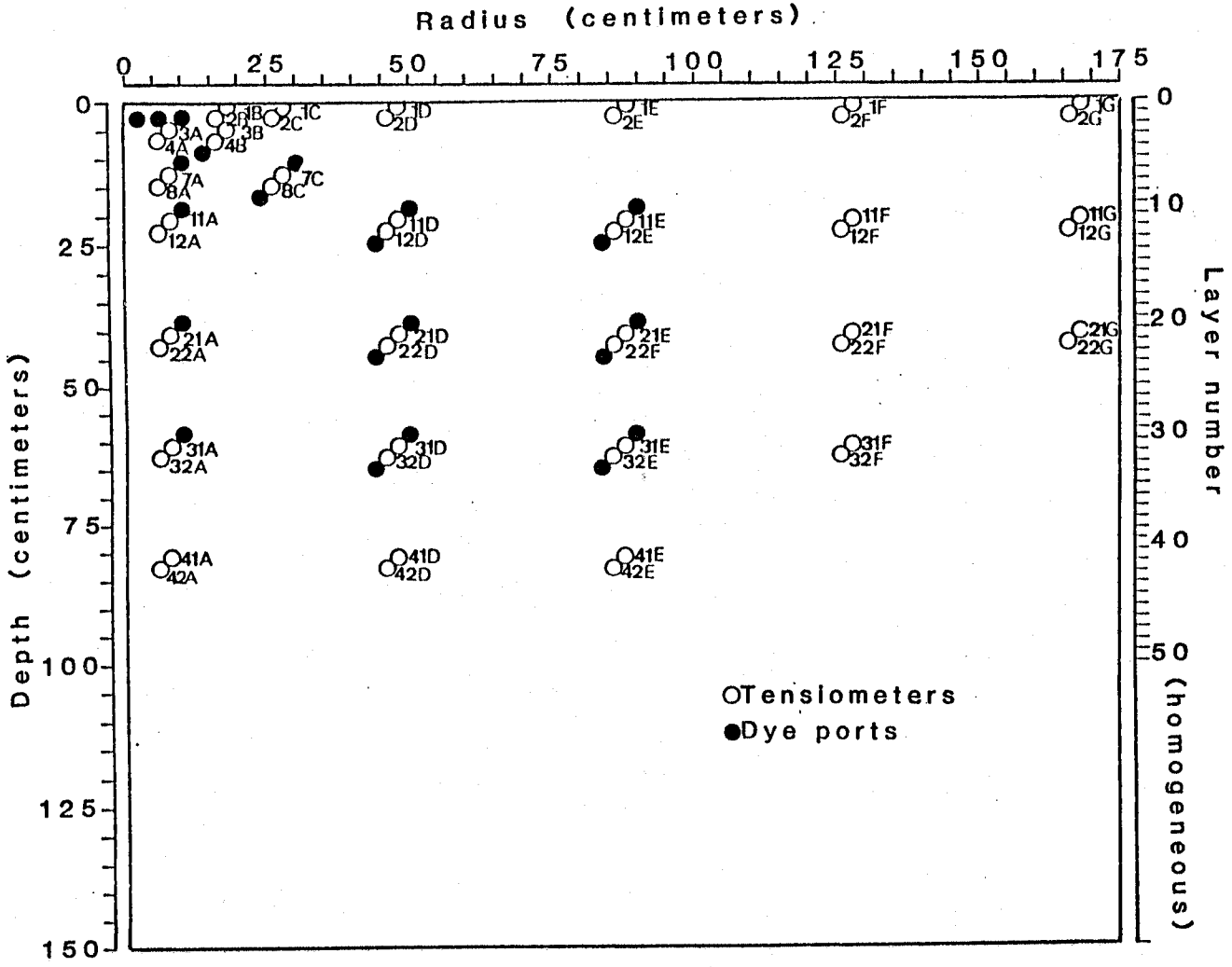

Figure A3.1. Nomenclature scheme for tensiometers used in experiment 1 and experiment 2.

Tensiometer data - Experiment 1 (Layer number 1)

(Pressure head values in cm-H_2O)

Time (min)	Tensiometer 1B	1C	1D	1E	1F
85	I/+5*				
180	-17.2				
220	-----	I/+7			
240	-19.1	-2.4			
300	-20.3	-17.6			
360	-20.8	-21.7			
480	-21.0	-22.4			
600	-21.0	-22.7			
650	-----	-----	I/+7		
720	-20.9	-22.8	-15.8		
1080	-22.0	-23.2	-22.0		
1440	-21.3	-21.0	-22.0		
1530	-20.8	-20.8	-21.7		
1800	-20.3	-19.7	-21.4		
2160	-20.3	-19.7	-21.4		
2200	-----	-----	-----	I/-29.2	
2880	-20.7	-20.1	-22.1	-26.9	
3240	-20.3	-19.9	-21.7	-29.5	
3600	-20.7	-19.9	-21.7	-32.0	I/(PT)**
4320	-22.2	-20.7	-22.3	-32.5	
4680	-21.3	-20.6	-22.1	-33.0	-18.9(?)

* Tensiometer intalled at this time and with noted initial pressure.

** Tensiometer read with pressure transducer

(Pressure head values in cm-H_2O)

Time (min)	Tensiometer 2B	2C	2D	2E	2F
210	I/+7				
240	-3.9				
280	-----	I/-28			
300	-5.1	-22.3			
360	-11.8	-22.6			
480	-14.0	-22.6			
600	-15.8	-22.6			
700	-----	-----	I/+7		
720	-17.0	-22.7	-4.5		
1080	-19.6	-23.5	-6.6		
1440	-20.8	-24.3	-21.8		
1530	-20.8	-24.3	-21.8		
1800	-21.1	-24.3	-22.2		
2160	-21.9	-25.5	-23.2		
2200	-----	-----	-----	I/-28.6	
2880	-23.0	-26.8	-26.2	-38.5	
3240	-22.6	-26.9	-26.6	-42.4	
3600	-22.5	-27.3	-27.7	-43.1	I/(PT)
4320	-21.7	-28.8	-30.4	-50.3	-37.3(?)
4680	-19.4	-28.2	-29.7	-55.0	-15.3(?)

Tensiometer data - Experiment 1 (Layer numbers 3 and 4)

(Pressure head values in cm-H_2O)

Time (min)	Tensiometer 3A	3B	4A	4B
100	I/+10			
125	-----	I/-80		
180	-11.8	-66.0		
240	-18.2	-41.4		
300	-19.3	-36.2		
360	-20.7	-30.5		
480	-21.2	-25.2		
580	-----	-----		
600	-21.3	-20.3		
720	-21.6	-23.3		
1080	-21.6	-22.9	I/-10.0	I/-10.0
1440	-24.6	-25.3	-12.7	-10.7
1530	-25.0	-25.7	-13.2	-11.0
1800	-25.6	-26.2	-14.4	-12.0
2160	-25.9	-26.4	-16.5	-14.5
2880	-25.0	-25.5	-20.3	-20.0
3240	-24.4	-24.8	-21.6	-21.8
3600	-23.9	-24.5	-25.2	-24.1
4320	-20.4	-21.9	-27.7	-26.4
4680	-21.3	-22.3	-28.4	-28.0

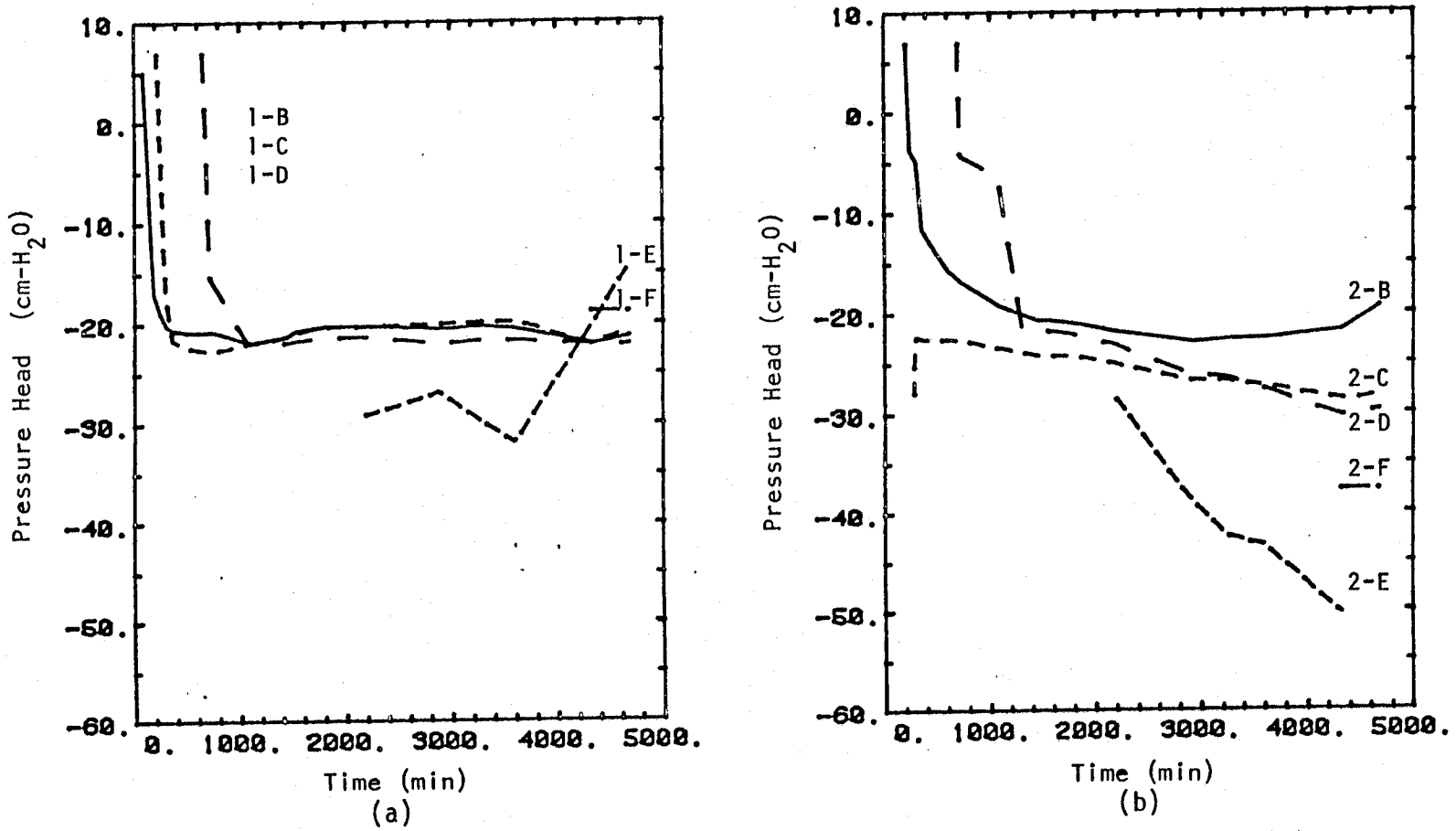

Figure A3.2 Tensiometer pressure heads versus time for experiments 1 and for (a) tensiomet in layer 1 (top layer, composed of Sevilleta dune sand) and (b)tensiometers in layer (medium blasting sand).

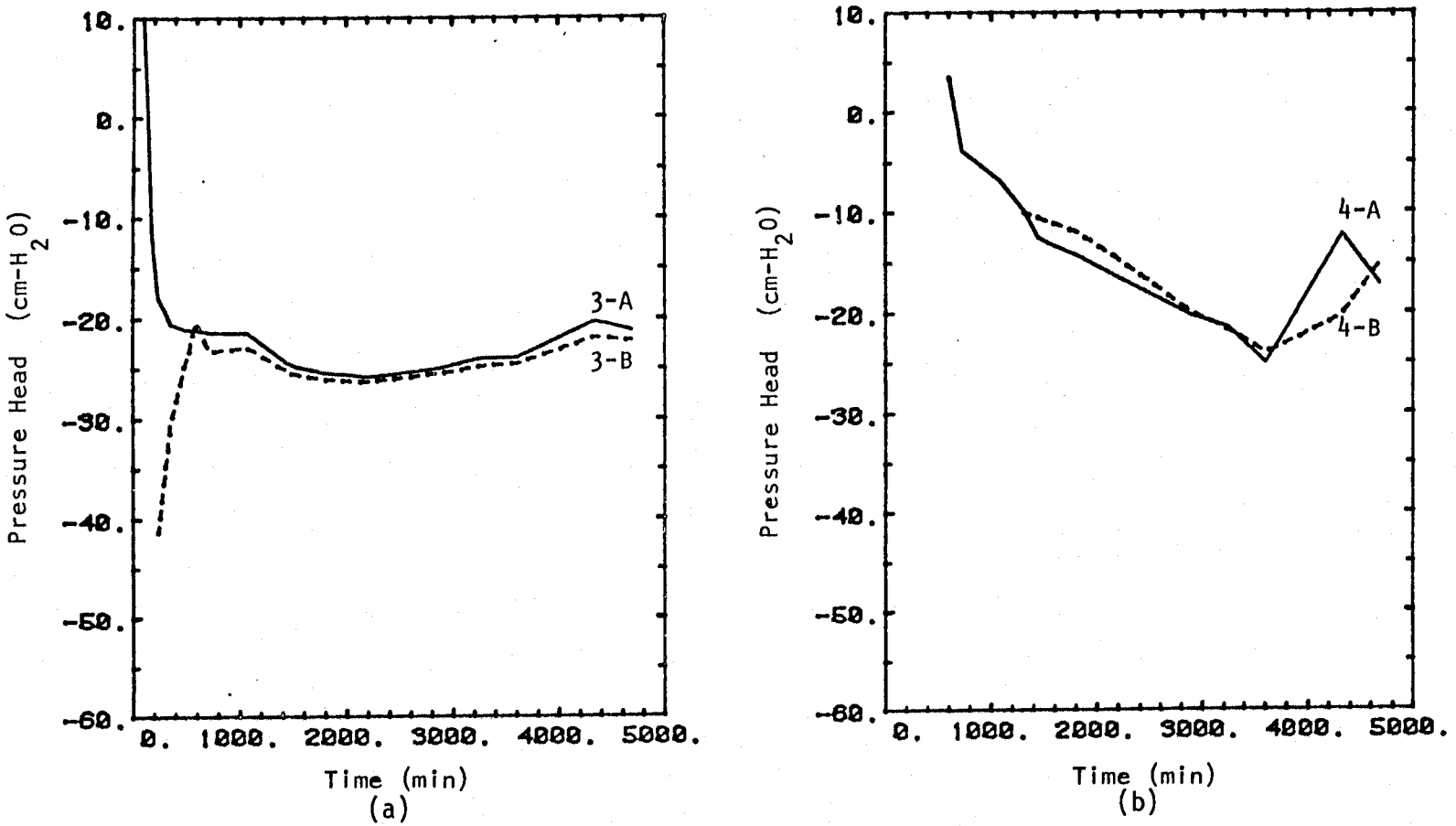

Figure A3.3. Tensiometer pressure heads versus time for experiment 1 and for (a) tensiometers in layer 3 (Sevilleta dune sand) and (b) layer 4 (medium blasting sand).

Tensiometer data - Experiment 2 (Layer number 1)

(Pressure head values in cm-H_2O)

	Tensiometers				
Time (min)	1B	1C	1D	1E	1F
10	I/-19.6*				
30	-----	I/-19.1			
55	-----	-----	I/-20.0		
90	-15.0	-16.4	-19.7		
120	-14.6	-15.7	-19.0		
180	-14.0	-14.8			
215	-----	-----	------	I/-27.5	
240	-11.8	-13.8	-16.7	-26.5	
300	-11.1	-13.2	-16.1	-24.5	
360	-10.8	-12.8	-15.6	-22.3	
480	-10.8	-12.6	-15.6	-21.0	
600	-10.3	-12.3	-15.2	-19.8	I/(PT)**
720	-11.1	-12.8	-15.3	-19.2	
780	-11.2	-12.8	-15.3	-19.2	
920	-11.2	-12.89	-15.3	-19.2	-20.

Tensiometer data - Experiment 2 (Layer number 2)

(Pressure head values in cm-H_2O)

	Tensiometers				
Time (min)	2B	2C	2D	2E	2F
190	I/-13.5				
195	-----	I/-21.7			
200	-----	-----	I/-19.8		
240	-11.2	-21.9	-19.9		
300	-11.1	-22.3	-20.6		
360	-10.9	-22.3	-20.8		
380	-----	-----	-----	I/-19.1	
480	-10.7	-21.5	-21.2	-19.9	
600	-10.1	-20.5	-21.2	-20.0	
720	-10.0	-19.0	-21.0	-19.0	I/(PT)
780	-10.0	-19.0	-21.0	-21.4	
920	-10.1	-18.8	-21.0	-21.7	-22.0

* Tensiometer intalled at this time and with noted initial pressure.

** Tensiometer read with pressure transducer.

Tensiometer data - Experiment 2 (Layer numbers 3 and 4)

(Pressure head values in cm-H_2O)

	Tensiometers			
Time (min)	3A	3B	4A	4B
20	I/-19.7			
35	-----	I/-18.3		
40	-----	-----	I/-21.0	
50	-----	-----	-----	I/-20.0
90	-12.2	-16.5	-15.2	-19.7
120	-12.2	-16.1	-13.8	-19.4
180	-12.5	-14.7	-11.3	-17.8
240	-12.7	-12.8	- 9.3	-14.6
300	-13.4	-12.2	- 8.7	-12.5
360	-13.7	-11.8	- 8.4	-11.2
480	-14.7(?)	-11.5	- 7.8	-10.3
600	-14.5(?)	-11.0	- 7.5	- 9.6
620	Changed tensiometer 3A to pressure transducer type			
720		-11.7	- 7.4	-10.2
780		-11.6	- 7.2	-10.0
920	- 4.	-11.5	-7.0	-10.0

Tensiometer data - Experiment 2 (Layer numbers 7 and 8)

(Pressure head values in cm-H_2O)

	Tensiometers			
Time (min)	7A	7C	8A	8C
90	I/-19.9			
120	-18.9			
180	-16.2			
210	-----	I/-11.9		
240	-14.3	-15.2		
300	-13.8	-17.0		
360	-11.6	-16.3		
390	-----	-----	I/-20.0	
480	-10.5	-15.2	-10.2	
510	-----	-----	-----	I/-20.5
600	-10.3	-14.3	-19.0	-20.5
720	-11.1	-14.3	-18.2	-20.1
780	-10.7	-14.0	-18.0	-20.0
920	-10.7	-13.8	-17.9	-19.2

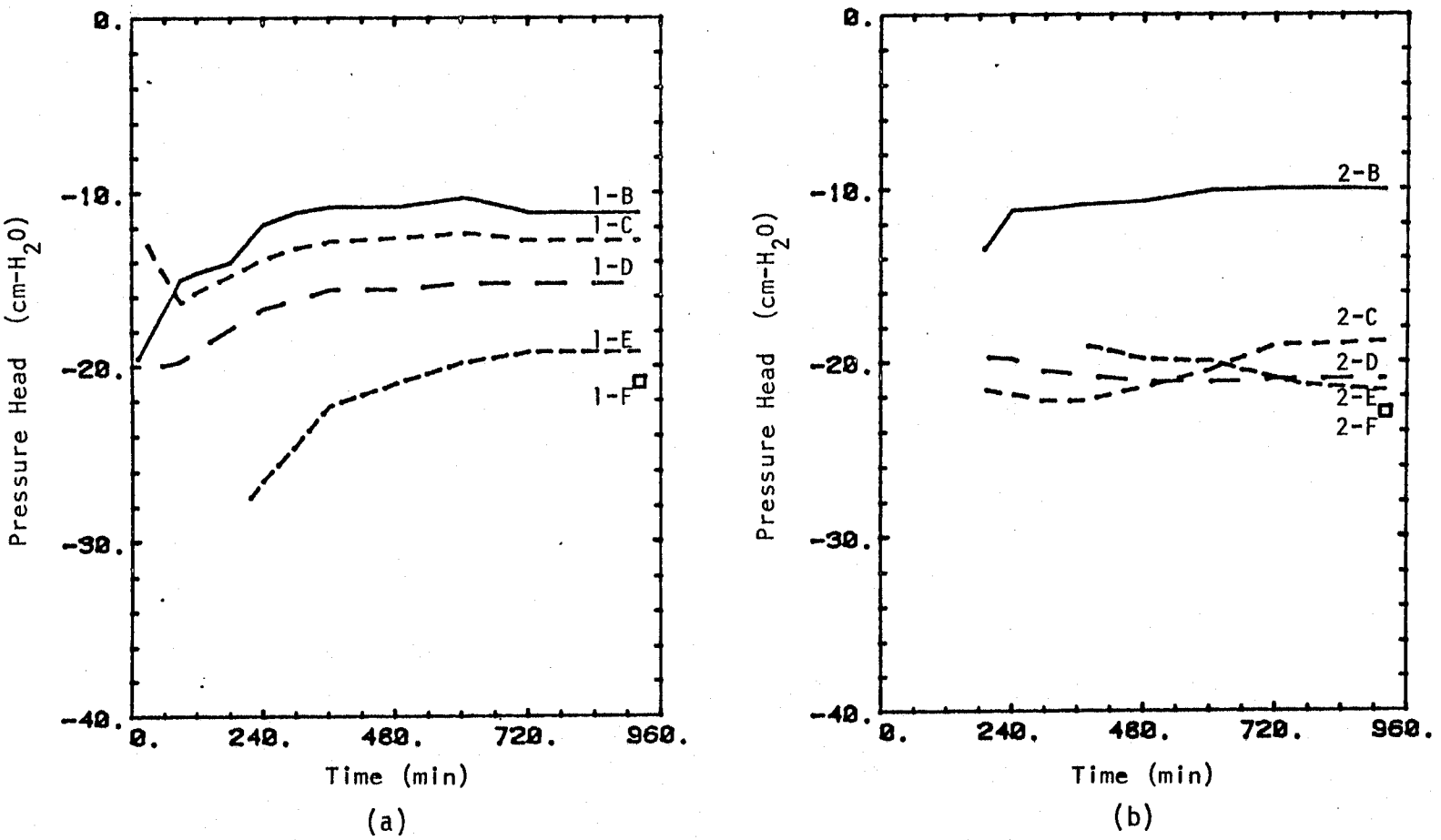

Figure A3.4. Tensiometer pressure heads versus time for experiment 2 and for (a) tensiometers in layer 1 (Sevilleta dune sand) and (b) layer 2 (medium blasting sand).

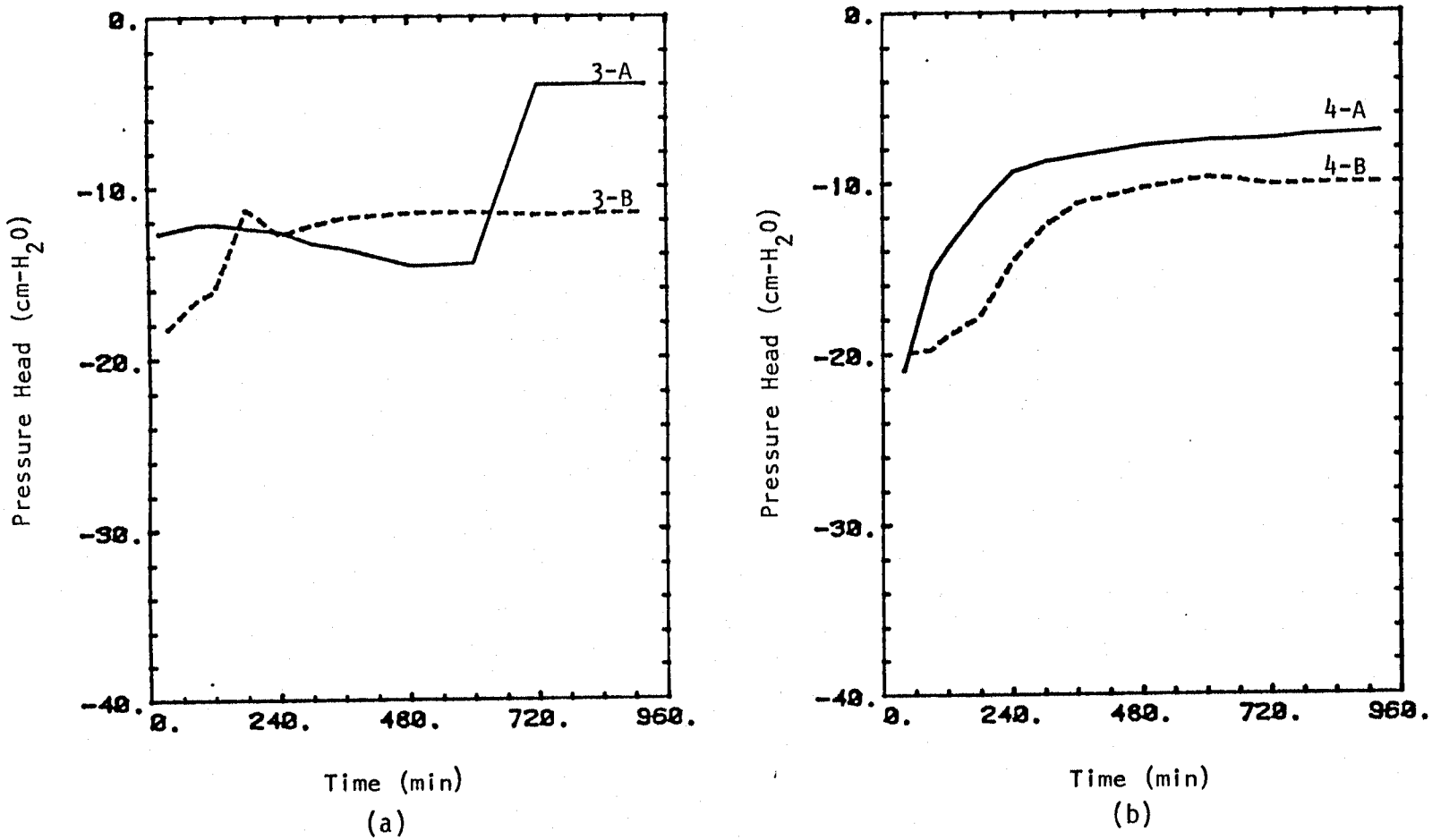

Figure A3.5. Tensiometer pressure heads versus time for experiment 2 and for (a) tensiometers located in layer 3 (Sevilleta dune sand), and (b) tensiometers located in layer 4 (medium blasting sand).

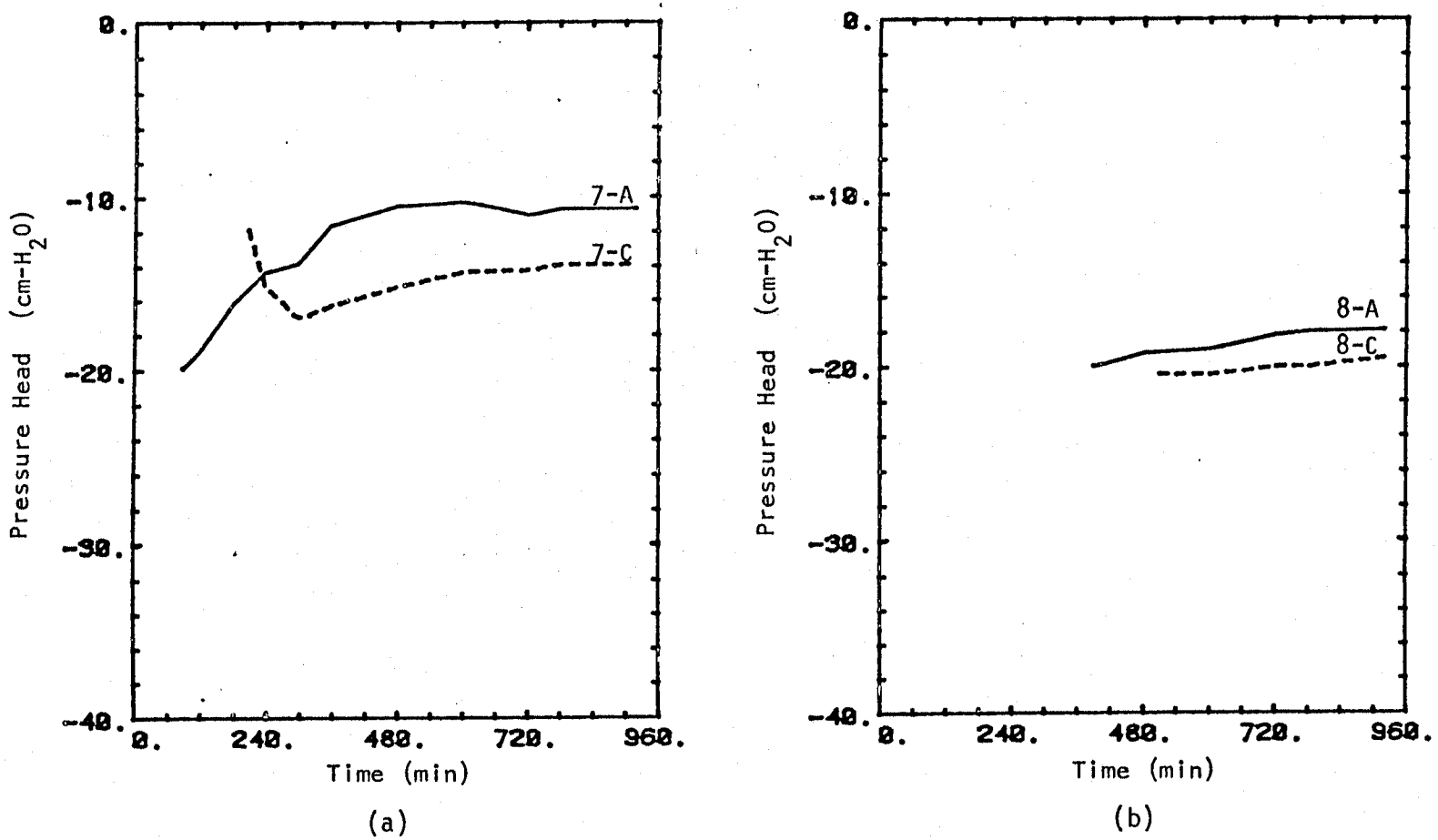

Figure A3.6. Tensiometer pressure heads versus time for experiment 2 and for (a) tensiometers located in layer 7 (Sevilleta dune sand), and (b) tensiometers located in layer 8 (medium blasting sand).

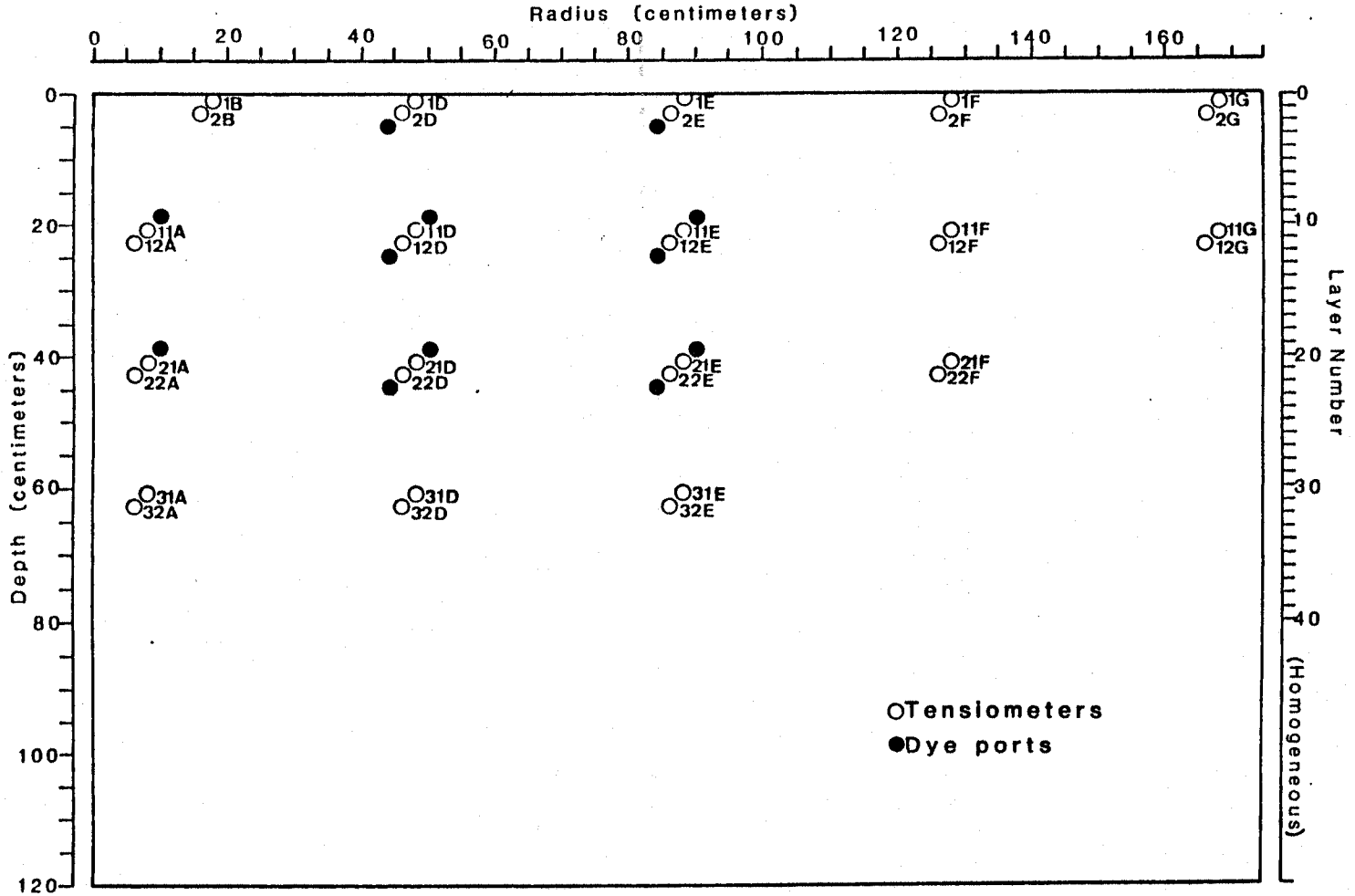

Figure A3.7. Nomenclature scheme for tensiometers used in experiment 3.

(Pressure head values in cm-H_2O)

Time (min)	Tensiometer 1B	1D	1E	1F
7	I/-13.1			
50	-----	I/-15.9		
70	-13.9	-17.1		
120	-13.7	-17.5		
190	-13.7	-17.1		
200	----	-----	I/-22.3	
270	-11.8(?)	-23.0	-22.3	
360	-13.5	-16.6	-22.6	
480	-13.0	-16.3	-22.6	I/-9.8
600	-13.9	-16.7	-22.5	-25.2
750	-13.7	-16.5	-22.5	-25.3

Tensiometer data - Experiment 3 (Layer number 2)

(Pressure head values in cm-H_2O)

Time (min)	Tensiometer 2B	2D	2E
60	I/-17.5		
70	-16.9		
120	-13.5		
190	-12.3		
210	------	I/-10.3	
230	-----	-----	I/-10.3
270	-12.3	-12.0	-10.4
360	-12.2	-13.2	-12.4
480	-11.6	-13.4	-14.2
600	-12.4	-14.0	-15.3
750	-12.0	-14.5	-16.2

* Tensiometer intalled at this time and with noted initial pressure.

** Tensiometer read with pressure transducer.

Tensiometer data - Experiment 3 (Layer number 11)

(Pressure head values in cm-H_2O)

Time (min)	Tensiometer 11A	11D	11E	11F
13	I/-12.9			
55	-----	I/-13.9		
70	-9.4	-15.3		
120	-9.8	-17.4		
190	-7.2	-17.3		
270	-7.2	-16.7		
340	------	-----	I/-12.5	
360	-7.2	-16.0	-22.2	
480	-7.9	-16.0	-20.0	
600	-8.4	-15.5	-19.4	
650	-----	-----	-----	I/(PT)
750	-8.2	-15.1	-18.8	-17. (?)

Tensiometer data - Experiment 3 (Layer number 12)

(Pressure head values in cm-H_2O)

Time (min)	Tensiometer 12A	12D	12E
18	I/-12.9		
70	-8.7		
120	-7.4		
190	-6.8		
210	-----	I/-10.8	
270	-6.7	-12.2	
340	-----	-----	I/-12.5
360	-6.6	-13.3	-12.5
480	-7.2	-14.2	-15.0
600	-7.3	-14.7	-16.3
750	-7.2	-14.8	-17.2

(Pressure head values in cm-H_2O)

Time (min)	Tensiometer 21A	21D	21E	21F
40	I/-10.0			
70	-8.8			
120	-7.5			
190	-7.0			
250	-----	I/-18.0		
270	-7.0	-17.3		
360	-6.8	-17.0		
480	-7.8	-17.1		
600	-7.5	-16.7		
620	-----	-----	I (PT)	I(PT)
750	-7.8	-16.2		
780	-----	-----	-17.	-22.

Tensiometer data - Experiment 3 (Layer number 22)

(Pressure head values in cm-H_2O)

Time (min)	Tensiometer 22A	22D	22E	22F
80	I/-11.8			
120	-9.7			
190	-8.0			
250	-----	I/-33.5		
270	-9.4	-33.2		
360	-7.2	-32.5		
480	-7.5	-31.0		
490	22D adjusted to a value of -19.2			
600	-7.4	-18.6		
640	-----	-----	I/(PT)	I(PT)
750	-8.4	-18.2		
780	-----	-----	-11.0	-16.0

Tensiometer data - Experiment 3 (Layer number 31)

(Pressure head values in cm-H_2O)

	Tensiometer		
Time (min)	31A	31D	31E
680	I(PT)	I(PT)	I(PT)
780	-7.	-14.	-18.

Tensiometer data - Experiment 3 (Layer number 32)

(Pressure head values in cm-H_2O)

	Tensiometer		
Time (min)	32A	32D	32E
680	I(PT)	I(PT)	I(PT)
780	-7	-18	-16

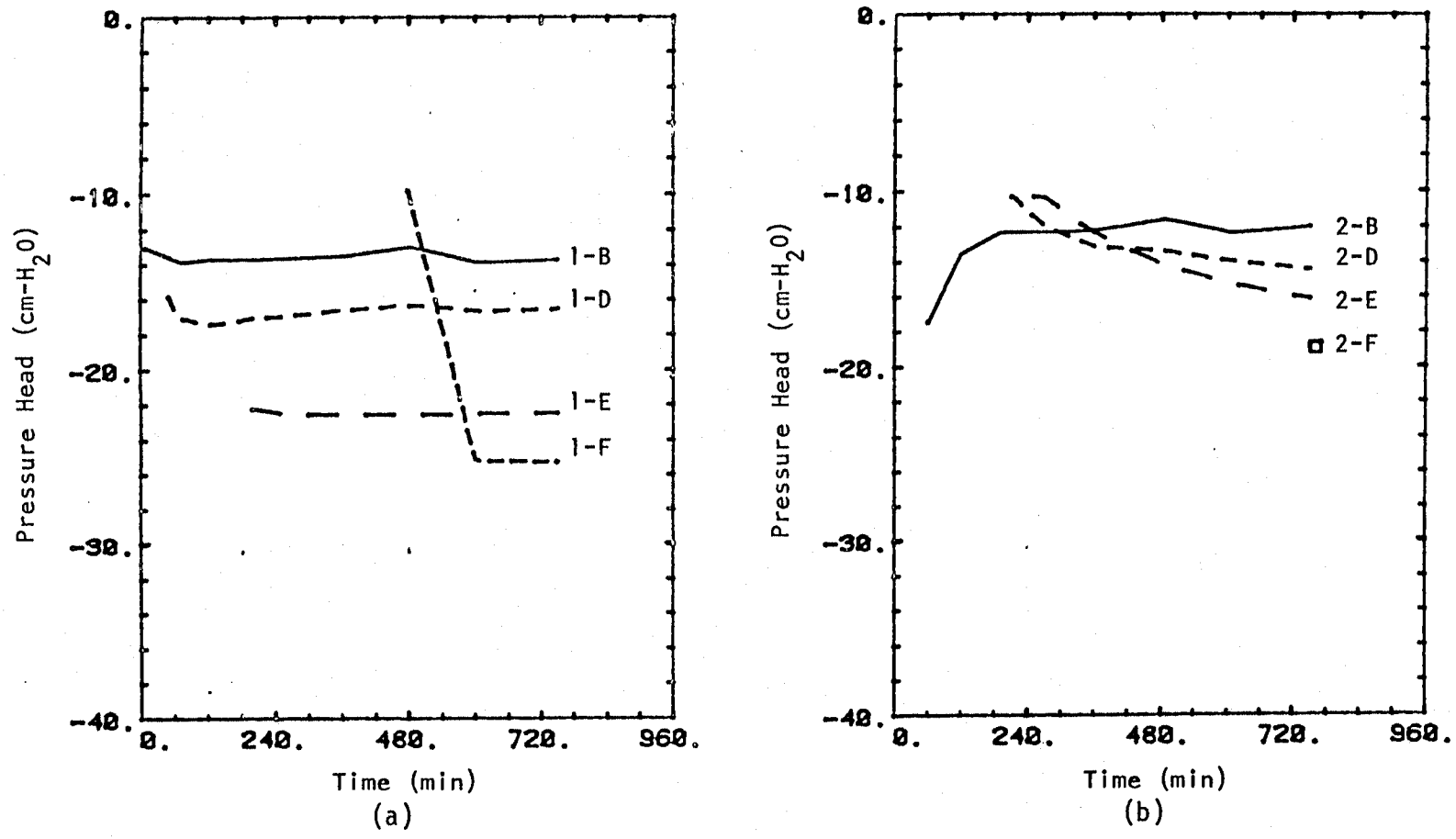

Figure A3.8. Tensiometer pressure head versus time for experiment 3 and for (a) tensiometers located in layer 1 (Sevilleta dune sand) and (b) tensiometers located in layer 2 (medium blasting sand).

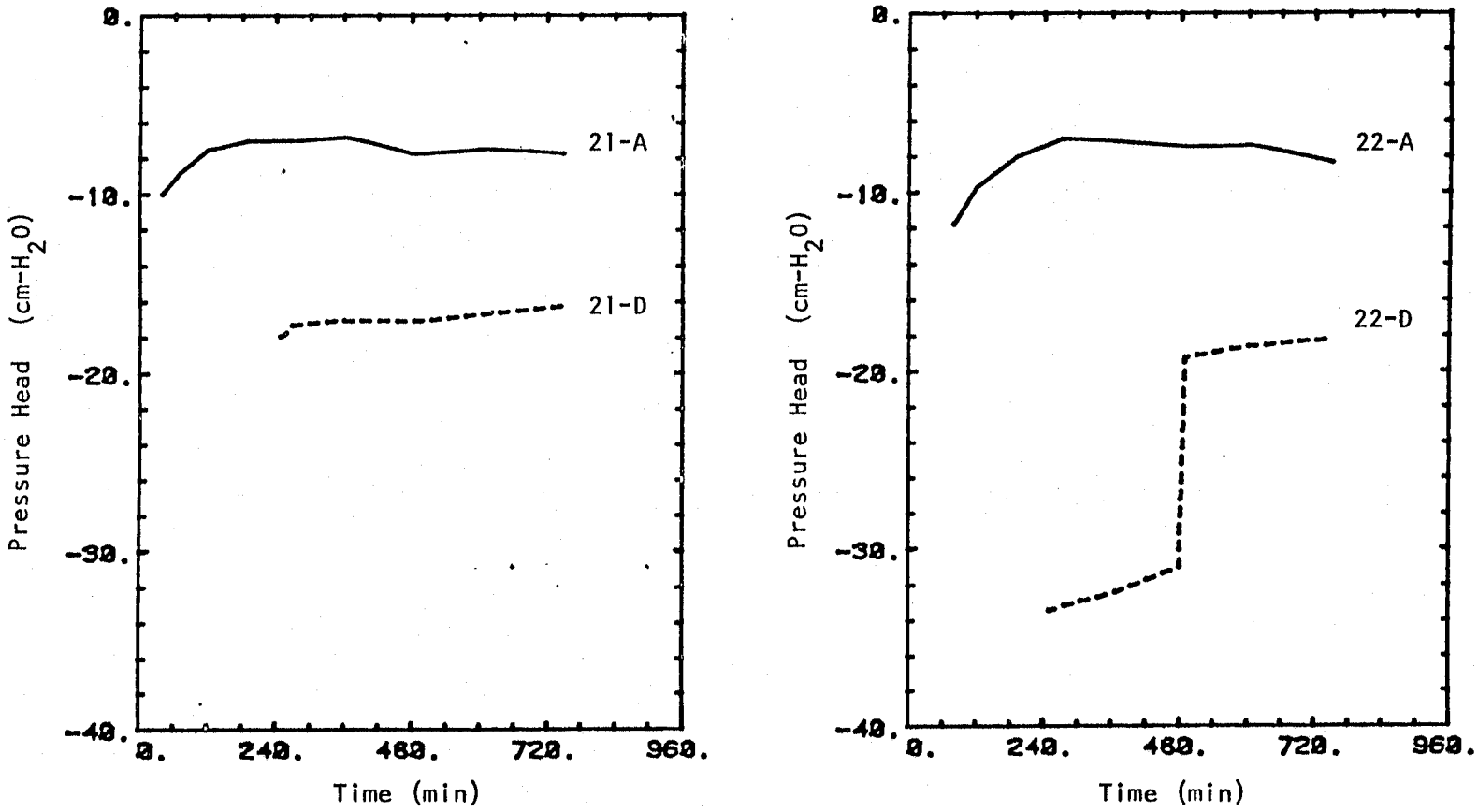

Figure A3.10. Tensiometer pressure heads versus time for experiment 3 and for (a) tensiometers located in layer 21 (Sevilleta dune sand) and (b) for tensiometers located in layer 22 (medium blasting sand).

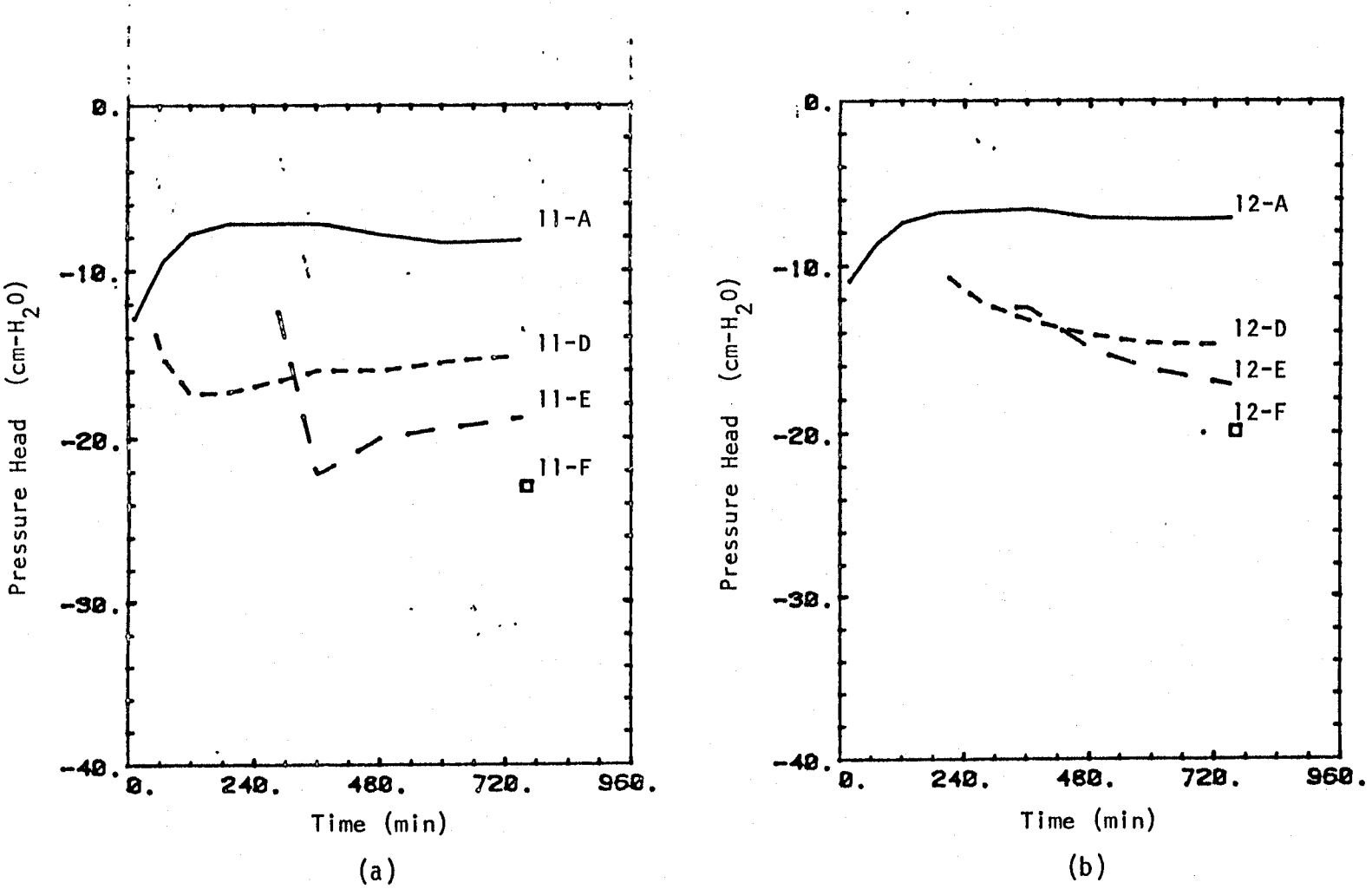

Figure A3.9. Tensiometer pressure heads versus time for experiment 3 and for (a) tensiometers located in layer 11 (Sevilleta dune sand) and (b) for tensiometers located in layer 12 (medium blasting sand).

Temperature Data

Temperature data was collected for each experiment from a 20 liter bucket of water located next to the reservoir that provided water to source. The experiment was conducted within an air-conditioned building during the summer months. Under these conditions, temperature fluctuations were minimal. Temperature data is presented in tabular form for each of the three experiments.

Experiment 1

Time Elapsed (min)	Temperature (^{o}C)
0	22.5
120	22.5
240	22.5
300	22.5
360	22.5
480	22.5
600	22.0
720	22.0
1080	20.5
1440	21.0
1800	22.0
2160	21.5
2880	21.0
3600	22.0
4320	20.0
4680	21.5

Experiment 2

Time Elapsed (min)	Temperature (^{o}C)
0	22.5
120	22.5
360	22.5
480	22.0
600	21.5
720	21.0

Experiment 3

Time Elapsed (min)	Temperature (^{o}C)
0	21.0
120	21.5
180	22.0
360	22.0
480	22.0
600	21.5
720	21.5